Technische Universität München
Fakultät für Chemie

Lehrstuhl für Technische Chemie II

Säure-Base katalysierte Synthese von Methanthiol

Manuel Weber-Stockbauer

Vollständiger Abdruck der von der Fakultät für Chemie der Technischen Universität München zur Erlangung des akademischen Grades eines

Doktors der Naturwissenschaften (Dr. rer. nat.)

genehmigten Dissertation.

Vorsitzender: Prof. Dr. Hubert A. Gasteiger
Prüfende der Dissertation:
1. Prof. Dr. Johannes A. Lercher
2. Prof. Dr. Ulrich K. Heiz

Die Dissertation wurde am 16.08.2019 bei der Technischen Universität München eingereicht und durch die Fakultät für Chemie am 14.01.2020 angenommen

“Man soll die Dinge nicht so tragisch nehmen, wie sie sind.”

- Karl Valentin

Für meine Familie

Statutory Declaration

I declare that I have authored this thesis independently and that I have solely used the declared (re)sources and that I have marked all material, which has been quoted either literally or by content from the used sources. At the end of each chapter all collaborators are named and their specific contribution is addressed. Published content of this thesis is clearly marked.

_____, _____

Acknowledgement

I would to thank my doctoral advisor, Professor Johannes A. Lercher for giving me the chance to do my PhD studies as a part of his group. Thank you for the trust and the freedom I got for my research. The next persons I want to thank are Dr Oliver Gutierrez and Dr. Ricardo Bermejo-Deval for being my co-advisors. The last three years we faced together many challenges coming from various sources, hard to imagine in the beginning they could ever occur. Thank you for our discussions and your help to put all the pieces together, which finally resulted in this thesis.

Many thanks to the staff members of TC II, Xaver Hecht, Bettina Federmann, Uli Sanwald, Stefanie Seibold, Kateryna Kryvko, Andreas Marx and Martin Neukamm. I always appreciated your work, easing our daily working life.

I also want to thanks my friends and colleagues, who went with me through the ups and downs of over three years PhD studies: Martin Baumgärtl, Felix Kirchberger, Andi Ehrmaier, Ferdinand Vogelgsang, Manuel Wagenhofer, Teresa Schachtl, Lara Milakovic, Laura Löppert, Daniel Melzer, Roland Weindl, Christoph Denk, Verena Höpfl, Niklas Pfriem Martina Aigner, Wanqiu Liu and all the others. Thanks for sharing the time with me and all the fun we had together. Also, I want to thank the students working with me; a special thanks goes to Matthias Singer and Matthias Rehner.

Of course, the biggest thanks is for my family and friends. My parents, for everything you did to give me the possibility to do what I wanted to do. My wife Veronika for supporting and pushing me when it was necessary. My wonderful daughter Anna for showing us every day what really matters; your smile always fixes everything. My grandmother, my parents in law and the rest of my family. Thank you all for your efforts to support us, your trust in me. Alexander and Florian Denk, Oliver Lenz, Maxine Schießl and all the rest; thank you for being my friends for more than twenty years.

Manuel

Abstract

Lewis acid-base pairs are the active sites in the thiolation of methanol, forming surface alcoholates and catalyze the corresponding substitution of the oxygen for the thiol groups in a Langmuir-Hinshelwood mechanism. Strong Lewis acid sites catalyze the condensation of methanol to form dimethyl ether, via the formation of methoxy groups that react with gas phase methanol. Suitable catalysts have weakly acidic Lewis acid sites and stronger base sites, such as cesium cation loaded metal oxides or Al_2O_3-MgO mixed oxides.

Kurzzusammenfassung

Lewis-Säure-Base-Paare sind die aktiven Zentren bei der Thiolierung von Methanol. Sie bilden Oberflächen-Alkoholate und katalysieren die Substitution des Sauerstoffs mit Thiolgruppen in einem Langmuir-Hinshelwood-Mechanismus. Starke Lewis-Säure-Zentren katalysieren die Kondensation von Methanol zu Dimethylether durch die Bildung von Methoxygruppen, die mit Methanol aus der Gasphase reagieren. Geeignete Katalysatoren weisen schwach saure Lewis-saure Zentren und stärker basische Zentren auf. Beispiel dafür sind mit Cäsium Kationen modifizierte Metalloxide oder Al_2O_3-MgO-Mischoxide.

Abbreviations

Abbreviation	*Description*
A	Anatase
AAS	Atomic absorption spectroscopy
AHFS	Ammonium hexafluorosilicate
AS	Acid site
BAS	Brønsted acid site
BEA	Zeolite Beta
BET	Brunnauer-Emmet-Teller
BS	Basic site
DMDS	Dimethyl disulfide
DME	Dimethyl ether
DMS	Dimethyl sulfide
FT	Fourier transform
GC	Gas chromatography
HC	hydrocarbons
HCL	Hallow-cathode lamp
IE	Ion exchange
IR	Infrared
IWI	Incipient wetness impregnation
LAS	Lewis acid site
LABS	Lewis acid-base site
LBS	Lewis basic site
MeOH	Methanol
MeSH	Methanethiol
MFC	Mass flow controller
MFI	Mordenite framework inverted
MS	Mass spectrometer
r.d.s	Rate determining step
R	Rutile
TCD	Thermal conductivity detector
X	Zeolite X
XRD	X-ray diffraction
Y	Zeolite Y

Symbols

Symbol	*Description*	*Unit*
c	concentration	[mol l^{-1}]
$E_{a,app}$	Apparent activation energy	[kJ mol^{-1}]
k	Reaction rate constant	[s^{-1}]
K	Equilibrium constant	-
m	mass	[g]
M	Molar ratio	-
n	Reaction order	-
p	Partial pressure	[bar]
P	Pressure	[bar]
Q	Volumetric flow rate	[mL min^{-1}]
r	reaction rate	[mol g^{-1} s^{-1}]
S	Selectivity	[%]
T	Temperature	[°C], [K]
TOF	Turnover frequency	[s^{-1}]
X	Conversion	[%]
Y	Yield	[%]
-	Mol percent	[mol.%]
-	Volume percent	[vol.%]
-	Weight percent	[wt.%]

Greek symbols

Symbol	*Description*	*Unit*
δ	Bending vibration	-
ν	Stretching vibration	-

Table of content

1. Introduction

1.1. Methanethiol

1.1.1. General

Methanethiol or methyl mercaptane (CH_3SH) is a colorless strongly smelling gas, with a smell of rotten cabbage. The boiling point is at 6 °C, the melting point at -123 °C. At high concentrations methanethiol is toxic, damaging the central nervous system. With a pK_a of 10.3, methanethiol is a weak acid.[2] Its main application is in the synthesis of the essential amino acid methionine, described in the next paragraph.

1.1.2. Main application of methanethiol – The Degussa process

The main application of methanol is in the industrial synthesis of methionine, the so-called Degussa process. In this reaction process, methanethiol (1) reacts in a first step with acrolein (2), forming 3-Methylmercaptopropionaldehyde (3). This aldehyde is further converted in a second step with hydrogen cyanide and ammonium hydrogen carbonate yielding 5-(2-ethylthioethyl)hydantoin (4). In an alkaline solution with excess of potassium carbonate, the hydantoin-derivate is hydrolyzed, giving $_{D,L}$-potassium methionate (5), CO_2 and NH_3 (from which ammonium hydrogen carbonate is recovered). Under acidification of the aqueous potassium methionate solution with CO_2 gives $_{D,L}$-methionine (6) is obtained.[3]

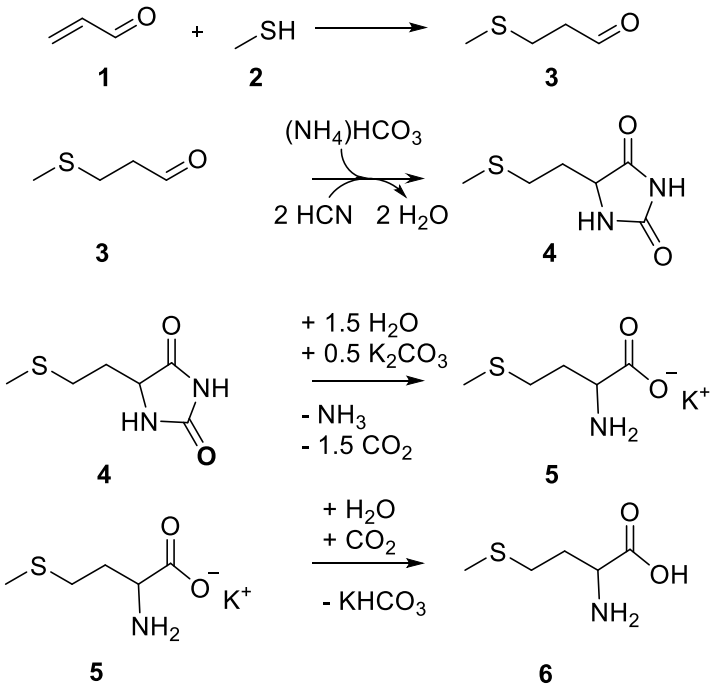

Figure 1.1 Reaction scheme of the Degussa process for the industrial synthesis of methionine. The reaction scheme is based on the scheme shown in [3].

1.2. Synthesis of methanethiol

1.2.1. Thiolation of methanol – State of the Art Process

The thiolation of methanol is the state of the art process for the selective synthesis of methanethiol in industry. The industrial synthesis of methanethiol is done over methanol thiolation, performed in the temperature range of 300 to 500 °C, at pressures from 1 to 25 bar using a fixed bed reactor with a variety of possible catalysts as described below (1.2.1.3). As the product stream can contain unreacted reactants, byproducts as dimethyl ether and dimethyl sulfide and gaseous species like CO, methane, nitrogen or hydrogen (1.2.1.2), purification is needed. For this, methanethiol pressure higher than 7 bar are required to enable the separation via e.g. washing the product stream with methanol at 25 °C. Lower product pressures requires condensation of methanethiol at -60 °C, to separate the liquid product from the product stream. From economic reasons, the second process is inconvenient, due to high energy costs. The used catalyst is Cs doped WS_2/Al_2O_3 with 15 to 40 wt.% Cs_2WS_4.[4]

1.2.1.1. Reaction mechanism

Mashkina et al. were the first to propose that the formation of methanethiol happens over the surface reaction of dissociated methanol and H_2S.[5] Mashkin postulated the following mechanism (Scheme 1.1): Methanol adsorbs on an acid-base pair of the metal oxide surface adjacent to a surface hydroxyl group, resulting in the formation of water and a surface methoxy species. In the second step adsorption of H_2S on the same acid-base pair leads to the formation of methanethiol, desorbing under recreation of the surface hydroxyl group.[6]

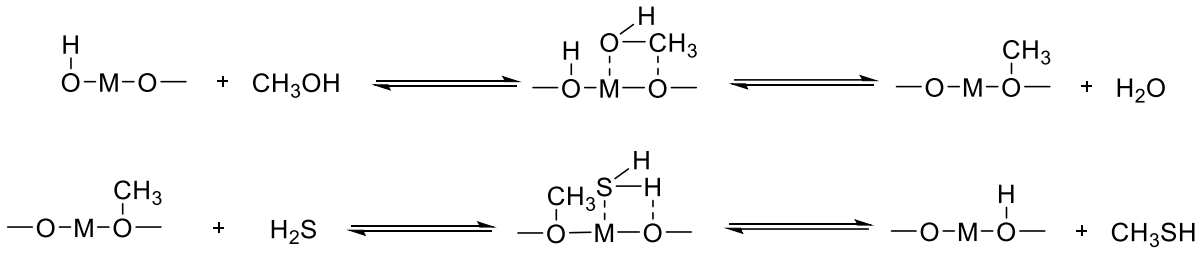

Scheme 1.1 Formation of methanethiol via 1) formation of surface methoxy species 2) reaction of the methoxy species with adsorbed H_2S, based on the work of Mashkin.[6]

Plaisance et al. studied different metal oxide catalysts and performed ab-initio calculations to determine the binding strength of different oxygen and sulfur compounds on the catalyst surface. From these experiments, they stated the following reaction mechanism for methanol and H_2S reacting over alumina: In a first step methanol and H_2S dissociatively adsorbs on Lewis acid-base pairs of the alumina. After that methanethiol can form over two different pathways: In the first pathway, the formed SH^- group can directly react with a neighbored methoxy group, forming the thiol. Ina second pathway, the hydrogen of the adsorbed SH^- can combine with a neighbored hydroxyl group, forming water and leaving behind a sulfide and a free Lewis acid site. The sulfide can react with an adsorbed methoxy group, forming an methanolate species, which can be protonated by a neighbored hydroxyl group, releasing again methanethiol. They observed reaction orders in H_2S of 1, respectively <1 in methanol.[7]

For the reaction of methanol and H_2S over H/alkaline zeolites Ziolek et al. proposed the following reaction scheme, involving Lewis and Brønsted acid sites (

Scheme **1.2**). On the Brønsted acid site pathway, dimethyl ether is formed by condensation of two methanol molecules, before undergoing secondary reactions, as conversion increases Formation of hydrocarbons or reaction with H_2S, giving dimethyl sulfide. On Lewis acid-base sites, methanol reacts with H_2S to methanethiol, which again can undergo secondary reactions on Brønsted acid sites, resulting in the formation of dimethyl sulfide and finally in hydrocarbons, if strong Brønsted acidic sites are present.[8]

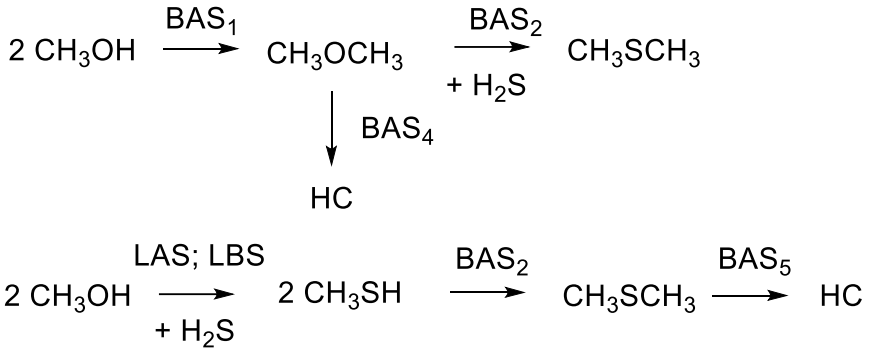

Scheme 1.2 Occurring reactions of methanol on acid-base sites of zeolites. BAS: Brønsted acid sites with different strength: $BAS_1 < BAS_2 < BAS_3 < BAS_4 < BAS_5$; LAS: Lewis acid sites; LBS: Lewis basic sites; HC: hydrocarbons.[8]

1.2.1.2. Reaction network

The complete reaction network as described by Pashigreva et al. is shown in Scheme 1.3.[1] In this network the desired reaction is the reaction of methanol and hydrogen sulfide to methanethiol (1). As possible side product, dimethyl ether can be obtained by condensation of methanol (2) which can undergo further reaction with H_2S, forming dimethyl sulfide. Methanethiol itself can undergo condensation reactions, resulting in the formation of dimethyl sulfide (4) or dimethyl ether (7). Other possible reactions are the dimerization under formation of dimethyl disulfide (5) and the hydrogenation of the thiol, resulting in methane formation (6).

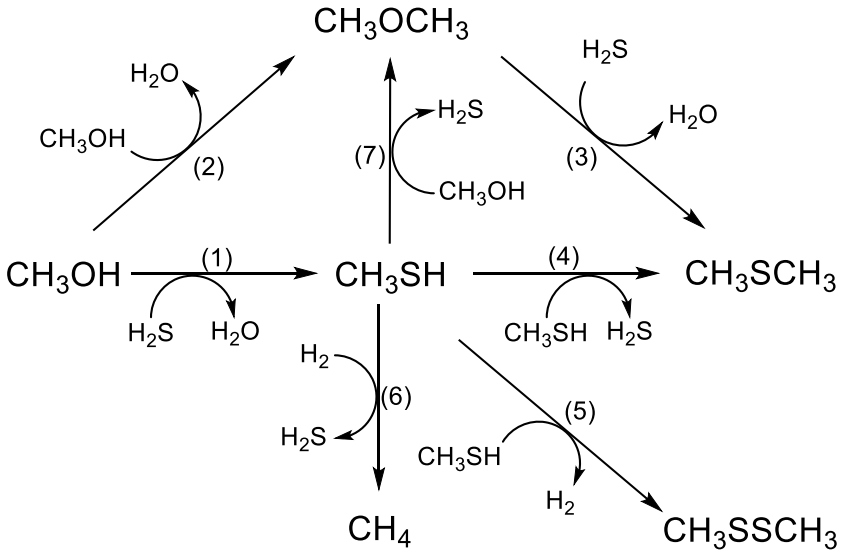

Scheme 1.3 Reaction network for the reaction of methanol with H_2S.[1]

1.2.1.3. Catalysts for methanol thiolation

The development of suitable thiolation catalysts is processing for over 100 years. After the fundamental work of Sabatier and Kramer in the beginning of the 20th century,[9, 10] it took about 30 more years for a real application for the thiol synthesize, when the industrial synthesize of methionine was invented. This process initiated the need of better thiolation catalysts, resulting in the development of the K_2WS_4/Al_2O_3 systems.[11] Further improvement of the catalytic performance was reached again 40 years later, as Sauer *et al.* found that replacing potassium by cesium, the performance of the catalyst increased. Figure 1.2 summarizes those most important steps in the development of the thiolation catalysts for industrial use.

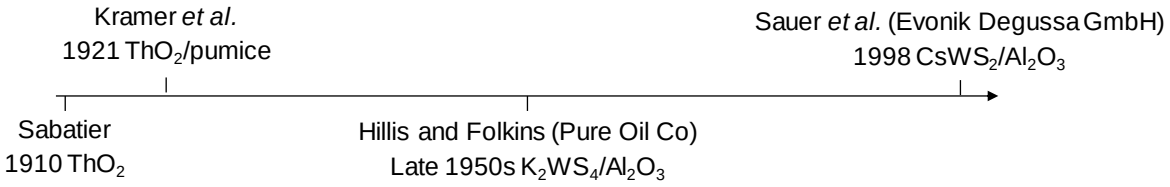

Figure 1.2 Milestones in the development of thiolation catalysts.

Next to the important milestones for the industrial application, the thiolation of methanol has been studied on a wide range of bulk and supported catalysts with different acid-base properties in academic research. An overview over the most important groups of catalysts is given in the following paragraphs, following similar classification as Mashkina.[12]

1.2.1.3.1. Metal oxides

The first to describe the synthesis of organic thiols was Sabatier, finding that ThO_2 was the most active material within a series of metal oxides to form isoamyl thiol.[9] Based on these first results, Kramer et al. studied different thoria systems. They found that in thoria supported on pumiced is able to catalyze the thiolation of different alcohol. (C_1 up to C_5).[10] Nearly 70 years later, the group of Mashkina systematically studied different metal oxides (being SiO_2, BeO_2, MgO, ZrO_2, ZnO, TiO_2, γ-Al_2O_3, η-Al_2O_3, WO_3 and V_2O_3) for their activity and selectivity in the reaction of methanol with H_2S. They found that referred to the surface area WO_3 and V_2O_3 showed the highest activity and selectivity to the thiol, followed by γ-Al_2O_3, η-Al_2O_3 and TiO_2 with one magnitude lower in activity. The over metal oxides were three orders of magnitude less active, compared to WO_3 and V_2O_3. In general they found that the specific activity increased with the ionization potential of the cation, indicating a possible dependency of the activity on the capacity of the cation to accept electrons.[12, 13]

Ziolek *et al.* compared metal oxides differing in acidity, they found that the conversion of methanol, as an indicator for the overall catalytic activity decreased in the order:

$$\gamma\text{-}Al_2O_3 > TiO_2(A) > ZrO_2 > CeO_2 > TiO_2(R) > MgAl_2O_4 > MgO$$

while the selectivity towards methanethiol decreased in the inverse order

$$MgO > ZrO_2 > TiO_2(R) > MgAl_2O_4 > CeO_2 > TiO_2(A) > \gamma\text{-}Al_2O_3.$$

selectivity to methanethiol respectively. As the other metal oxides posse both, Lewis acid and basic sites, no simple correlation of activity and selectivity can be found.

Studying the adsorption of methanol via IR they found that chemisorbed methanol is necessary for reaction taking place; taking into account the stability of the chemisorbed methanol species, they concluded that the high stability of the methoxy species and the lack of HS^- leads to the low activity of MgO.[14]

They concluded that the acid-base properties of the metal oxides play a critical role in activity and selectivity of the metal oxides. They found that the most basic material (MgO) showed the lowest activity but highest selectivity towards the thiol, while the material with the lowest basicity, γ-Al_2O_3, showed the highest activity in methanol conversion and selectivity to DMS, lowest

1.2.1.3.2. Supported basic catalysts

Next to metal oxides, often providing acidic and basic functionalities, alkaline doped metal oxides and sulfides were used as basic catalysts for the reaction of methanol and H_2S. The use of such systems was developed and patented already back in the ninety fifties by Pure Oil Co. The reason for these efforts was the development of the industrial synthesis of methionine, demanding methanethiol and the findings that the thoria systems, developed by Kramer (1.21.2.1) had serious disadvantages (*E.g*. erosion tendency did not allow the use in fixed bed reactors, low activity under industrial relevant conditions and deactivation with time on stream).[11] These new catalysts were potassium or sodium oxides, carbonates or the alkaline salts of group VI metals supported on metal oxides, with γ-Al_2O_3 being found to be highly suitable.[15-18] Kudenov *et al*. did first academic research on these materials, investigating potassium and sodium doped γ-Al_2O_3. They found that samples containing either alkaline carbonate or hydroxide, stronger basic sites were obtained, compared to the alkaline tungstate. Additionally, the concentration of aprotic sites was 2.5 times lower on the former systems compared to the later one. Main product on all the catalysts was indeed methanethiol, with DMS as byproduct. Minor side products were DME (T<450 °C reaction temperature) and CH_4 and CO_2 (>450 °C reaction temperature). The activity decreases in the order K_2CO_3/Al_2O_3 > KOH/Al_2O_3 ~$NaOH/Al_2O_3$ > K_2WS_{34}/Al_2O_3. Among the potassium samples, the DMS formation rate was 3-4 times higher on K_2CO_3/Al_2O_3 and KOH/Al_2O_3, compared to K_2WS_4/Al_2O_3.[19] The same group investigated the influence of using different tungsten species in potassium and sodium doped W_xS_Y/Al_2O_3 systems. They found that similar properties were obtained using mono and different polynuclear tungsten-oxocomplexes, hinting for similar surface properties of all catalysts. Highest selectivity towards methanethiol was achieved using an alkaline/tungsten ratio of 2:1.[20] Ziolek *et al*. studied the influence of increasing Na doping on ZrO_2 and Al_2O_3 onto catalytic properties in the methanol thiolation. They found that increasing the Na loading from 0 (pure Al_2O_3) up to 4.5% Na, respectively 0 to 1 % on ZrO_2, decreases the methanol consumption rate. Following the conclusions about metal oxides (1.2.1.2.1) higher basicity increases selectivity towards methanethiol while lowering overall activity.[21] In 1998, Sauer *et al.* found that replacing potassium by cesium, the catalyst activity increased up to 25%, referred to the catalyst mass, making those $Cs_2WS_4/A_{l2}O_3$ catalyst to the state of the art catalyst for methanol thiolation even today.[22] For a better understanding of these industrially well-applied systems, the group of Lercher systematically characterized these catalysts. They fund that the good performance and high selectivity (around 95 % at full conversion) of alkaline doped systems in general comes from the suppression of the support induces by the support and the generation of basic sites by the alkaline phase itself.[1] In a subsequent work of the same group, it was shown that the activity in methanol thiolation

increases within the group of alkaline metals from lithium to cesium due to the lower Sanderson electronegativity and the higher induced basicity of the corresponding anion.[23]

1.2.1.3.3. Supported acid catalysts

Also supported catalysts with mainly acidic character were studied for the reaction of H_2S with methanol. An overview of acidic materials used as catalysts for methanol thiolation was given by Mashkina (Table 1.1).[12] Those materials show a very limited selectivity towards methanethiol, hardly exceeding 50 %, with high yields of DMS. Compared to the high selectivity of the supported alkaline catalysts, such systems are not suitable for high selective thiol synthesis.

Table 1.1 Activity and selectivity of supported acid catalysts in the reaction of methanol with hydrogen sulfide at 360 °C, *x* = 80 % and methanol concentration of 38-62 vol.%; (M = H_2S/CH_3OH; taken from [12]).

Catalyst	M = 0.6			M = 1.6		
	w/mmol g^{-1} h^{-1}	S		*w*/mmol g^{-1} h^{-1}	S	
		CH_3SH	$(CH_3)_2S$		CH_3SH	$(CH_3)_2S$
$HSiW/SiO_2$	-	-	-	21	49	51
Cr_2O_3/SiO_2	5	40	60	-	-	-
WO_3/SiO_2	12	23	74	21	46	43
WO_3/AlSi	-	-	-	102	43	49
γ-Al_2O_3	340	15	54	637	37	35
Cr_2O_3/Al_2O_3	460	10	80	832	22	50
MoO_3/Al_2O_3	330	20	70	767	53	47
V_2O_5/Al_2O_3	400	40	40	661	54	31
WO_3/Al_2O_3	214	2	70	547	51	37
HF/Al_2O_3	307	4	20	1338	34	51
B_2O_3/Al_2O_3	-	-	-	554	41	47
H_2SO_4/Al_2O_3	-	-	-	612	37	38

1.2.1.3.4. Zeolites

Another important group of materials, studied in the thiolation of methanol were protonic and alkaline exchanged zeolites. Mashikna et al. compared HZSM-5 with partially and fully alkaline exchanged faujasite zeolites. Similar to the metal oxides (0) they found that the activity drastically decreased with decrease in acidity and increase in basicity in the order

HZSM-5 > HNaY >> NaX > NaY

In the same order, the selectivity towards methanethiol, respective to dimethyl sulfide increased from 5 – 20 % on HZSM-5 to 60-88 on NaX, respectively 69-76 % on NaY. They stated that the high activity of the protonic zeolites and the high dimethyl sulfide selectivity is based on the high concentration of strong surface acid sites. On NaX, the lack of those strong acid sites results in a lower catalytic activity (factor 2 to 10), due to a lower activation of methanol. A higher activity to methanethiol is based on the presence of paired acid-base sites, being Na^+ and lattice oxygen on which H_2S adsorbs under dissociation, giving surface thiol groups. Lower activity from on NaY to NaX is explained by the lower concentration of extra framework sodium in NaY, while the reaction mechanism was stated to be the same, due to similar selectivities.[24, 25]

Ziolek et al. studied a series of partial protonic faujasite catalysts, containing different alkaline metals. They found that on acidic zeolites not only the thiolation reactions to methanethiol and dimethyl sulfide occurred, but the conversion of methanol to hydrocarbons. With decreasing acid strength, the selectivity to methanethiol, respective to dimethyl sulfide increased. In general, the basicity influenced the yield of methanethiol. Medium acidic zeolites like LiHNaY and NaHY were not stable under reaction condition, as competitive reactions increased with time on stream, while such increase was not found on low acidic catalysts like KHNaY, RbHNaY and CsHNaY.[8]

1.2.1.3.5. Alternative synthesis routes

Over the past years, various research groups investigated the direct methanethiol synthesis from H_2S containing synthesis gas. Kaufmann *et al.* described a two-stage process: In the first step, CO or CO_2, H_2 and elemental sulfur[26, 27] react in liquid phase to form carbonyl sulfide COS, which was catalytically converted to methanethiol under the presence of H_2 and H_2S, using K doped MoS_4/SiO_2 as catalyst.[27-29] The promotion of MoS_4/SiO_2 with transition metals like Ni or Co was found to increase the catalytic activity[30, 31] and suppresses side reactions like CO_2 formation.[32] Mul *et al.* used supported Vanadium catalysts to convert CO, H_2 and H_2S directly into methanethiol. They also found that COS and CS_2 were formed as intermediates, being further hydrogenated to methanethiol.[33] A similar one step process was studied by Chen *et al.*, using $KMoS_4/SiO_2$ as catalyst.[34]

A different reaction system has been studied by Wang et al. using CS_2 as S source instead of H_2S for thiolation of methanol, using (Co)KWS_2/Al_2O_3 as catalyst.[35, 36] The different synthesis strategies for methanethiol are summarized in Table 1.2.

Table 1.2: Catalytic processes for the synthesis of methanethiol.

Reaction	Catalyst	Reference
$CO/CO_2 + H_2 + S \longrightarrow COS + H_2O + H_2S$	No catalyst	[26, 27]
$COS + H_2 + H_2S \longrightarrow CH_3SH + H_2O$	$KMoS_4/SiO_2$	[27-32]
$CO + H_2 + H_2S \longrightarrow CH_3SH + H_2O$	$KMoS_4/SiO_2$, V_2O_5 on metal oxides	[33, 34]
$CH_3OH + CS_2 \longrightarrow CH_3SH + H_2O$	(Co)KWS_2/Al_2O_3	[35, 36]
$CH_3OH + H_2S \longrightarrow CH_3SH + H_2O$	Various metal oxides/sulfides, alkaline doped metal oxides/sulfides, zeolites	[9-25]

1.3. Scope of this thesis

The scope of this thesis is to understand how thiolation catalysts work, including a detailed understanding of the role of single catalyst components to understand catalyst activity and selectivity, being active sites for different reaction pathways. Clarifying the role of different components enable a development of tailor-made methanol thiolation catalyst, with optimized properties for maximum thiol yield.

For that purpose, in the second chapter of this thesis the role of Cs^+ and the WS_2 phase of cesium doped WS_2/Al_2O_3 catalysts is studied. The study includes kinetic measurements using different catalyst compositions, as well as the use spectroscopy and other physicochemical methods to study the state of the catalyst and the adsorption of probe molecules. The combination of the obtained results gives a clear picture of the processes on the surface.

In the third chapter, the changes in catalyst activity in the thiolation of methanol induced by Cs doping are studied on different metal oxide, being γ-Al_2O_3 ZrO_2 and TiO_2. Physicochemical characterization and evaluation of changes in the reaction kinetics are going to show changes on the metal oxide surface, coming along with the Cs deposition and correlate those to changes on the reaction pathways of methanol. Acid properties of the obtained catalysts are evaluated by pyridine adsorption and the obtained catalyst compared to Cs supported on alumina, as benchmark system.

Zeolites as support materials for the active Cs species are studied in chapter four. Cs is deposited on HBEA is loaded via incipient wetness impregnation and on ion exchange. Also, a series of AHFS treated Cs exchanged MFI zeolites with changing Si/Al ratio are synthesized, to study the activity of single Cs sites and exclude the effect of extra framework alumina on the reaction.

The fifth chapter deals with magnesium-aluminum mixed oxides which are proposed to be highly active for the conversion of methanol, while the selectivity is affected by the magnesium/aluminum ratio. First, a series of magnesium-aluminum mixed oxides with increasing aluminum content is synthesized. Studying those materials as catalysts in the thiolation reaction of methanol, together with the characterization of acid-base properties is going to reveal the optimum Mg/Al ratio for the methanol thiolation.

1.4. Literature

[1] https://pubchem.ncbi.nlm.nih.gov/compound/878 (accessed Nov. 14, 2018), in, 2018.

[2] A.V. Pashigreva, E. Kondratieva, R. Bermejo-Deval, O.Y. Gutiérrez, J.A. Lercher, Methanol thiolation over Al2O3 and WS2 catalysts modified with cesium, Journal of Catalysis, 345 (2017) 308-318.

[3] M. Breuer, K. Ditrich, T. Habicher, B. Hauer, M. Keßeler, R. Stürmer, T. Zelinski, Industrial Methods for the Production of Optically Active Intermediates, Angewandte Chemie International Edition, 43 (2004) 788-824.

[4] J. Sauer, W. Boeck, L.v. Hippel, W. Burkhardt, S. Rautenberg, D. Arntz, W. Hofen, Catalyst, process for its preparation, and use for synthesis of methyl mercaptan in: E.D. GmbH (Ed.), 1998.

[5] A.V. Mashkina, E.A. Paukshtis, E.N. Yurchenko, V.N. Yakovleva, A.V. Popov, Effect of acid-base properties of catalysts on their activity in methylmercaptane synthesis, Reaction Kinetics and Catalysis Letters, 34 (1987) 407-412.

[6] V.Y. Mashkin, Kinetic study of dimethylsulfide and methanethiol synthesis, Applied Catalysis A: General, 109 (1994) 45-61.

[7] C.P. Plaisance, K.M. Dooley, Zeolite and Metal Oxide Catalysts for the Production of Dimethyl Sulfide and Methanethiol, Catal Lett, 128 (2009) 449-458.

[8] M. Ziolek, J. Czyzniewska, J. Kujawa, A. Travert, F. Mauge, J.C. Lavalley, Reactions of alcohols with hydrogen sulphide on zeolites. Part 7: the effect of Brønsted acidity of faujasite type zeolites on methanol hydrosulphurisation, Microporous and Mesoporous Materials, 23 (1998) 45-54.

[9] S. Sabatier, C.R. Mailhe, General Methods for Direct Preparation of Mercaptans by Catalysis Starting with the Alcohols, Comptes rendus chimie, 150 (1910) 1217-1221.

[10] R.L. Kramer, E.E. Reid, THE CATALYTIC PREPARATION OF MERCAPTANS.1, Journal of the American Chemical Society, 43 (1921) 880-890.

[11] H.O. Folkins, E.L. Miller, Synthesis of Mercaptans, Industrial & Engineering Chemistry Process Design and Development, 1 (1962) 271-276.

[12] A.V. Mashkina, Heterogeneous catalytic synthesis of alkanethiols and dialkyl sulfides from alcohols and hydrogen sulfide, Russian Chemical Reviews, 64 (1995) 1131.

[13] M.E.A. A. V., Paukshtis; V. N. Yakovleva, Synthesis of methyl mercaptan from methanol and hydrogen sulfide on acidic catalysts, Kinetic and Catalysis, 29 (1988) 596-602.

[14] M. Ziolek, J. Kujawa, O. Saur, J.C. Lavalley, Metal oxides as catalysts for the reaction between methanol and hydrogen sulfide, The Journal of Physical Chemistry, 97 (1993) 9761-9766.

[15] H.O. Folkins, Production of organic thiols in: P.O. Co (Ed.), 1957.

[16] H.O. Folkins, E.L. Miller, Preparation of organic thiols in: P.O. Co (Ed.), 1958.

[17] H.O. Folkins, E.L. Miller, K. Adolph, Preparation of prganic thiols, in: P.O. Co (Ed.), 1958.

[18] H.O. Folkins, M. Elmer, Production of organic thiols from ether and hydrogen sulfide over promoted alumina catalysts in: P.O. Co (Ed.), 1958.

[19] V.M. Kudenkov, E.A. Paukshtis, A.V. Mashkina, Synthesis of methylmercaptane in the presence of base catalysts, Reaction Kinetics and Catalysis Letters, 38 (1989) 199-203.

[20] A.V. Mashkina, R.I. Maksimovskaya, V.N. Yakovleva, E.P. Starodubtseva, Activity of tungstate catalysts in the synthesis of metylmercaptane from methanol and hydrogen sulfide, Reaction Kinetics and Catalysis Letters, 36 (1988) 159-164.

[21] M. Ziolek, J. Kujawa, J. Czyzniewska, I. Nowak, A. Aboulayt, O. Saur, J.C. Lavalley, Effect on the reaction between methanol and hydrogen sulphide of Na or Mo doping on zirconia and alumina, Applied Catalysis A: General, 171 (1998) 109-115.

[22] J. Sauer, W. Boeck, L.v. Hippel, W. Burkhardt, S. Rautenberg, D. Arntz, W. Hofen, Metal oxides as catalysts for the reaction between methanol and hydrogen sulfide, in: E.D. GmbH (Ed.), 1998.

[23] R. Bermejo-Deval, R.M.H. Walter, O.Y. Gutierrez, J.A. Lercher, On the role of the alkali cations on methanol thiolation, Catalysis Science & Technology, 7 (2017) 4437-4443.

[24] A.V. Mashkina, V.N. Yakovleva, L.N. Khairulina, Synthesis of dimethyl sulfide in the presence of zeolites, Reaction Kinetics and Catalysis Letters, 43 (1991) 405-411.

[25] A.V. Mashkina, V.N. Yakovleva, Kinetics and Catalysis, 32 (1991).

[26] C. Kaufmann, O.Y. Gutiérrez, Y. Zhu, J.A. Lercher, Effect of H2 in the synthesis of COS using liquid sulfur and CO or CO2 as reactants, Research on Chemical Intermediates, 36 (2010) 211-225.

[27] O.Y. Gutiérrez, C. Kaufmann, A. Hrabar, Y. Zhu, J.A. Lercher, Synthesis of methyl mercaptan from carbonyl sulfide over sulfide K2MoO4/SiO2, Journal of Catalysis, 280 (2011) 264-273.

[28] Y.Q. Yang, Y.Z. Yuan, S.J. Dai, B. Wang, H.B. Zhang, The catalytic properties of supported K2MoS4/SiO2 catalyst for methanethiol synthesis from high H2S-content syngas, Catal Lett, 54 (1998) 65.

[29] O.Y. Gutiérrez, C. Kaufmann, J.A. Lercher, Synthesis of Methanethiol from Carbonyl Sulfide and Carbon Disulfide on (Co)K-Promoted Sulfide Mo/SiO2 Catalysts, ACS Catalysis, 1 (2011) 1595-1603.

[30] O.Y. Gutiérrez, L. Zhong, Y. Zhu, J.A. Lercher, Synthesis of Methanethiol from CS2 on Ni-, Co-, and K-Doped MoS2/SiO2 Catalysts, ChemCatChem, 5 (2013) 3249-3259.

[31] S.J. Dai, Y.Q. Yang, Y.Z. Yuan, D.L. Tang, R.C. Lin, H.B. Zhang, On methanethiol synthesis from H2S-containing syngas over K2MoS4/SiO2 catalysts promoted with transition metal oxides, Catal Lett, 61 (1999) 157-160.

[32] Y. Hao, Y. Zhang, A. Chen, W. Fang, Y. Yang, Study on Methanethiol Synthesis from H2S-Rich Syngas Over K2MoO4 Catalyst Supported on Electrolessly Ni-Plated SiO2, Catal Lett, 129 (2009) 486-492.

[33] G. Mul, I.E. Wachs, A.S. Hirschon, Catalytic synthesis of methanethiol from hydrogen sulfide and carbon monoxide over vanadium-based catalysts, Catalysis Today, 78 (2003) 327-337.

[34] A. Chen, Q. Wang, Q. Li, Y. Hao, W. Fang, Y. Yang, Direct synthesis of methanethiol from H2S-rich syngas over sulfided Mo-based catalysts, Journal of Molecular Catalysis A: Chemical, 283 (2008) 69-76.

[35] W. Wang, Y. Li, X. Zhang, W. Fang, Y. Yang, Catalytic synthesis of methanethiol from methanol and carbon disulfide over KW/Al2O3 catalysts, Catalysis Communications, 69 (2015) 104-108.

[36] W. Wang, J. Li, Q. He, S. Peng, Y. Yang, M. Li, Synthesis of Methanethiol from Methanol and Carbon Disulfide over CoKW/Al2O3 Catalysts: The Possible Reaction Network and Reaction Mechanism, ChemistrySelect, 3 (2018) 9663-9671.

2. The role of weak Lewis acid sites for methanol thiolation

Reproduced from

M. Weber-Stockbauer, O.Y. Gutiérrez Tinoco, R. Bermejo-Deval, J.A. Lercher, The role of weak Lewis acid sites for methanol thiolation, Catalysis Science & Technology, (2019).[a]

With permission from the Royal Society of Chemistry.

[a] M.W.-S. planned, designed and conducted the experiments (Except Raman spectroscopy, H_2S and CO_2 adsorption and kinetic data of Cs_2WS_4/Al_2O_3, which were done by R.B.-D.), analyzed and interpreted the data and wrote the manuscript. R.B.-D., O.Y.G. and J.A.L. contributed to the discussion of the results and the correction of the manuscript anytime.

2.1. Abstract

Weak Lewis acid combined with strong base sites of Cs^+ supported on WS_2 and γ-Al_2O_3 act as active sites in the thiolation of methanol. The acid-base pairs dissociate methanol upon adsorption. The formed surface alcoholate and the corresponding sulfuryl groups enable the substitution of oxygen for sulfur in a Langmuir-Hinshelwood mechanism. Stronger Lewis acid sites catalyze dimethyl ether formation *via* an Eley-Rideal mechanism in which methoxy groups react with gas phase methanol. The results demonstrate the importance of adjusting the acid-base strength in oxides to selectively catalyze substitution reactions.

2.2. Introduction

The synthesis of methanethiol is a key intermediate step in the industrial production of the amino acid methionine,[1–4] petrochemicals, pesticides and pharmaceuticals.[5,6] An effective route is the direct use of syngas and H_2S, with the formation of chemical intermediate CS_2 and other byproducts.[6–10] Another route is the thiolation of methanol, which involves the simultaneous addition of the SH nucleophile and the elimination of the hydroxyl species in a concerted step (SN_2 nucleophilic substitution). However, the strongly basic hydroxide ion (HO^-) is challenging to replace with a weaker base, such as SH^-.

A broad variety of mixed metal oxides have been proposed as catalysts. [11–17] High basic strength induced by alkali cations, such as Cs^+, is required to achieve high selectivity. [18,19] As the nature of the support for Cs^+ appears not to alter its catalytic activity in methanol thiolation and even sulfide materials have not induced marked changes, it is hypothesized that the catalyzed steps take place on cesium chalcogenides domains supported on oxides or sulfides. [20] Thus, we decided to explore the mechanism and kinetics of methanol thiolation on supported Cs^+ on WS_2 and γ-Al_2O_3. Detailed physicochemical characterization of the surface properties by probe molecules is combined with detailed kinetic measurements in order to derive a mechanism and the associated kinetic parameters. This insight should guide next generations of catalysts for the synthesis of thiols via nucleophilic substitution reactions.

2.3. Experimental

2.3.1. Catalyst preparation

Catalysts were prepared by incipient wetness impregnation of γ-Al_2O_3 (grain size of 0.15-0.25 mm) with aqueous solutions, added dropwise to the agitated solid. For the synthesis of CsW/Al_2O_3, the wt.% composition was within the optimum activity and selectivity to methanethiol.[5] CsW/Al_2O_3 was synthesized using 5.0 g of γ-Al_2O_3 with target tungsten loading of 20.5 wt. %, using a solution of 1.94 g of ammonium metatungstate hydrate (Sigma Aldrich, 99.99%) in 4 mL of H_2O. The sample was dried at room temperature overnight. After drying, the sample was calcined at 455 °C for 4h, with an increment of 5 °C/min. Subsequently, 2 g of this solid sample were impregnated with 640 mg of cesium acetate (Sigma Aldrich, ≥99.99%) dissolved in 1.6 mL of H_2O. The catalyst was then dried and calcined as before. Cs/Al_2O_3 was prepared following the same procedure without the use of ammonium metatungstate. All samples were activated by treatment in H_2S with flow rate of 20 mL/min at 360 °C for 2 hours.

Cs_2WS_4/Al_2O_3 was synthesized as followed: Cs_2WS_4 crystals were formed by precipitation, mixing a solution of 350 mg of $(NH_4)_2WS_4$ in 20 mL of H_2O and 325 mg of Cs_2CO_3 (Sigma Aldrich, 99%) in 20 mL of H_2O. A yellow precipitate was formed. These solids were filtered, washed with ice cold water and 1-propanol. Due to the low solubility of Cs_2WS_4, 450 mg of these were dissolved in 150 mL of water. Then 2 g of Cs/Al_2O_3 were added to the solution. The water was eliminated by evaporation in continuous rotation, precipitating the Cs_2WS_4 crystals on the solid sample. The sample was dried at room temperature overnight, calcined and activated in H_2S.

2.3.2. Chemical and physicochemical characterization

The BET surface area and the pore size distribution of the catalysts were determined by N_2 adsorption–desorption at -196 °C using a PMI Automated BET Sorptomatic 1900 Series instrument. Prior to the adsorption, the samples were evacuated at 250 °C for 2 h. Elemental analysis was carried out in the Microanalytical Laboratory at the TU München. The crystalline structure of the catalysts was determined by powder X-ray diffraction. XRD patterns were collected with a Philips X'Pert System (Cu Kα radiation, 0.1542 nm) operating at 45 kV/40 mA, using a nickel Kβ-filter and solid-state detector (X'Celerator). The measurements were carried out with a step size of 0.017° and scan time of 0.31 s per step. Raman spectra of active catalysts were recorded with a Renishaw Raman Spectrometer (Type 1000), equipped with a CCD detector, a Leica microscope and a 514 nm Ar laser at ambient conditions shortly after sulfidation conditions. The calibration was done using a Si (111) crystal prior to the measurements. The wavenumber accuracy was within 1 cm^{-1}. Adsorption followed by temperature programmed desorption of H_2S was performed with a pulse technique using a

flow apparatus equipped with a mass spectrometer (QME 200, Pfeiffer Vacuum). A sample of 100 mg of catalyst was loaded in a quartz reactor and activated in situ under 4.2 vol. % H_2S/He with a flow of 6 mL/min at 360 °C for 2 h. For H_2S adsorption, the temperature was set to 360 °C and the sample was flushed with He for 1 h prior to adsorption. Pulses of 4.4 vol. % of H_2S in He (V_{Total} = 3.1 mL, duration ~1 s) were introduced every 30 min (5.0 µmol/min of H_2S) during continuous He flow (6 mL/min). The total concentration of gas adsorbed was calculated as the sum of the uptakes per pulse. 24 pulses were performed per experiment.

Adsorption of pyridine and CH_3OH was monitored by IR spectroscopy in transmission absorption mode (samples pressed into self-supporting wafers). All studied materials were treated in situ with H_2S prior to the measurements, using a gas flow system. Once the wafer was in place, the cell was purged with He (10 mL/min) and the temperature was increased from 50 °C to 360 °C (increment of 10 °C/min). After reaching 360 °C, sulfidation took place, using 10 vol. % H_2S in N_2 (10 mL/min) for 1.5h. After sulfidation, the cell was flushed with He for 0.1 h, followed by evacuation to 10^{-5} mbar. Methanol was adsorbed at 50 °C, stepwise increasing the methanol partial pressure (0.1 mbar, 0.5 mbar and 1 mbar) followed by an increase in temperature to 300°C. For pyridine adsorption the cell was cooled down to 50 °C and the sample was exposed to 1 mbar of pyridine, followed by decreasing the pyridine partial pressure. Further evacuation to 10^{-5} mbar resulted in no pyridine adsorbed on Cs/Al_2O_3 and CsW/Al_2O_3. Thus, spectra from different catalysts were compared at 0.1 mbar. Spectra were recorded on a Nicolet 6700 FTIR spectrometer (64 scans were collected to obtain each spectrum) and presented after background subtraction and normalization to mass of the wafer. The concentrations of coordinating pyridine were calculated using the molar extinction coefficient 0.96 cm·µmol^{-1} determined for the characteristic band at 1450 cm^{-1}.[21]

2.3.3. Catalytic testing and kinetic experiments

Kinetic experiments at varying temperature were performed using 0.125 g catalyst (granule diameter 0.15-0.25 mm) diluted with 1 g of SiC (granules diameter 0.075-0.100 mm) at 9 bar, in the temperature range of 300-360 °C. Standard calculations of the Weisz–Prater modulus showed that it was < 1 for all catalysts under all conditions, and, therefore, it can be concluded that the kinetics results were unaffected by internal mass transfer effects.[22] For on-line analysis a Shimadzu GC 2014 equipped with a HSQ 80 column and a TCD detector was used. GC samples were taken after 4h of the reaction running at the defined temperature, when steady state was reached. The reactant flows were: CH_3OH 10 mL/min in gas phase, H_2S 20 mL/min, N_2 20 mL/min. Before testing, the catalysts were activated by flushing with 20 mL/min of pure H_2S at 360 °C and 9 bar for 2 h.

Experiments at varying residence time were performed at 360 °C with catalyst loading of 0.05-0.2 g, total pressure of 9 bar, using the same concentration of reactants as described before.

Reaction orders were determined at 360 °C. For reaction order in H_2S, the partial pressure of methanol was kept constant at 2.2 bar, while the H_2S partial pressure was varied between 1.1 and 5.6 bar. To measure methanol reaction orders, the H_2S partial pressure was set to 4.5 bar and the methanol partial pressure varied from 0.6 to 2.2 bar gaseous methanol. The N_2 gas flow was adjusted to compensate volume flow changes and keep the total volume flow constant at 80 mL/min. The amount of catalyst used in each experiment was adjusted accordingly, to ensure methanol conversion lower 10 %. Reaction orders for cesium-modified materials were measured with 0.01 g of catalyst, while 0.001 g was sufficient for γ-Al_2O_3. To avoid channeling effects, γ-Al_2O_3 was physically mixed with SiO_2, being known to be inactive in the studied reaction, in a ratio of 1:9.

2.4. Results and Discussion

2.4.1. Physicochemical properties

The corresponding X-ray diffractograms of the catalysts investigated are compiled in the supporting information (Figure S1). All of the materials exhibited reflections of the γ-Al_2O_3 support (PDF no. 96-101-0462). The X-ray diffractogram of Cs_2WS_4/Al_2O_3 showed a pattern consistent with the Cs_2WS_4 phase (PDF no. 96-221-4428), while CsW/Al_2O_3 exhibited both the Cs_2WS_4 and the WS_2 (PDF no. 96-591-0004) phases. The presence of sharp reflections in the Cs_2WS_4/Al_2O_3 diffractogram indicates the presence of large crystalline Cs_2WS_4 domains. A sharp peak was observed in the diffractogram of Cs_2WS_4/Al_2O_3 at 27.9° 2Θ corresponding to the 004 basal plane, indicative of crystal growth on that plane. The average particle diameter of the Cs_2WS_4 crystals was approximately 100 nm (calculated from XRD data by the Scherrer equation). Due to the large particle size of Cs_2WS_4, these crystals were concluded to be precipitated on the surface of Cs/Al_2O_3. Such large crystals would not cover the alumina surface. In contrast, the lower intensity of Cs_2WS_4 and WS_2 for CsW/Al_2O_3, suggests the presence of much smaller crystals. Cs_2CO_3 bands were observed on all catalyst prior to sulfidation (not shown), however, H_2S treatment removed these phases.

In the Raman spectrum of Cs_2WS_4/Al_2O_3 (Figure 1) the bands at 482 and 459 cm^{-1} have been attributed to v_{as}(WS) and v_s(WS).[23–25] This confirms the presence of the Cs_2WS_4 phase in addition to Cs^+ supported on Al_2O_3 support, as observed on the X-ray diffractogram. In the case of CsW/Al_2O_3, two additional bands appear at 418 and 352 cm^{-1}, which are characteristic of WS_2 vibration modes.[26,27] The first band corresponds to the first-order A_{1g} (T) optical mode, while the latter corresponds to an overlap between the first-order E^1_{2g} (T) optical mode and the second order longitudinal phonons (2LA (M)). Both the X-ray diffractograms and Raman spectra of Cs_2WS_4/Al_2O_3 showed a much higher intensity of WS_2 than of Cs_2WS_4. This suggests that during sulfidation Cs^+ is segregating forming an apparent separate phase after sulfidation. [7,28]

Table 2.1 Physical and adsorption properties of Cs_2WS_4/Al_2O_3, CsW/Al_2O_3, $Cs/\gamma\text{-}Al_2O_3$ and γ-Al_2O_3. From left to right: W and Cs content, pore volume, BET surface area and H_2S adsorbed.

Catalyst	W (wt. %)	Cs (wt. %)	Pore Vol. ($cm^3 \cdot g^{-1}$)	BET Sa ($m^2 \cdot g^{-1}$)	Ads. H_2S ($\mu mol \cdot g^{-1}$)	Ads. H_2S ($\mu mol \cdot m^{-2}$)
Cs_2WS_4/Al_2O_3	5.1	20.6	0.20	141	18	0.13
CsW/Al_2O_3	16.4	15.2	0.11	68	11	0.16
Cs/Al_2O_3	--	15.6	0.24	117	22	0.20
γ-Al_2O_3	--	--	0.34	222	--	--

Surprisingly, this segregation into two phases reversed after reactions (Figure 2S4). The concentration of Cs_2WS_4 was significantly higher than that of the WS_2 phase as judged from Raman spectra. It is unclear at present whether how this change is atomistically related to the methanol thiolation. In addition to the Cs^+ cation balancing the negative charge of WS_4^{-2}, other Cs oxide or sulfide species could be formed interacting with the WS_2 phase. [20]

In the absence of W, other bands appear for Cs/Al_2O_3 (Figure 2.1) in the region between 1100-200 cm^{-1} which are assigned to different sulfur oxyanions such as sulfite (SO_3^{2-}), thiosulfate ($S_2O_3^{2-}$), dithionate ($S_2O_6^{2-}$), pyrosulfite ($S_2O_5^{2-}$) and dithionite ($S_2O_4^{2-}$).[29–32] As it has been shown for different alkali cations supported on γ–Al_2O_3,[18] these sulfur oxyanions can be formed in the presence of water as an oxidizing agent following the elementary reactions proposed in Figure S2.2. These sulfur oxyanions were formed on the γ–Al_2O_3 support only in the presence of H_2S. [32] Additional bands in between 500-800 cm^{-1} of the CsW/Al_2O_3 catalyst correspond to additional S-O bonds of the sulfur oxyanions in the presence of WS_2 and Cs_2WS_4 phases. [33] These bands were much weaker in intensity than the W-S bands previously discussed. IR spectroscopy confirmed the presence of the sulfur oxyanions in all three catalysts (Cs_2WS_4/Al_2O_3, CsW/Al_2O_3 and Cs/Al_2O_3, Figure 2S3). The surface sulfates on γ–Al_2O_3 and WS_2 (in CsW/Al_2O_3) are balancing the Cs^+, W^{4+} or Al^{3+} cations, providing oxygen

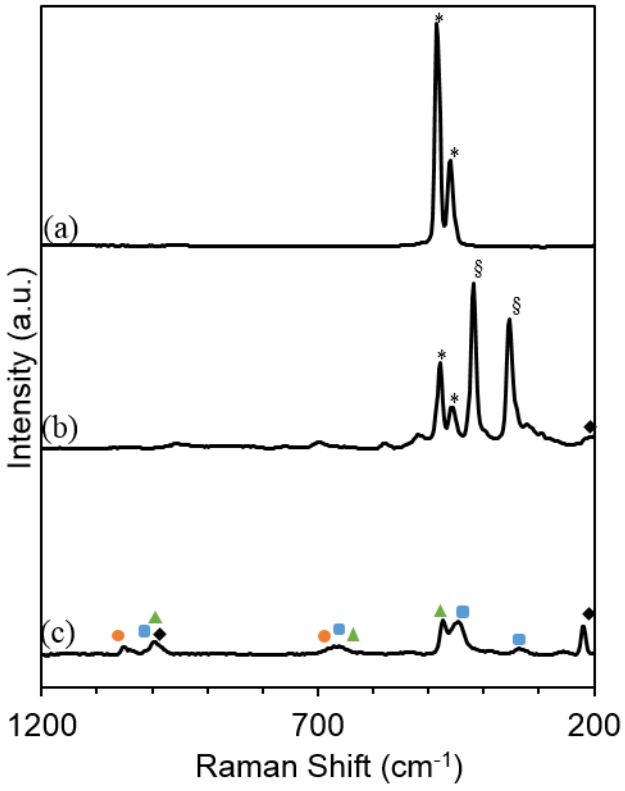

Figure 2.3 Raman spectra of a) $CsWS_4/γ\text{-}Al_2O_3$, b) $CsW/γ\text{-}Al_2O_3$ and c) $Cs/γ\text{-}Al_2O_3$. The symbols (*) and (§) are assigned to the WS_4^{-2} and WS_2 phases. The following symbols are for the anions: sulfite (green triangle), thiosulfate (blue square), dithionate (black diamond) and pyrosulfite (orange dot).

atoms to form a Lewis acid-base pairs with different charge distributions. Small Cesium clusters were not observed with the current physicochemical characterization methods.

Using IR spectroscopy, previous studies have shown that H_2S adsorbs dissociatively on both Cs/Al_2O_3 and CsW/Al_2O_3. [20] In addition, Cs atoms on γ-Al_2O_3, WS_2 or Ru increased the surface basicity, enhancing the adsorption of the H_2S molecule.[18,20,34–36] The Cs/Al_2O_3 catalyst resulted in the highest uptake of H_2S per unit area (0.20 μmol/m^2, Table 2.1). The addition of the Cs_2WS_4 crystals to Cs/Al_2O_3 (Cs_2WS_4/Al_2O_3) does not seem to enhance the H_2S adsorption capacity (0.13 μmol/m^2), however these crystals decrease the concentration of H_2S on the surface. The uptake of H_2S on CsW/Al_2O_3 (0.16 μmol/m^2) was lower than on the Cs/Al_2O_3 catalyst. The involvement of some of the Cs^+ in the formation of the Cs_2WS_4 is hypothesized to decrease the availability of Cs^+ to adsorb H_2S in the CsW/Al_2O_3 catalyst. We also hypothesize that in Cs_2WS_4 Cs^+ interact only weakly with H_2S, due to the low reactivity of the Cs_2WS_4 phase in methanol thiolation (see below).

Acid-base sites

IR spectra of adsorbed pyridine were used to evaluate qualitatively and quantitatively the acidity of the different materials (Figure 2.2). For qualitative evaluation, the assignment by Morterra *et al.* [37] was used. The bands between 1580 and 1620 cm^{-1} are assigned to the 8a ring vibration mode of coordinatively bound pyridine to LAS in γ-Al_2O_3, *i.e.* strong LAS associated to a vacancy in a tetrahedral coordination (>1600 cm^{-1}); weak LAS associated to a vacancy in an octahedral coordination (<1600 cm^{-1}) and H-bond pyridine, adsorbed on weakly acidic surface hydroxyl groups. The band at 1573 cm^{-1} is attributed to the 8b vibrational mode. After the addition of Cs^+ on the γ–Al_2O_3 support, a new band at lower wavenumber (1581 cm^{-1}) was observed. It is attributed to pyridine adsorbed on weak LAS, induced by the interaction of the Cs^+ cation with the Al_2O_3 support. This is also observed on CsW/Al_2O_3, showing the dominance of the weak LAS of the Cs cation with the support.

The bands at 1450 cm^{-1} were used for quantitative and qualitative analysis of the concentration of LAS on the catalysts. [20] The bands at 1448 and 1444 cm^{-1} correspond to strong LAS of γ–Al_2O_3, while the presence of Cs^+ results in a band of lower wavenumber (1440 cm^{-1}). The Lewis acid site concentration decreased from 680 μmol g^{-1} for γ-Al_2O_3 to 490 μmol g^{-1} for Cs/Al_2O_3. In the case of the CsW/Al_2O_3, a lower concentration of acid sites (38 μmol g^{-1}) was observed. [20]

The high LAS heterogeneity observed in γ-Al_2O_3 was also observed previously on the surface of WS_2/Al_2O_3. [20] This heterogeneity in Lewis acid strength will be reflected in the methanol thiolation selectivity, since these sites have different chemical affinity to adsorb the reactants CH_3OH and H_2S (Chart 2.1). The presence of Cs^+ increases the basicity, due to its lower

Sanderson electronegativity. [38,39] In addition, the presence of large Cs^+ cations blocks the access to stronger Lewis acid sites of γ-Al_2O_3 and/or WS_2.

Due to the changes in the acid-base properties of γ-Al_2O_3 and WS_2 upon Cs addition, we would like to discern the chemical interaction of methanol with these Lewis acid-base pairs prior to the mechanistic studies of methanol conversion.

Adsorption of CH_3OH

The IR bands of methanol adsorbed on CsW/Al_2O_3, Cs/Al_2O_3 and γ-Al_2O_3 between 2950 and 2800 cm^{-1} are assigned to the asymmetric and symmetric CH_3 stretching vibrations (ν_{as} and ν_s, respectively), split up by Fermi resonance with overtones of the methyl bending vibrations. [40] The spectra suggests that methanol adsorbs on both strong Lewis acid and strong basic sites in CsW/Al_2O_3, Cs/Al_2O_3 and γ-Al_2O_3 (Figures 2S5-2S7).[3] The molecular adsorption of methanol is concluded to take place on strong Lewis acid sites at 50°C. Upon heating, dissociation is favored, leading to the formation of bridging methoxides in the strong Lewis acid sites (Species I, 2940 cm^{-1} and 2840 cm^{-1}), mainly observed in γ-Al_2O_3 (Figure 2S7).

At 50 °C the acid-base pairs with a weaker Lewis acid cation and stronger base anion result in the dissociation of the methanol O-H group and the alcoholate formation (Species II, 2800-2820 cm^{-1} and 2930-2945 cm^{-1}).[43,44]

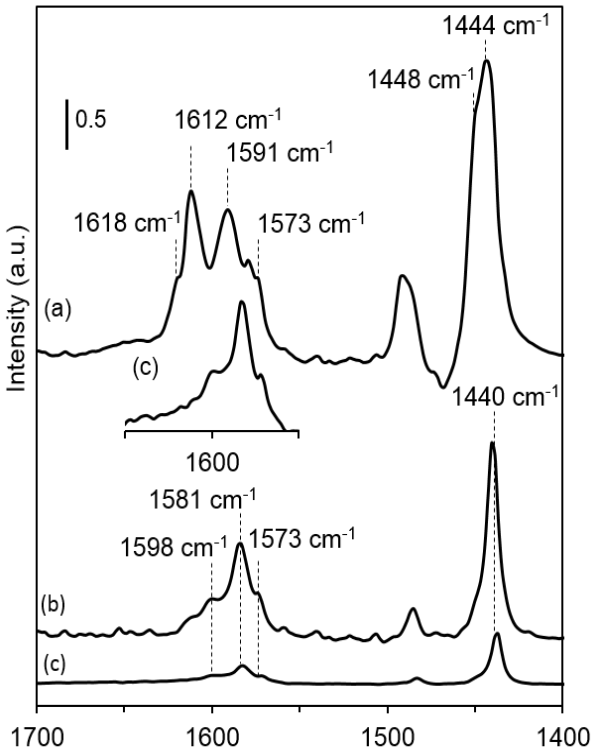

Figure 2.4 Spectra of Pyridine adsorbed on a) γ -Al_2O_3 b) Cs/Al_2O_3 and c) CsW/Al_2O_3 (50 ºC and evacuated). An inset on the top shows an expansion of the spectrum of CsW/Al_2O_3.

Upon heating, the intensity of the bands characteristic for methoxy decreased without other major changes in the IR spectra. Upon adsorption at 50 °C at 10^{-1} mbar, the alcoholate formation on the stronger base anion dominated on all catalysts (Figure 2.4), in contrast to parent γ-Al_2O_3. The variation in wavenumbers between Species II on CsW/Al_2O_3 and Cs/Al_2O_3 is attributed to the differences between the electronegativity of W and Al. We attribute this to the fact that the base strength of the former catalysts is significantly higher than that of γ-Al_2O_3, allowing for a more facile methanolate formation.

Indeed, the formation of bridging methoxides on strong Lewis acids and alcoholate on strong bases had equal contributions on WS_2/Al_2O_3 upon evacuation,[20] similarly to γ-Al_2O_3. We hypothesize at this point that the relative concentrations of methoxide and alcoholate on the catalysts surface influence the selectivity to methanethiol and dimethyl ether.

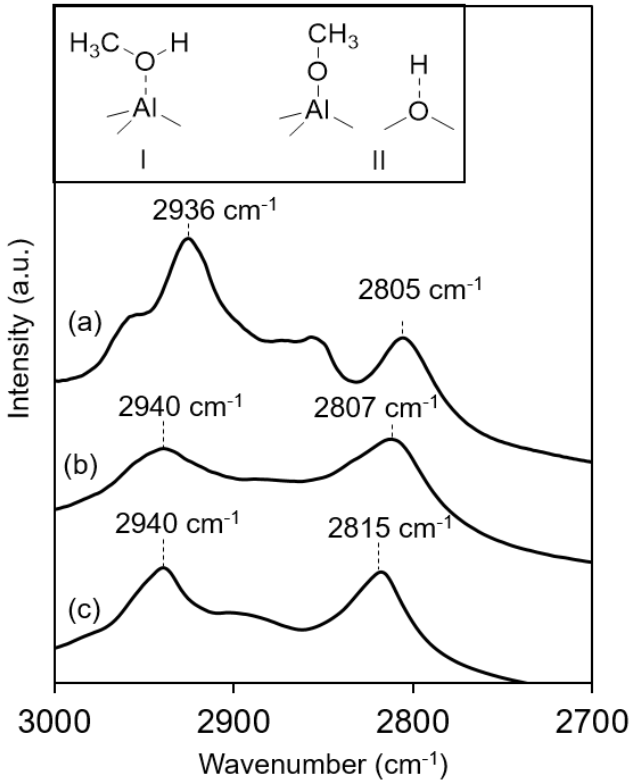

Figure 2.5 Spectra of methanol adsorbed on a) CsW/ Al_2O_3 b) Cs/ Al_2O_3 and c) γ-Al_2O_3 (50 ºC and 0.1 mbar methanol partial pressure). An inset on the top left shows the adsorption of methanol on Lewis acid-base pairs. [**36]**

2.4.2. Kinetics of methanethiol formation

The rates of methanol consumption and methanethiol formation between 300 and 360 °C for Cs_2WS_4/ Al_2O_3, CsW/ Al_2O_3, Cs/ Al_2O_3 and γ-Al_2O_3 are shown in Figures 4 and 5, respectively. The highest rate in methanol consumption was observed for γ-Al_2O_3 (2.3-5.0·10^{-5} $mol_{CH3OH}/s/g_{cat}$), i.e. 2-3 times higher than the other catalysts. The rate of formation of all products increased with temperature, except for dimethyl ether (DME) that passed through a maximum in between 320-340 °C (Figure 2S8). This rate was at least 2 orders of magnitude higher with γ-Al_2O_3 (1.8-2.4·10^{-5} $mol_{(CH3)2O}/s/g_{cat}$) than with CsW/Al_2O_3 (0.0-1.3·10^{-7} $mol_{(CH3)2O}/s/g_{cat}$). DME was not observed with Cs/Al_2O_3 and Cs_2WS_4/Al_2O_3 catalysts. γ-Al_2O_3, CsW/ Al_2O_3 and Cs/γ-Al_2O_3 followed similar trends for the rate of methanethiol (CH_3SH) formation with temperature. The rates of formation of dimethyl sulfide (DMS, Figure 2S9), dimethyl disulfide (DMDS, Figure 2S10) and methane (Figure 2S11) were orders of magnitude lower than that to methanethiol (Figure 2.5).

Figure 2.6 shows the product yield variations as a function of methanol conversion at 360°C on γ-Al_2O_3. linear increase of CH_3SH and DME at low conversion show that both are primary products with γ-Al_2O_3, as well as with WS_2/γ-Al_2O_3. [20] For γ-Al_2O_3, CH_3SH formation from DME was observed at conversions above 50% (Reaction 6, Scheme 2.1). DMS formation is suggested to form via H_2S elimination from CH_3SH (Reaction 3, Scheme 2.1).

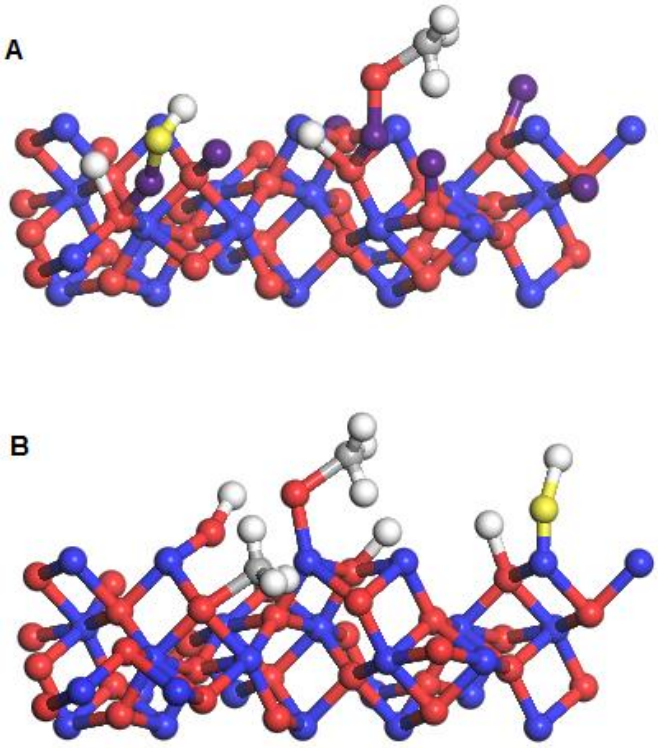

Chart 2.1 Schematic representation of the adsorption of substrates methanol and hydrogen sulphide on the different catalysts A) Cs/Al_2O_3 and B) γ-Al_2O_3, B) Cs/Al_2O_3. The H, C, O, S, Al and Cs atoms are presented in white, grey, red, yellow, blue and purple, respectively.

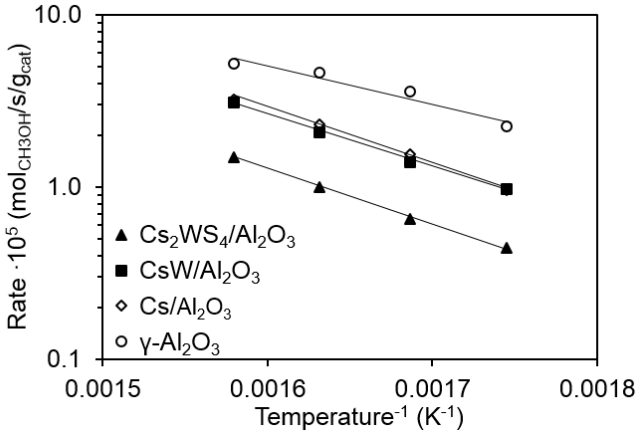

Figure 2.4 Methanol consumption rate for $Cs_2WS_4/\gamma\text{-}Al_2O_3$, $CsW/\gamma\text{-}Al_2O_3$, Cs/Al_2O_3 and $\gamma\text{-}Al_2O_3$, in between 300-360 °C.

Similarly, DMDS and methane (not shown in Figure 2.6 and 2.7) were secondary products (Reaction 4 and 5, Scheme 2.1). For Cs/Al_2O_3, methanethiol was the only primary product (Figure 2.7), since its yield increases linearly with methanol conversion. At high conversions the yields of DMS and DMDS were higher with Cs/Al_2O_3 than with $\gamma\text{-}Al_2O_3$. The higher selectivity to methanethiol with Cs/Al_2O_3 is hypothesized to lead to higher concentrations of DMS and DMDS. The presence of the W sulfide phases in CsW/Al_2O_3 (WS_2 and WS_4^{2-}) and Cs_2WS_4/Al_2O_3 (WS_4^{2-}) increased the hydrogenolysis of methanethiol[13,45,46] (Reaction 5, Scheme 2.1) or methanol to methane.[13] However, the rates were three orders of magnitude lower than those to methanethiol. The similarity in catalytic properties of all Cs^+ containing catalysts led us to conclude that the strong basic sites induced by Cs^+ were the key factor to achieve high catalytic activity. Surprisingly, the apparent activation energies of both CsW/Al_2O_3 and Cs/Al_2O_3 were lower (67 and 69 kJ/mol, respectively), than that observed with $\gamma\text{-}Al_2O_3$ (113 kJ/mol) (Table 2.2).

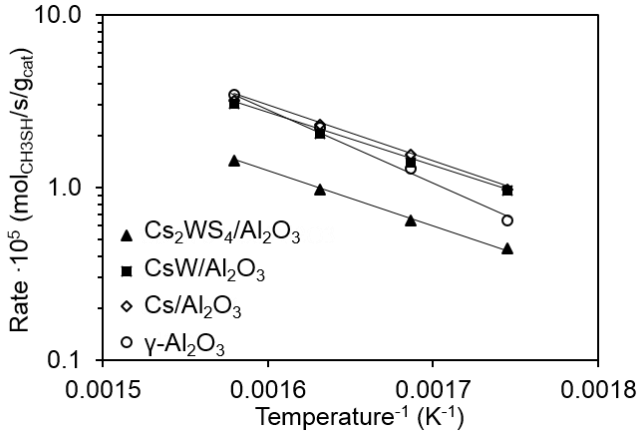

Figure 2.5 Methanethiol formation rate for Cs_2WS_4/ Al_2O_3, CsW/ Al_2O_3, $Cs/\gamma\text{-}Al_2O_3$ and $\gamma\text{-}Al_2O_3$, in between 300-360 °C.

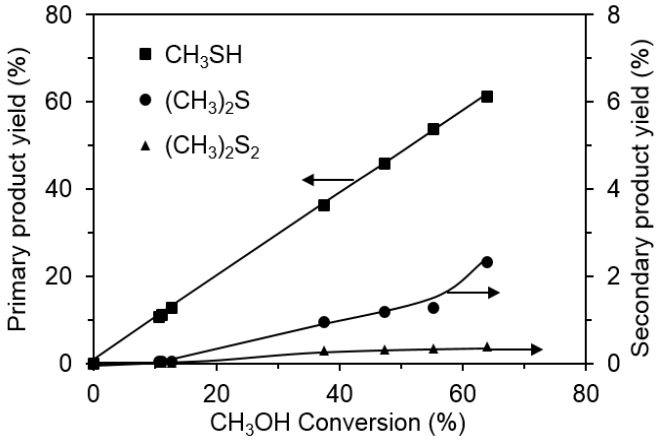

Figure 2.6 Product yields during reaction of methanol and H_2S over Cs/Al_2O_3 (360°C, 9 bar).

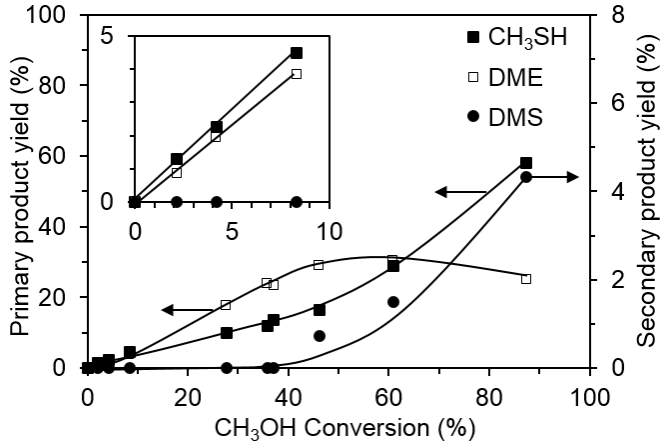

Figure 2.7 Product yields during reaction of methanol and H_2S over γ-Al_2O_3 (360°C, 9 bar).

The observed reaction order of 1.4 in CH_3OH (Figure 2S11) for the formation of dimethyl ether with γ-Al_2O_3 suggests a partial coverage of methanol in an Eley-Rideal type bimolecular reaction (SI Section 3). The reaction is taking place between a methoxy group bound to a strong Lewis acid site and weakly adsorbed methanol. [43,47] Upon formation (Step 4, Scheme 2.2), DME desorbs from the surface, leaving behind a proton that recombines with an OH group to form water (Step 8). The rate determining step (r.d.s) involves the nucleophilic attack of the weakly sorbed methanol with the CH_3^+ group. [48] Therefore, the rate expression for the formation of DME is (complete derivation in Section 3 of SI):

$$r_{CH_3OCH_3} = \frac{k_4 K_1 [CH_3OH]^{1.5}}{a} \qquad (1)$$

with $a = (1 + K_1^{0.5}[CH_3OH]^{0.5} + [H_2O]^{0.5}/K_8^{0.5})$.

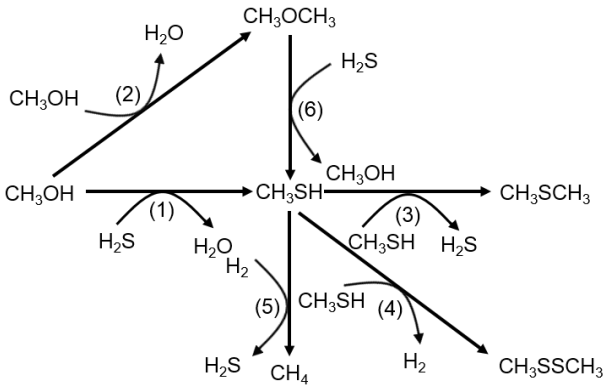

Scheme 2.1 Reaction network for the reaction of methanol with H_2S over Cs-free (the dominant reactions are (2) and (1)) and Cs-modified catalysts (the dominant reaction is (1)). The numbers in parenthesis correspond to the reaction numbers as described in the text. This figure is based on Scheme 1 of our previous work.[16]

The observed reaction order was of 0.4 for both CH_3OH and H_2S in the formation of methanethiol with γ-Al_2O_3. These values are close to those expected for a reaction involving dissociated methanol and dissociated hydrogen sulfide (0.5 for both reactants, SI Section 3) in a Langmuir-Hinshelwood type mechanism. In the formation of CH_3SH the r.d.s. involves the nucleophilic substitution of the oxygen atom in the methanolate with an SH (Step 5, Scheme 2.1). [20]

Table 2.2 Apparent activation energies and rates of methanethiol formation normalized per gram and surface area at 360ºC and 9 bar.

	Rate CH_3SH ($mol \cdot s^{-1} \cdot g^{-1}$)	Rate CH_3SH ($mol \cdot s^{-1} \cdot m^2$)	$E_{a,app}$ ($kJ \cdot mol^{-1}$)
CsW/Al_2O_3	$4.3 \cdot 10^{-5}$	$6.4 \cdot 10^{-7}$	67
Cs/Al_2O_3	$4.5 \cdot 10^{-5}$	$3.9 \cdot 10^{-7}$	69
γ-Al_2O_3	$3.1 \cdot 10^{-4}$	$1.4 \cdot 10^{-6}$	113

Therefore, the rate expression for the methanethiol formation is

$$r_{CH_3SH} = \frac{k_5 K_2 K_3 [CH_3OH]^{0.5} [H_2S]^{0.5}}{b^2} \qquad (2)$$

with $b = (1 + K_2^{0.5}[CH_3OH]^{0.5} + K_3^{0.5}[H_2S]^{0.5} + [CH_3SH]^{0.5}/K_6^{0.5} + [H_2O]^{0.5}/K_7^{0.5})$.

The observed reaction order was 0.7 and 0.6 for CH_3OH and H_2S for the formation of CH_3SH with Cs/Al_2O_3 (Figure 2S13), indicating a similar mechanism as the one proposed with γ-Al_2O_3. This was also observed previously with WS_2/Al_2O_3 and CsW/Al_2O_3, [20] with reaction orders of 0.5 in both CH_3OH and H_2S (Figure 2.10). Therefore, the methanolate and the SH species follow a bimolecular Langmuir-Hinshelwood reaction mechanism (Scheme 2.3). Upon addition of Cs^+ on the surface of γ-Al_2O_3 we are able to alter its Lewis acid-base properties, forming a stronger base (anion) next to the cation. [38,39]

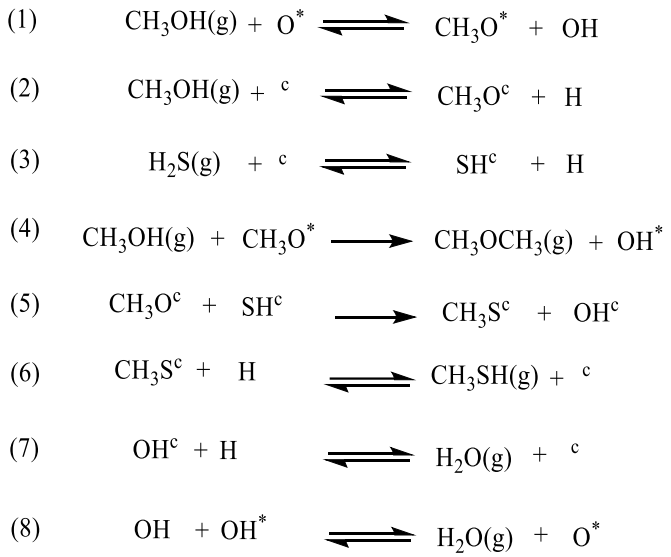

Scheme 2.2 Elementary reaction steps for the formation of dimethyl ether (DME) and CH_3SH, with (*) being the anion next to a strong Lewis acid and (c) the cation next to a strong basic site. Both of these are Lewis acid-base pairs.

To test the hypothesis that only the Cs^+ induced basic sites are causing the catalytic activity, Cs/SiO_2 was also explored. Pure silica did not show activity in methanol thiolation. The presence of Cs^+ cations on silica, however, induced activity for methanol thiolation (Figure 2S14). We conclude, therefore, that basic sites associated with alkali cations, and in particular here with Cs^+ suffice to generate strong basic sites, independent of the specific nature of the support. Therefore, we are currently working on dispersing Cs^+ on supports without strong LAS and a strong interaction with the Cs^+ cation.

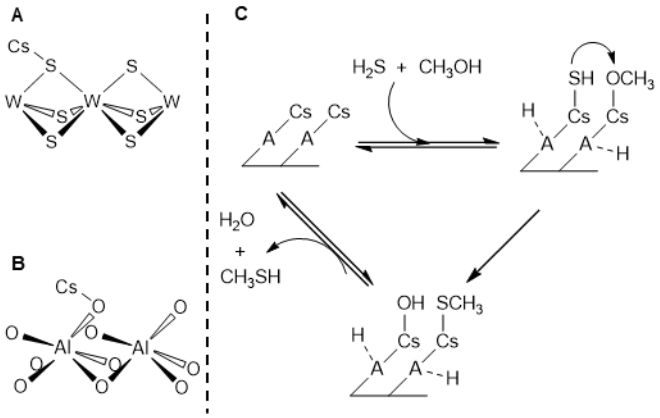

Scheme 2.3 A) WS_2 phase with Cs^+ cations, B) γ-Al_2O_3 with Cs^+ cations, and C) Proposed mechanism for the thiolation of methanol on Lewis acid-base pairs formed, regardless of the anion (A) interacting with the Cs^+ cation.

2.5. Conclusion

Strong basic sites are concluded to be the active sites for methanol thiolation. Addition of Cs^+ enhances the base strength, independent of the support and the presence Al-O and/or W-S bonds. In the absence of Cs^+ cations γ-Al_2O_3 catalyzes also the formation of DME. The dehydration of methanol into DME with γ-Al_2O_3 follows an Eley-Rideal mechanism between a methoxy group and a weakly sorbed methanol on strong Lewis acid sites. Pyridine and methanol adsorption, as well as the reaction order close to 0.5 in methanol thiolation with γ-Al_2O_3 and Cs/Al_2O_3, clearly indicate the dissociative adsorption of methanol and hydrogen sulfide on strong basic sites are necessary for the SN_2 nucleophilic substitution to methanethiol. However, the similar apparent activation energy and pyridine bands in the IR with both Cs/Al_2O_3 and CsW/Al_2O_3 (69 and 67 kJ/mol, respectively), and the higher apparent activation energy for γ-Al_2O_3, 113 kJ/mol, show the intrinsic properties of the strong basic sites to determine the energetic barriers in the methanol thiolation. Thus, future design of catalysts for methanol thiolation should entail only the presence of strong basic sites and a strong interaction of the Cs^+ cation with the support.

2.6. Literature

[1] Y. Zhang, S. Chen, M. Wu, W. Fang and Y. Yang, *Catal. Commun.*, 2012, **22**, 48–51.

[2] D. Kumar and J. Gomes, *Biotechnol. Adv.*, 2005, **23**, 41–61.

[3] W. Leuchtenberger, K. Huthmacher and K. Drauz, *Appl. Microbiol. Biotechnol.*, 2005, **69**, 1–8.

[4] T. Willke, *Appl. Microbiol. Biotechnol.*, 2014, **98**, 9893–9914.

[5] US Patent, US 5 852 219, 1998.

[6] W. Taifan and J. Baltrusaitis, *Catal. Sci. Technol.*, 2017, **7**, 2919–2929.

[7] O. Y. Gutiérrez, C. Kaufmann, A. Hrabar, Y. Zhu and J. A. Lercher, *J. Catal.*, 2011, **280**, 264–273.

[8] O. Y. Gutiérrez, C. Kaufmann and J. A. Lercher, *ChemCatChem*, 2011, **3**, 1480–1490.

[9] C. Kaufmann, O. Y. Gutiérrez, Y. Zhu and J. A. Lercher, *Res. Chem. Intermed.*, 2010, **36**, 211–225.

[10] O. Y. Gutiérrez, C. Kaufmann and J. A. Lercher, *ACS Catal.*, 2011, **1**, 1595–1603.

[11] M. Ziolek, J. Kujawa, J. Czyzniewska, I. Nowak, A. Aboulayt, O. Saur and J. C. Lavalley, *Appl. Catal. A Gen.*, 1998, **171**, 109–115.

[12] M. Ziolek, J. Kujawa, O. Saur and J. C. Lavalley, *J. Phys. Chem.*, 1993, **97**, 9761–9766.

[13] T. J. Paskach, G. L. Schrader and R. E. Mccarley, *J. Catal.*, 2002, **211**, 285–295.

[14] A. V. Mashkina, *Russ. Chem. Rev.*, 1995, **64**, 1131–1147.

[15] US Patent, 7,691,776 B2, 2010.

[16] W. M. Wang, J. J. Li, Q. J. He, S. Peng, Y. Q. Yang and M. Li, *ChemistrySelect*, 2018, **3**, 9663–9671.

[17] A. Eftekhari, *J. Mater. Chem. A*, 2017, **5**, 18299–18325.

[18] R. Bermejo-Deval, R. M. Walter, J. A. Gutierrez and J. A. Lercher, *Catal. Sci. Technol.*, 2017, **7**, 4437–4443.

[19] D. Kiani, G. Belletti, P. Quaino, F. Tielens and J. Baltrusaitis, *J. Phys. Chem. C*, 2018, **122**, 24190–24201.

[20] A. V. Pashigreva, E. Kondratieva, R. Bermejo-Deval, O. Y. Gutiérrez and J. A. Lercher, *J. Catal.*, 2017, **345**, 308–318.

[21] S. M. Maier, A. Jentys and J. A. Lercher, *J. Phys. Chem. C*, 2011, **115**, 8005–8013.

[22] K. Bischoff and G. Froment, *Chemical Reactor analysis and design*, New York, 1990.

[23] B. R. Srinivasan, C. Näther and W. Bensch, *Acta Crystallogr. Sect. E*, 2007, **63**, 167.

[24] M. J. F. ; Leroy and G. Kaufmann, *Bull. Soc. Chim. Fr.*, 1966, 3090.

[25] I. R. Beattie, P. J. Jones, A. D. Willson and N. A. Young, *J. Chem. Soc. Dalt. Trans.*, 1988, 2047–2049.

[26] A. Berkdemir, H. R. Gutiérrez, A. R. Botello-Méndez, N. Perea-López, A. L. Elías, C.-I. Chia, B. Wang, V. H. Crespi, F. López-Urías, J.-C. Charlier, H. Terrones and M. Terrones, *Sci. Rep.*, 2013, **3**, 1–8.

[27] M. Thripuranthaka, R. V. Kashid, C. Sekhar Rout and D. J. Late, *Appl. Phys. Lett.*, 2014, **104**, 81911.

[28] R. R. Chianelli, M. H. Siadati, M. P. De la Rosa, G. Berhault, J. P. Wilcoxon, R. Bearden and B. L. Abrams, *Catal. Rev. - Sci. Eng.*, 2006, **48**, 1–41.

[29] H. Takahashi, N. Kaneko and K. Miwa, *Spectroquimica Acta*, 1982, **38**, 1147–1153.

[30] P. D. Clark, N. I. Dowling, M. Huang, O. Okemona, G. D. Butlin, R. Hou and W. S. Kijlstra, *Appl. Catal. A Gen.*, 2002, **235**, 61–69.

[31] D. Santamara-Pérez, A. Vegas, C. Muehle and M. Jansen, *J. Chem. Phys.*, 2011, **135**, 1–8.

[32] J. S. Church and D. J. Evans, *Spectrochim. Acta - Part A Mol. Biomol. Spectrosc.*, 2008, **69**, 256–262.

[33] A. J. Van der Vlies, G. Kishan, J. W. Niemantsverdriet, R. Prins and T. Weber, *J. Phys. Chem. B*, 2002, **106**, 3449–3457.

[34] E. Schachtl, E. Kondratieva, O. Y. Gutiérrez and J. A. Lercher, *J. Phys. Chem. Lett.*, 2015, **6**, 2929–2932.

[35] C. Petit, F. Mauge and J. Lavalley, *Stud. Surf. Sci. Catal.*, 1997, **106**, 157–166.

[36] A. Ishihara, J. Lee, F. Dumeignil, R. Higashi, A. Wang, E. W. Qian and T. Kabe, *J. Catal.*, 2003, **217**, 59–68.

[37] C. Morterra and G. Magnacca, *Catal. Today*, 1996, **27**, 497–532.

[38] R. T. Sanderson, *J. Am. Chem. Soc.*, 1983, **105**, 2259–2261.

[39] R. T. Sanderson, *J. Chem. Educ. Part 1. Gen. Nat.*, 1988, **65**, 112–118.

[40] J. Derouault, J. Le Calve and M. T. Forel, *Spectrochim. Acta Part A Mol. Spectrosc.*, 1972, **28**, 359–371.

[41] L. J. Burcham, L. E. Briand and I. E. Wachs, *Langmuir*, 2001, **17**, 6164–6174.

[42] G. Busca, P. F. Rossi, V. Lorenzelli, M. Benaissa, J. Travert and J. Lavalley, *J. Phys. Chem.*, 1985, **89**, 5433–5439.

[43] J. H. de Boer, R. B. Fahim, B. G. Linsen, W. J. Visseren and W. F. N. M. de Vleesschauwer, *J. Catal.*, 1967, **7**, 163–172.

[44] G. Busca, P. Forzatti, E. Tronconi and J. C. Lavalley, *Stud. Surf. Sci. Catal.*, 1985, **20**, 15–24.

[45] T. Todorova, R. Prins and T. Weber, *J. Catal.*, 2005, **236**, 190–204.

[46] R. L. Wilson and C. Kemball, *J. Catal.*, 1964, **3**, 426–437.

[47] S. Buchang and B. H. Davis, *J. Catal.*, 1995, **157**, 359–367.

[48] Z. Zuo, W. Huang, P. Han, Z. Gao and Z. Li, *Appl. Catal. A Gen.*, 2011, **408**, 130–136.

2.7. Supporting Information

S.1. Characterization

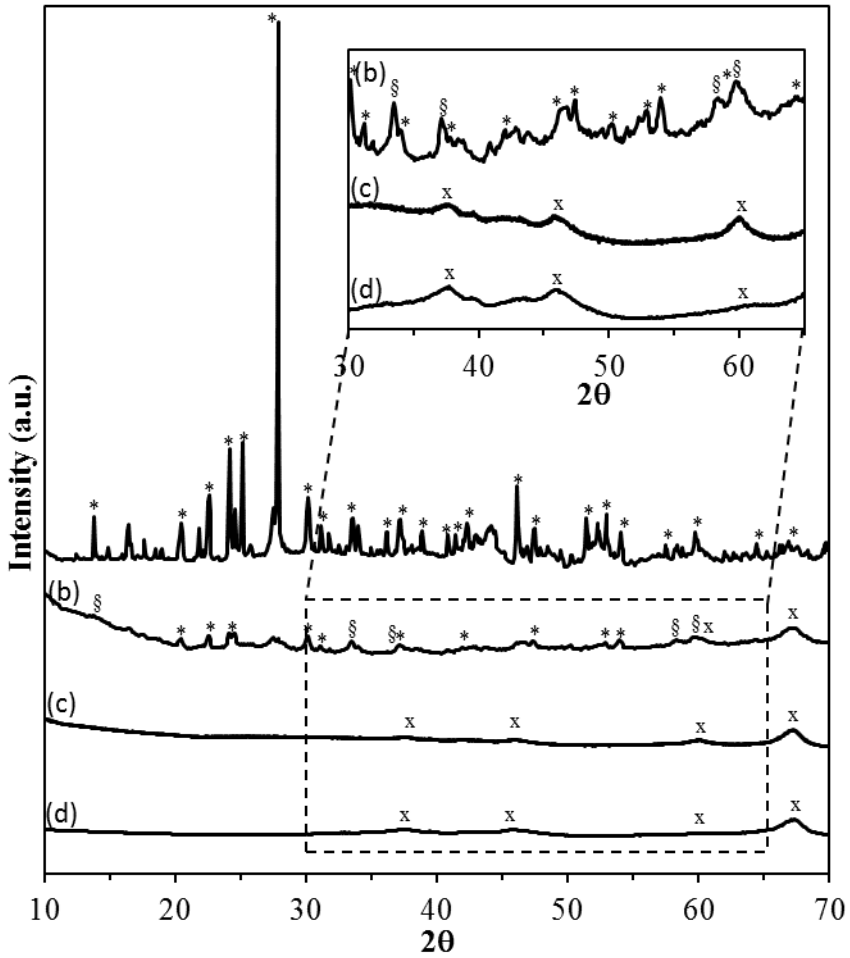

Figure S2.1 X-ray diffraction after sulfidation of a) Cs_2WS_4 /Al_2O_3, b) CsW/Al_2O_3, c) Cs/Al_2O_3 and d) γ-Al_2O_3. The symbols are represented as: * as Cs_2WS_4, § as WS2 and x as γ-Al_2O_3.

Table S2.1 Raman shifts and assignments from the different sulfur anions.

Anion	Raman Shift (cm^{-1})	Assignment
Sulfite (SO_3^{-2})	496	(E) Antisymmetric SO_3 deformation
Sulfite (SO_3^{-2})	647	(A_1) Symmetric SO_3 deformation
Sulfite (SO_3^{-2})	986	(E) Antisymmetric SO_3 stretching
Thiosulfate ($S_2O_3^{-2}$)	323	(E) Symmetric S-S-O deformation
Thiosulfate ($S_2O_3^{-2}$)	452	(A_1) Symmetric SO_3 deformation
Thiosulfate ($S_2O_3^{-2}$)	656	(A_1) Symmetric S-SO_3 stretching
Thiosulfate ($S_2O_3^{-2}$)	1016	(A_1) Symmetric SO_3 stretching
Dithionate ($S_2O_6^{-2}$)	204	(E_u) Symmetric SO_3 deformation
Dithionate ($S_2O_6^{-2}$)	1000	(A_{2u}) Symmetric stretching
Pyrolsulfite ($S_2O_5^{-2}$)	660	(A_1) Symmetric SO_3 deformation
Pyrolsulfite ($S_2O_5^{-2}$)	1050	(A_1) Symmetric SO_3 stretching
Dithionite ($S_2O_4^{-2}$)	508	---

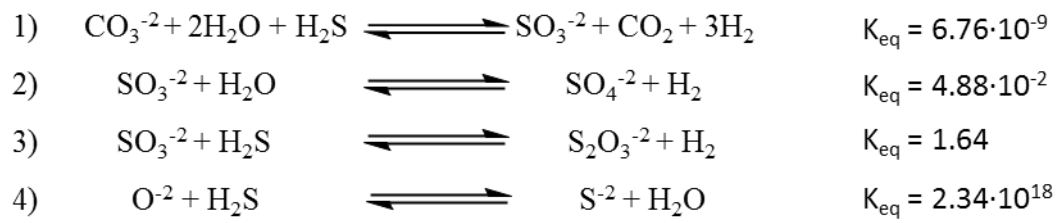

Figure S2.2. Plausible reactions yielding sulfur oxyanions and the corresponding equilibrium constants at 400 °C and 1 atm. The equilibrium constants were calculated with the HSC-chemistry software. The decomposition of CO_3^{-2} into SO_3^{-2} and CO_2 would be driven, under flow conditions, by the continuous removal of CO_2 and H_2 from the system pushing the equilibrium towards the product side.

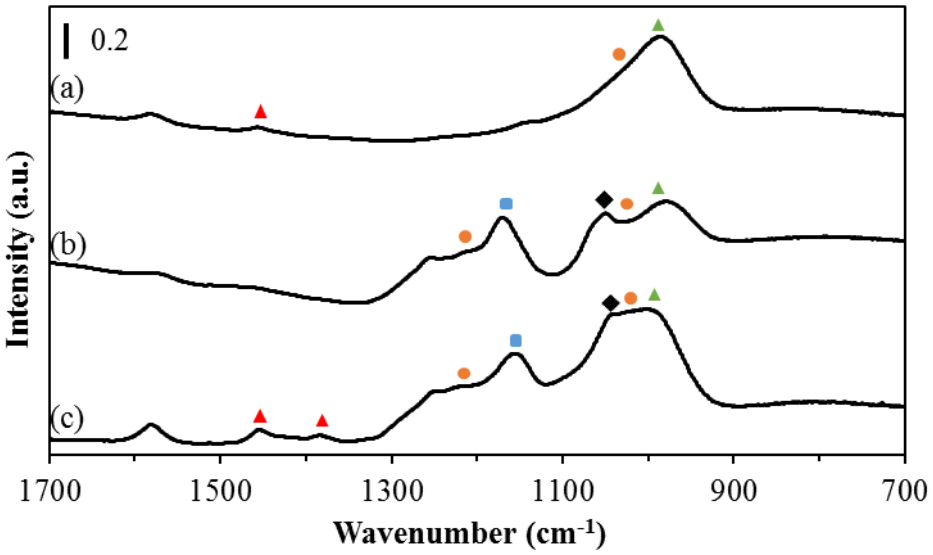

Figure S2.3. Infrared spectroscopy after sulfidation of a) $CsWS_4/Al_2O_3$, b) CsW/Al_2O_3 and c) Cs/Al_2O_3. The symbols are represented by anions: thiosulfate (blue square), dithionate (black diamond), pyrosulfite (orange dot), pyrosulfate (red triangle) and sulfite (green triangle).

Table S2.2 Infrared bands and assignments from the different sulfur anions.

Anion	IR band (cm^{-1})	Assignment
Sulfite (SO_3^{-2})	968	(A_1) Symmetric SO_3 stretching
Thiosulfate ($S_2O_3^{-2}$)	1146	(E) Antisymmetric SO_3 stretching
Dithionate ($S_2O_6^{-2}$)	1000	(A_{2u}) Symmetric stretching
Pyrolsulfite ($S_2O_5^{-2}$)	970	(A_2) Symmetric SO_2 stretching
Pyrolsulfite ($S_2O_5^{-2}$)	1196	(A_2) Symmetric SO_3 stretching
Pyrosulfate ($S_2O_7^{-2}$)	1380	--
Pyrosulfate ($S_2O_7^{-2}$)	1450	--

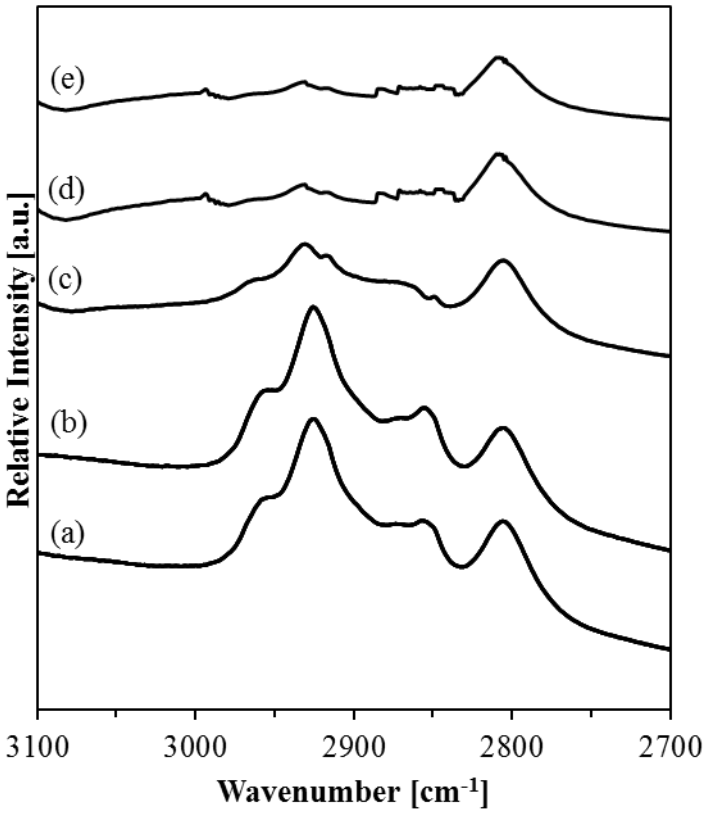

Figure S2.4 IR Spectra of methanol adsorbed on CsW/Al_2O_3 (previously sulfided) at a) 0.1 mbar and 50 °C, b) 1 mbar and 50 ºC, c) 1 mbar and 100 ºC, d) 1 mbar and 150 ºC, e) 10-5 mbar and 300 ºC.

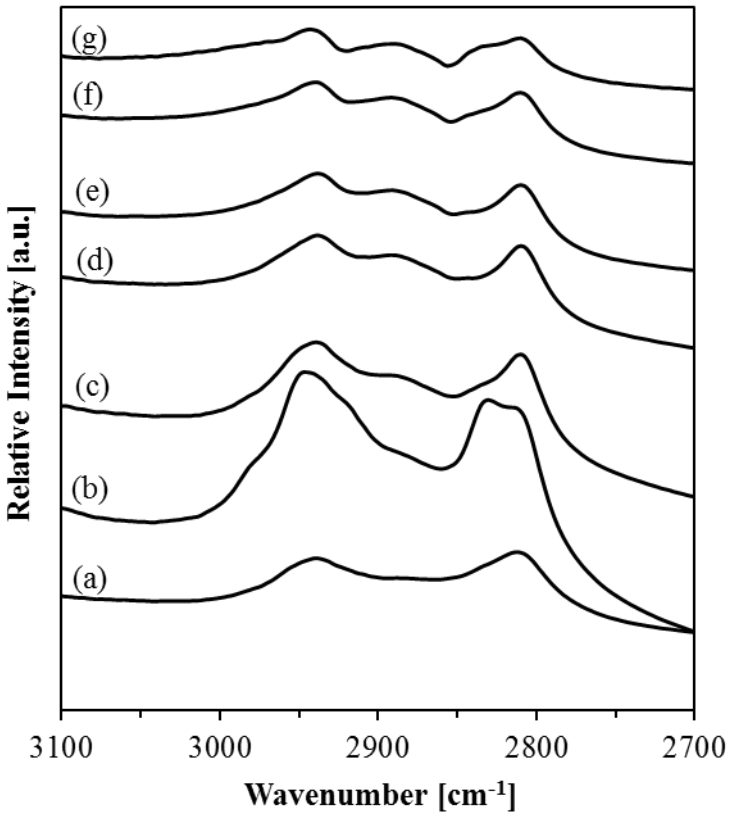

Figure S2.5 IR Spectra of methanol adsorbed on Cs/Al_2O_3 (previously sulfide) at a) 0.1 mbar and 50 °C, b) 1 mbar and 50 ºC, c) 1 mbar and 100 ºC, d) 1 mbar and 150 ºC, e) 1 mbar and 200 ºC, e) 1 mbar and 250 ºC and e) 1 mbar and 300 ºC.

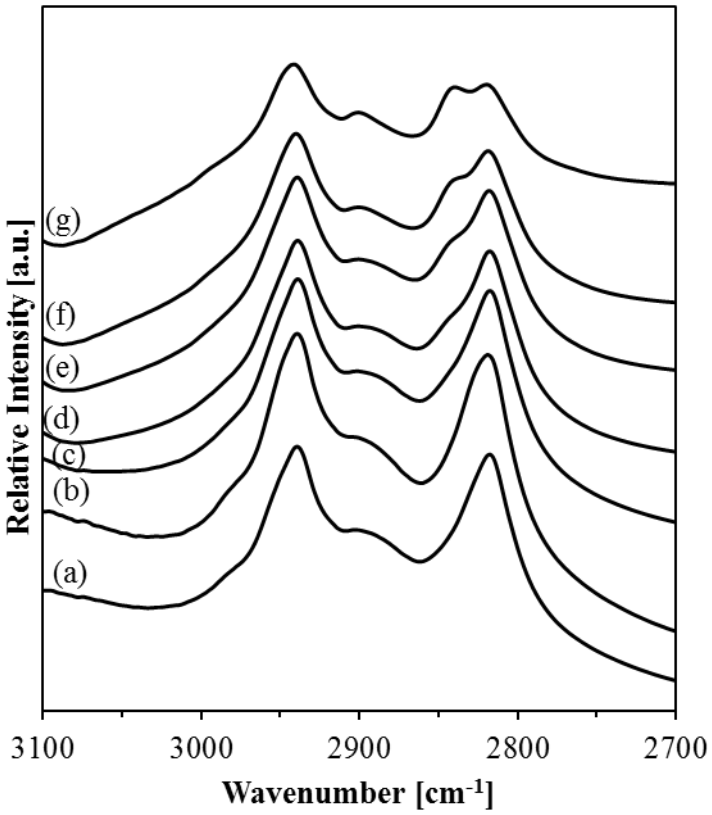

Figure S2.6 IR Spectra of methanol adsorbed on γ-Al_2O_3 (previously sulfided) at a) 0.1 mbar and 50 °C, b) 1 mbar and 50 ºC, c) 1 mbar and 100 ºC, d) 1 mbar and 150 ºC, e) 1 mbar and 200 ºC, e) 1 mbar and 250 ºC and e) 1 mbar and 300 ºC.

S.2 Catalytic Testing and Kinetic Data

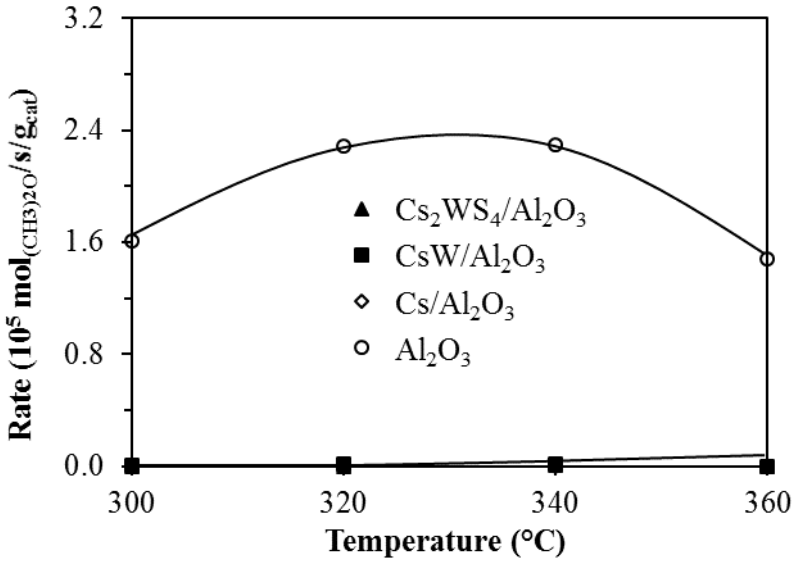

Figure S2.7 Dimethyl ether rate formation for Cs_2WS_4/Al_2O_3, CsW/Al_2O_3, Cs/Al_2O_3 and γ-Al_2O_3, in between 300-360 °C.

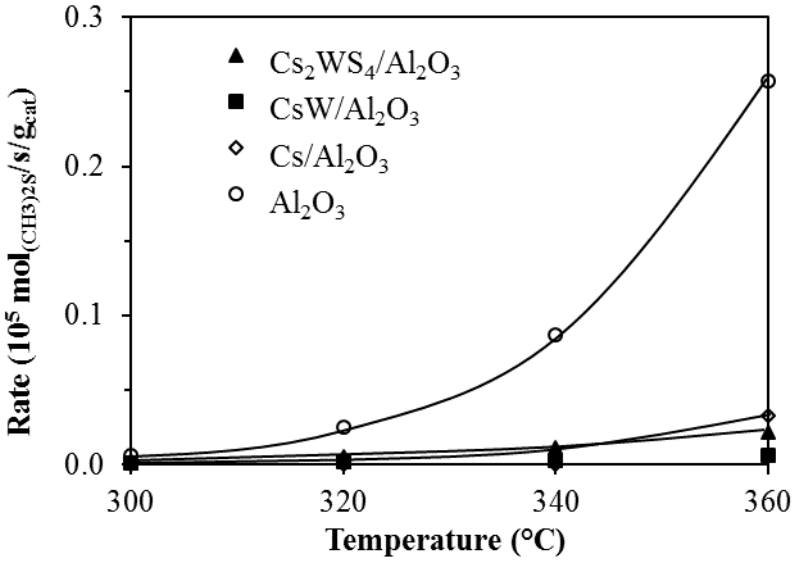

Figure S2.8 Dimethyl sulfide rate formation for Cs_2WS_4/Al_2O_3, CsW/Al_2O_3, Cs/Al_2O_3 and γ-Al_2O_3, in between 300-360 °C.

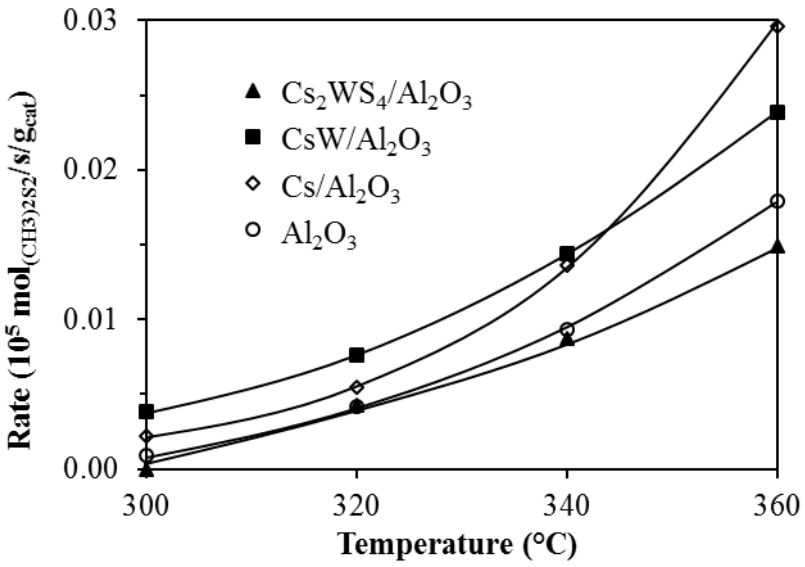

Figure S2.9 Dimethyl disulfide rate formation for Cs_2WS_4/Al_2O_3, CsW/Al_2O_3, Cs/Al_2O_3 and γ-Al_2O_3, in between 300-360 °C.

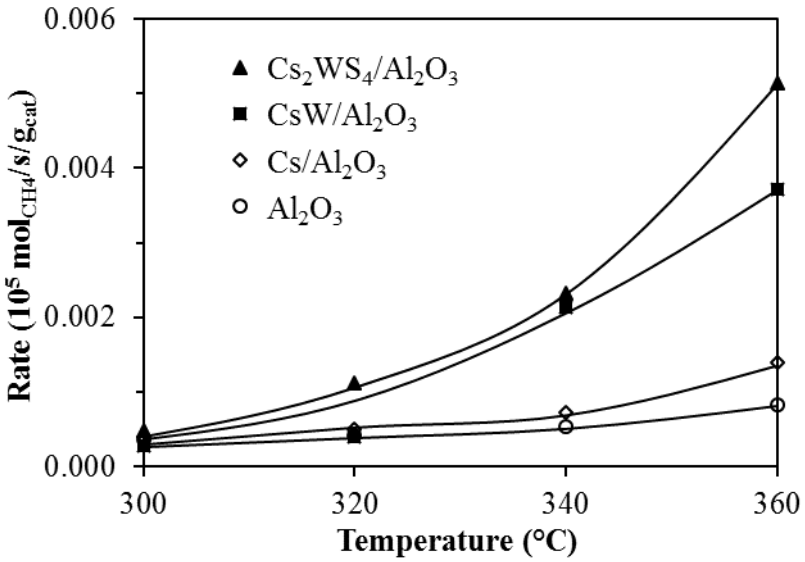

Figure S2.10 Methane rate formation for Cs_2WS_4/Al_2O_3, CsW/Al_2O_3, Cs/Al_2O_3 and γ-Al_2O_3, in between 300-360 °C.

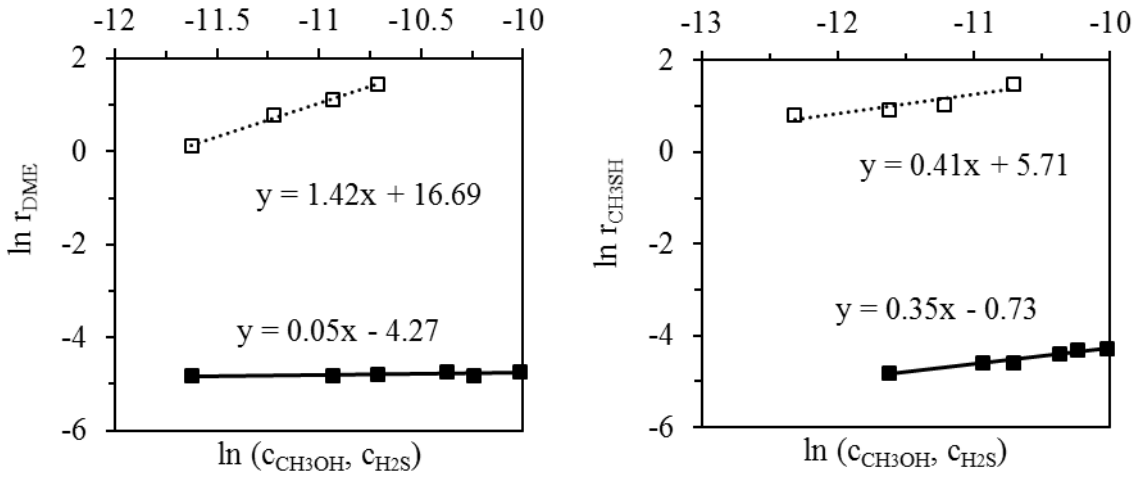

Figure S2.11 Left: Plot of ln rates of dimethyl ether production (Ln r_{DME}) along with ln of concentration of methanol (C_{CH3OH}, empty squares) or H_2S (c_{H2S}, filled squares) with Al_2O_3 catalyst at 300°C and 9 bar. Right: Plot of ln rates of methanethiol production (Ln r_{CH3SH}) along with ln of concentration of methanol (c_{CH3OH}, empty squares) or H_2S (c_{H2S}, filled squares) with Al_2O_3 catalyst at 300°C and 9 bar.

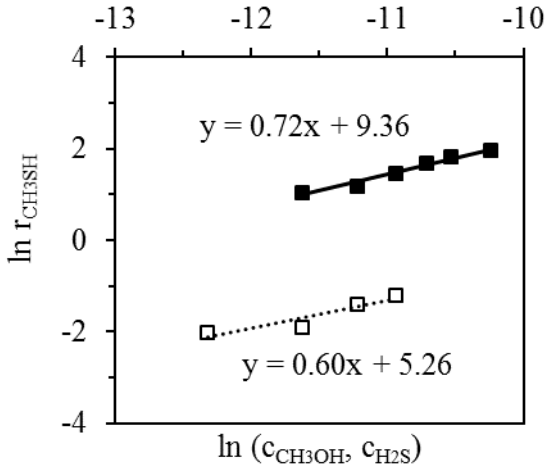

Figure S2.12 Plot of ln rates of methanethiol production (Ln r_{CH3SH}) along with ln of concentration of methanol (c_{CH3OH}, empty squares) or H_2S (c_{H2S}, filled squares) with Cs/Al_2O_3 catalyst at 300°C and 9 bar.

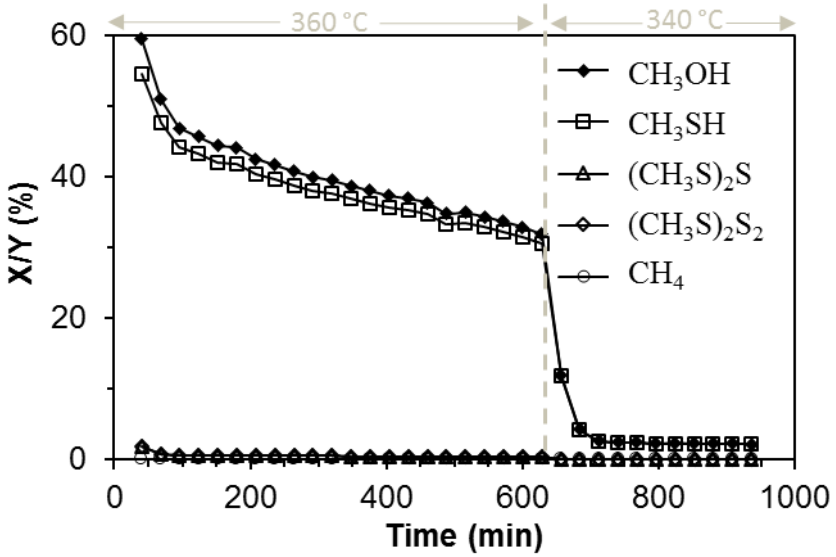

Figure S2.13 Methanol conversion and product yields during reaction of methanol and H_2S over Cs/SiO_2 at 360 and 340 °C under same conditions as catalytic tests.

S.3 Derivation of bimolecular rate equations for the formation of dimethyl ether and methanethiol

The following reaction steps describe the formation of dimethyl ether (CH_3OCH_3) and methanethiol (CH_3SH):

(1) $CH_3OH(g) + O^* \rightleftharpoons CH_3O^* + OH$ $\quad K_1 = [CH_3O^*]^2/([CH_3OH]\cdot[O^*])$

(2) $CH_3OH(g) + {}^c \rightleftharpoons CH_3O^c + H$ $\quad K_2 = [CH_3O^c]^2/([CH_3OH]\cdot[{}^c])$

(3) $H_2S(g) + {}^c \rightleftharpoons SH^c + H$ $\quad K_3 = [SH^c]^2/([H_2S]\cdot[{}^c])$

(4) $CH_3OH(g) + CH_3O^* \rightarrow CH_3OCH_3(g) + OH^*$

(5) $CH_3O^c + SH^c \rightarrow CH_3S^c + OH^c$

(6) $CH_3S^c + H \rightleftharpoons CH_3SH(g) + {}^c$ $\quad K_6 = [CH_3SH]\cdot[{}^c]/([(CH_3S^c][H])$

(7) $OH^c + H \rightleftharpoons H_2O(g) + {}^c$ $\quad K_7 = [H_2O]\cdot[{}^c]/([OH^c])\cdot[H])$

(8) $OH + OH^* \rightleftharpoons H_2O(g) + O^*$ $\quad K_8 = [H_2O]\cdot[O^*]/([OH^*])\cdot[OH])$

Scheme S2.1 Reaction kinetic steps for the formation dimethyl ether (DME) and CH_3SH, being (O^*) the strong Lewis acid site and (^{c}) the strong basic site of the Lewis acid-base pairs. The synthesis of DME follows an Eley-Rideal bimolecular reaction while the synthesis of CH_3SH follows a Langmuir-Hinshelwood bimolecular reaction.

The Lewis acid-base pair (LABS) sites are taking part in the formation of the methoxy on a strong Lewis acid site and the alcoholate on a strong basic site. In both cases there is a dissociation of the methanol having both respective equal number on acid and base sites ([^{c}]

or [*]). Assuming the Most Abundant Reaction Intermediates (MARI) and vacant sites ([c]) for strong Lewis acid sites:

$$[LABS^c] = [^c] + [CH_3O^c] + [SH^c] + [OH^c] + [CH_3S^c]$$

$$[LABS^c] = [^c]\,(1 + K_2^{0.5}\cdot[CH_3OH]^{0.5} + K_3^{0.5}\cdot[H_2S]^{0.5} + K_6^{-0.5}\cdot[CH_3S^H]^{0.5} + K_7^{-0.5}\cdot[H_2O]^{0.5})$$

Following the same rationale for the formation of dimethyl ether with strong Lewis acid sites:

$$[LABS^*] = [^*]\,(1 + K_1^{0.5}\cdot[CH_3OH]^{0.5} + K_8^{-0.5}\cdot\,[H_2O]^{0.5})$$

Assuming reaction 3 and 4 (Scheme S1) are the rate determining steps in the formation of dimethyl ether and methanethiol, respectively, the rate expressions for these two products are the following:

$$r_{CH_3SH} = k_5\cdot[CH_3O^c]\cdot[SH^c] = k_5\cdot K_2^{0.5}\cdot K_3^{0.5}\cdot[CH_3OH]^{0.5}\cdot[H_2S]^{0.5}\cdot[^c]^2$$

$$r_{CH_3OCH_3} = k_4\cdot[CH_3OH]\cdot[CH_3O^*] = k_4\cdot K_1^{0.5}\cdot[CH_3OH]^{1.5}\cdot[^*]$$

Substituting the site balance gives:

$$r_{CH_3OCH_3} = \frac{k_4 K_1^{0.5}[CH_3OH]^{1.5}}{1 + K_1^{0.5}[CH_3OH]^{0.5} + \frac{[H_2O]^{0.5}}{K_8^{0.5}}}[LABS*]$$

$$r_{CH_3SH} = \frac{k_5 K_2^{0.5} K_3^{0.5}[CH_3OH]^{0.5}[H_2S]^{0.5}}{(1 + K_2^{0.5}[CH_3OH]^{0.5} + K_3^{0.5}[H_2S]^{0.5} + \frac{[CH_3SH]^{0.5}}{K_6^{0.5}} + \frac{[H_2O]^{0.5}}{K_7^{0.5}})^2}[LABS\ c]$$

3. Effects of acid-base properties of metal oxides on methanol thiolation

Reprinted (adapted) with permission from Manuel Weber-Stockbauer, Oliver Y. Gutiérrez, Ricardo Bermejo-Deval, and Johannes A. Lercher, Cesium Induced Changes in the Acid–Base Properties of Metal Oxides and the Consequences for Methanol Thiolation, ACS Catalysis Copyright (2019) American Chemical Society[a]

[a] M.W.-S. planned, designed and conducted the experiments, analyzed and interpreted the data and wrote the manuscript. R.B.-D., O.Y.G. and J.A.L. contributed to the discussion of the results and the correction of the manuscript anytime.

3.1. Abstract

Cs^+ modified γ-alumina, titania anatase and zirconia in the absence of WS_2 are excellent catalysts for methanol thiolation. The Cs^+ cations induce higher concentrations and strength of base sites. Reaction rates were very similar on all three catalysts indicating that the Cs^+ cations are part of the dominating active sites. Methanol thiolation showed similar apparent activation energies, decreasing with Cs^+ concentration. Reaction orders close to 0.5 for both reactants show that all three metal oxides and their alkali metal modified counterparts follow the identical base-catalyzed Langmuir-Hinshelwood mechanism. A reaction between the surface alcoholate and the corresponding sulfhydryl groups is hypothesized to be the pathway for reaction.

3.2. Introduction

Methanethiol is an important base chemical for the industrial synthesis of methionine. [1] Various synthesis routes have been developed, including the hydrogenation of carbonyl sulfide[2, 3, 4] and/or methanol thiolation. [1, 5, 6, 7] The latter is currently the most frequently used process with Cs^+ modified WS_2/Al_2O_3 as catalyst. [8]

We have shown that Cs^+ increases the surface basicity of WS_2/Al_2O_3 and suppresses the formation of dimethyl ether.[1] The Lewis acid-base pairs catalyze methanol thiolation via surface alcoholates, while the stronger Lewis acid sites catalyze the formation of dimethyl ether. [9] In addition, methanethiol formation rates are higher with Cs^+ than with other alkaline metals (Rb^+ and K^+), due its lower Sanderson electronegativity. [1,10] Even though similar rates were observed with Cs/Al_2O_3 and CsW/Al_2O_3, the strong interaction of the Cs^+ cations with WS_2 results in a higher stability. This suggests that high interaction strength of Cs^+ with the support is critical for catalyst stability.

The present manuscript explores, therefore, the anchoring of Cs^+ cations on two transition metal oxides known to have strong ability to anchor oxide particles, such as TiO_2 and ZrO_2, as catalyst for methanol thiolation, comparing them with γ-Al_2O_3. Acid site distributions are probed by IR spectra of adsorbed probe molecules. Combining kinetic and spectroscopic results allow to explain the relations between physicochemical and catalytic properties and provide further guidance to catalyst development in the absence of WS_2.

3.3. Experimental

3.3.1. Catalyst preparation

Cs^+ containing catalysts were prepared by incipient wetness impregnation of γ-Al_2O_3 (Spheralite 101, Axens), TiO_2 (Hombikat 100 UV, Sachtleben), and ZrO_2 (SZ 61152, Norpro) with an aqueous solution of CH_3COOCs cesium acetate, added dropwise to the agitated solid. 160.5 mg of cesium acetate (Sigma Aldrich, ≥99.99%) were dissolved in 0.5 mL H_2O per 1 g of support targeting a Cs^+ loading of 10 wt.% and 361.0 mg cesium acetate for 20 wt.% Cs^+ loading. The impregnated metal oxides were dried over night at 70 °C and successively calcined (0.5 °C min^{-1}, 400 °C, 2 h, in flowing synthetic air, 100 ml min^{-1}). All samples were activated by treatment in H_2S with flow rate of 20 ml/min at 360 °C for 2 hours before use.

3.3.2. Chemical and physicochemical characterization

The elemental composition of the prepared materials was determined by AAS. The measurements were performed on an *UNICAM 939 AA*-Spectrometer. The textural properties were determined by N_2 physisorption using a *Porous Materials Inc. BET-121* sorptometer. After activation at 250 °C for 2 h under vacuum, N_2 was adsorbed at 77.4 K. The specific surface area was calculated using the BET-method. The crystalline structure of the catalysts was

determined by powder X-ray diffraction with a Philips X'Pert System (Cu Kα radiation, 0.1542 nm) operating at 45 kV/40 mA, using a nickel Kβ-filter and solid-state detector (X'Celerator). A step size of 0.017° and scan time of 0.31 s per step were used.

Adsorption of CO and pyridine were monitored via IR spectroscopy in transmission absorption mode (samples pressed into self-supporting wafers) to measure its Lewis acidity. Before adsorption, the samples were heated to 360 °C with heating ramp of 10 °C min^{-1} in a He flow of 10 mL min^{-1}. Then, the samples were sulfided at 0.5 h at 360 °C in 10 mL min^{-1} of 10 vol% H_2S in N_2. To remove physisorbed H_2S, the sample was flushed with He of 10 mL min^{-1} for another 15 min, before it was evacuated to 10^{-7} mbar and cooled to 50 °C. For pyridine adsorption, the sample was exposed to 1 mbar of pyridine at 50 °C, followed by decreasing the pyridine partial pressure. Evacuation to 10^{-5} mbar resulted in pyridine not being adsorbed on Cs^+ containing samples. Thus, spectra from different catalysts were compared at 0.1 mbar, before evacuation. The concentrations of coordinating pyridine were calculated using the molar integrated extinction coefficient of 0.96 cm·µmol^{-1} determined for the characteristic band at 1450 cm^{-1}. [11] Adsorption of CO via IR was measured at -150 °C, using liquid nitrogen. The spectra were recorded at a CO partial pressure of five mbar.
Methanol was adsorbed at 50°C, stepwise increasing the methanol partial pressure (0.1 mbar, 0.5 mbar, 1 mbar and 5 mbar) followed by an increase in temperature to 300°C. All spectra were recorded on an Nicolet 6700 FTIR spectrometer (64 scans were collected to obtain each spectrum). All spectra are presented after background subtraction and normalized to mass of the wafer.

3.3.3. Kinetic experiments

Catalytic thiolation of methanol was performed in a plug flow reactor. Before the reaction, 125.0 mg of catalyst (125-250 µm), diluted in 1 g of SiC, were sulfided in a flow of 20 mL min^{-1} H_2S at 360 °C and 9 bar. To determine activation energies, the reaction was performed with a flow of gaseous methanol of 10 mL min^{-1} mixed with H_2S (20 mL min^{-1}) and N_2 (20 mL min^{-1}), varying the temperature between 300 and 360 °C. Standard calculations of the Weisz–Prater modulus showed that it was < 1 for all catalysts under all conditions, and, therefore, it can be concluded that the kinetics results were unaffected by internal mass transfer effects.

Online analysis of the product flow was done using a *Shimadzu GC-2014* equipped with a HP-PLOT Q column (2.7 m, 2.0 mm inner diameter), using a TCD detector. Reaction rate constants were calculated using the integrated rate law for a 0.5 order reaction in methanol and H_2S for methanethiol. To study the product distribution over the whole range of conversion, the residence time was adjusted, keeping partial pressure of CH_3OH at 2.2 bar and N_2 and H_2S at 3.3 bar at 360 °C.

Reaction orders were determined at 360 °C. For reaction orders in H_2S, the partial pressure of methanol was kept constant at 2.2 bar, while the H_2S partial pressure was varied between 1.1 and 5.6 bar. To measure methanol reaction orders, the H_2S partial pressure was set to 4.5 bar and the methanol partial pressure varied from 0.6 mbar to 2.2 gaseous methanol. The N_2 gas flow was adjusted to compensate volume flow changes and keep the total volume flow constant at 80 ml/min. The amount of catalyst used in each experiment was adjusted accordingly, to ensure methanol conversion below 10 %. Reaction orders for Cs-modified materials were measured with 10.0 mg catalysts, while 5.0 mg for TiO_2 and ZrO_2 and 1.0 mg of γ-Al_2O_3 was sufficient. In the case of γ-Al_2O_3, the catalyst was homogeneously mixed with SiO_2 in a ratio of 1:9, to avoid channeling.

3.4. Results

3.4.1. Characterization

The elemental analysis and surface area determination of the studied catalysts are summarized in Table 3.1. The specific surface area of the three catalysts, Cs^+/Al_2O_3, Cs^+/TiO_2 and Cs^+/ZrO_2 decreased with increasing Cs^+ loading.

Table 3.1: Chemical composition and specific surface aread of studied catalysts.

Cs loading	C(Cs) (mmol g^{-1})			S_{BET} (m^2 g^{-1})		
(wt.%)	Al_2O_3	TiO_2	ZrO_2	Al_2O_3	TiO_2	ZrO_2
0	0	0	0	283	314	126
10	0.7	0.7	0.8	239	232	70
20	1.4	1.5	1.5	154	109	50

X-ray diffraction (Figure S3.1) showed the expected patterns of γ-Al_2O_3, anatase and tetragonal zirconia. Upon Cs^+ addition the X-ray diffractograms were hardly altered. Only one additional diffraction band at 45° was observed with γ-Al_2O_3 and TiO_2, indicative of Cs_2CO_3. The carbonate is formed by the reaction of Cs^+ with atmospheric CO_2. Upon sulfidation, these carbonate bands disappeared, leading to the formation of sulfur oxyanions not detected by X-ray diffraction.[9] The specific surface area decreased with increasing Cs^+ loading; this can be attributed to the increased density of the catalyst and coverage of the surface with Cs^+.

3.4.1.1. Characterization of acid base properties

The acidity of the metal oxides was characterized by IR spectra of adsorbed pyridine (Figure 3.1). [12] On γ-Al2O3 several bands were observed at 1620, 1612, 1593, 1577, 1450 and 1440 cm-1. [12,13] The bands at 1620 and 1612 cm^{-1} are assigned to the 8a vibrational mode of pyridine coordinatively bound to Lewis acid sites (LAS) of different acid strength (the wavenumber increases with acid strength), [12,13] while the band at 1577 cm^{-1} is assigned to the 8b vibrational mode. The band at 1593 cm^{-1} is assigned to the 8a vibrational mode of H-

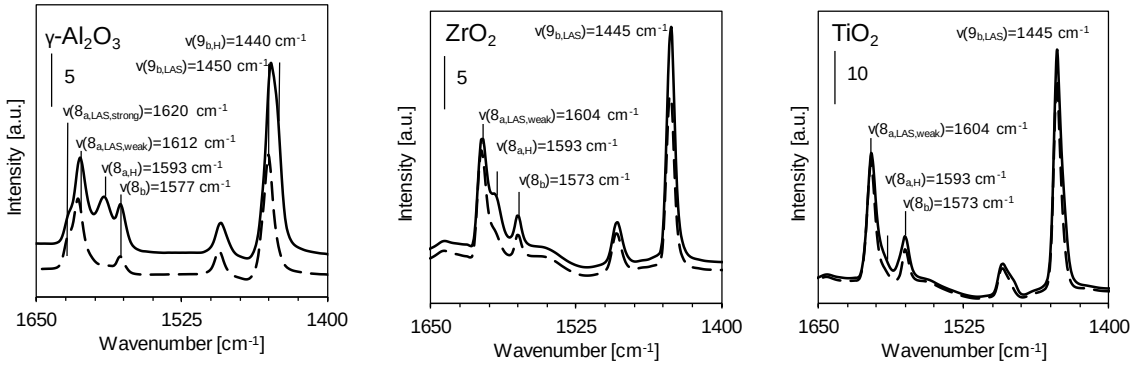

Figure 3.1. Subtracted IR spectra of adsorbed pyridine on the three studied metal oxides at 50 °C; the black line was taken at 0.1 mbar pyridine, dashed line show the sample after evacuation at 10^{-6} mbar.

bonded pyridine, caused by the interaction of pyridine with weak acidic surface hydroxyl groups.

We attribute the signal at 1450 cm^{-1} to the 9b vibration of pyridine on LAS, while the band at 1440 cm^{-1} is assigned again to pyridine H-bonded to hydroxyl groups. Pyridine coordinatively bound to LAS (1450 cm^{-1}, 1612-1620 cm^{-1},) was stable against evacuation, while the H-bonded pyridine bands (1440 and 1593 cm^{-1}) disappeared after evacuation, due to their weak interaction with the probe molecule.[14] The IR spectra of pyridine on ZrO_2 and TiO_2 led to bands at 1604, 1593, 1573 and 1445 cm^{-1}. The 1604 cm^{-1} band is assigned to the 8a mode of pyridine bound to LAS of ZrO_2 and TiO_2, the 1573 cm^{-1} band to its 8b mode and the 1593 cm^{-1} H-bond pyridine.[13,15,16,17] As for γ-alumina, this latter band disappeared after evacuation. The band at 1445-1450 cm^{-1} is attributed to the 9b vibration of pyridine adsorbed on LAS. Using this band to quantify the LAS concentration led to 454 µmol g^{-1} for γ-Al_2O_3, 220 µmol g^{-1} for ZrO_2 and 749 µmol g^{-1} for TiO_2. The higher wavenumber with γ-Al_2O_3 (1450 cm^{-1}) than with ZrO_2 and TiO_2 (1445 cm^{-1}) points to higher Lewis acid strength of the alumina.

The addition of Cs^+ led to subtle changes in nature and concentration of acid sites (Figure 3.2). On Cs^+(10)/γ-Al_2O_3, the 8a bands characteristic of strongly adsorbing LAS (1620 cm^{-1}) was no longer detected, as well as the signal of H-bonded pyridine. The remaining band is assigned to weak Lewis acid sites to 1612 cm^{-1}. A new band appeared at 1583 cm^{-1}, corresponding to the 8a vibrational mode of pyridine coordinatively bound to a weak Lewis acidic alkali, i.e., Cs^+ [14,18,19] with lower Lewis acid strength than those measured on γ-Al_2O_3.[14,18] Upon addition of Cs^+ to ZrO_2 and TiO_2, Cs^+(10)/ZrO_2 and Cs^+(10)/TiO_2, bands characteristic of pyridine adsorbed to LAS of ZrO_2 and TiO_2 were not observed. As for Cs^+/γ-Al_2O_3, bands at 1602, 1583 and 1573 cm^{-1} appeared, corresponding to the 1 + 6a, 8a and 8b overtone vibrations of pyridine adsorbed on Cs^+, respectively. [12] After evacuation, these bands largely disappeared, but traces were still seen with Cs^+(10)/γ-Al_2O_3 and Cs^+(10)/TiO_2.

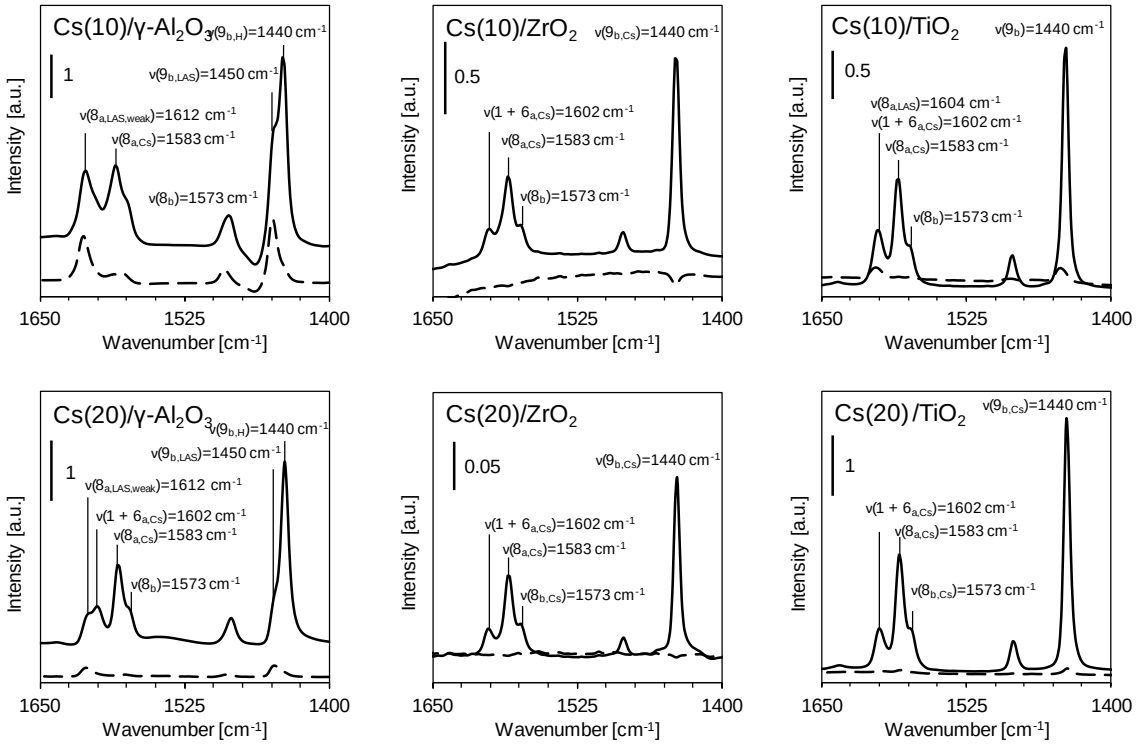

Figure 3.2. Subtracted IR spectra of adsorbed pyridine on the Cs+ doped metal oxides at 50 °C; the black line was taken at 0.1 mbar pyridine, dashed line demonstrate the samples after evacuation at 10^{-7} mbar.

Even higher concentrations of Cs^+ ($Cs^+(20)/\gamma\text{-}Al_2O_3$) led to a lower intensity of the band at 1612 cm^{-1} and the appearance of a new band at 1602 cm^{-1} attributed to the 1+6a overtone vibration of pyridine on Cs^+.[14] The mentioned 1583 cm^{-1} 8a vibration of pyridine on Cs^+ sites and 1573 cm^{-1} 8b vibration of pyridine on LAS and Cs^+ are the same as for $Cs^+(10)/\gamma\text{-}Al_2O_3$. Thus, the gradual addition of Cs^+ led to the replacement of strong LAS from $\gamma\text{-}Al_2O_3$ with weaker LAS from Cs-oxide/hydroxide supported particles. Pyridine adsorption on $Cs^+(20)/ZrO_2$ and $Cs^+(20)/TiO_2$ showed only pyridine on Cs^+ sites (8a, 8b and 1+6a vibrational modes). [18] For these ZrO_2 and TiO_2 based catalysts all pyridine was concluded to be desorbed after evacuation, while a minor fraction remained on $Cs^+(20)/\gamma\text{-}Al_2O_3$.

The bands and their assignments are summarized in Table S1 (metal oxides) and Table S2 (Cs^+ containing catalysts). The IR spectra indicate substantial heterogeneity of LAS sites in $\gamma\text{-}Al_2O_3$, while TiO_2 and ZrO_2 strongly indicate one type of LAS of similar strength. [12,13,15,16,17] We hypothesize that Cs^+ replaces hydrogen atoms of surface hydroxyl groups, [14,18,19] increasing the overall basicity. At high Cs^+ loading, the surface is dominated by Cs^+, forming supported Cs-oxide/hydroxide particles. [18,19]

IR spectra of adsorbed CO are shown in Figure S3.2. The assignments of the CO bands are compiled in Table S3.3. The bands at 2180-2190 cm^{-1} are assigned to the CO adsorption on LAS and those at 2150 cm^{-1} to adsorption on surface hydroxyls. [15,20,21] Those on LAS decreased in the sequence of $\gamma\text{-}Al_2O_3$ (2188 cm^{-1}), TiO_2 (2181 cm^{-1}), ZrO_2 (2177 cm^{-1}). This points to a decrease in the interaction strength following that order.

The addition of 10 wt.% Cs^+ on the three oxides led to a red-shift of the wavenumber of adsorbed CO to 2136 cm^{-1}, indicating that CO interacted primarily with Cs^+ cations.[22,20] For $Cs^+(10)/\gamma\text{-}Al_2O_3$, an additional band appeared at 2179 cm^{-1}, corresponding to LAS in the $\gamma\text{-}Al_2O_3$ support altered by the alkali cation. [19,22] Bands of CO adsorbed on OH groups were not observed. On $Cs^+(20)/TiO_2$ and $Cs^+(20)/\gamma\text{-}Al_2O_3$ only the band for CO on Cs^+ cations was detected. Also for $Cs^+(20)/ZrO_2$ bands of CO were not observed after equilibration with 5 mbar CO at -150°C.

The red-shift of the CO stretching vibration on LAS with Cs^+ is caused by its lower acid strength compared to Al^{3+}, Ti^{4+}, and Zr^{4+}. As in the case of the pyridine, Cs^+ is the dominating site for CO adsorption.

3.4.1.2. Methanol adsorption

The IR spectra of adsorbed methanol on the studied metal oxides are shown in Figure 3.3, exhibiting bands in the 3000-2750 cm^{-1} region (alkyl (sp^3) C-H vibrations). Bands between 3000-2900 cm^{-1} are assigned to the asymmetric stretch of ($\nu_{as}(CH_3)$) or its Fermi resonance with CH_3 deformation vibrations ($2\delta_s(CH_3)$), while lower bands are assigned to symmetric stretching vibrations ($\nu_s(CH_3)$). [23-25]

Different intensities were observed for the C-H stretching vibration bands assigned to the adsorption of methanol on strong Lewis acid sites and strong basic sites, for both the ν_{as} and the ν_s at 50°C (Figure 3.3 and S3.3). The adsorption of CH_3OH on strong Lewis acid sites results in non-dissociated methanol (molecularly adsorbed), [26,27] while the adsorption of CH_3OH on a strong basic site results in the dissociation of an alcoholate (dissociation of the OH group).[26,27] Molecularly adsorbed methanol bands are observed for both the ν_{as} (2943, 2948 and 2944 cm^{-1} for γ-Al_2O_3, ZrO_2 and TiO_2) and the ν_s (2845, 2852 and 2844 cm^{-1} for γ-Al_2O_3, ZrO_2 and TiO_2). Vibration bands of dissociated methanol are observed for both the ν_{as} (2939, 2931 and 2923 cm^{-1} for γ-Al_2O_3, ZrO_2 and TiO_2) and the ν_s (2821, 2827 and 2821 cm^{-1} for γ-Al_2O_3, ZrO_2 and TiO_2). On ZrO_2 a relatively higher concentration of the methanolate compared to the molecularly adsorbed methanol was observed, increasing further for TiO_2.[28] In the case of γ-Al_2O_3, heating would transform the non-dissociated methanol into a bridging methoxy species (Figure S3.4). No major changes were observed upon heating for the other two metal oxides. The relative intensities of methanol on the surface species directly leads to the conclusion that the general acidic character of the metal oxide to a more basic one decreases in the order of: γ-Al_2O_3 > ZrO_2 ~ TiO_2.

Probing the Cs^+ modified metal oxides with methanol showed a number of differences with respect to the parent metal oxide materials. The bands assigned to molecularly adsorbed methanol decreased with increasing Cs+ loading, shifting to lower wavenumbers the signal assigned to the alcoholate formation. The decrease in these bands can be explained by the reduction of the LAS concentration, as discussed with pyridine and CO. The variation in

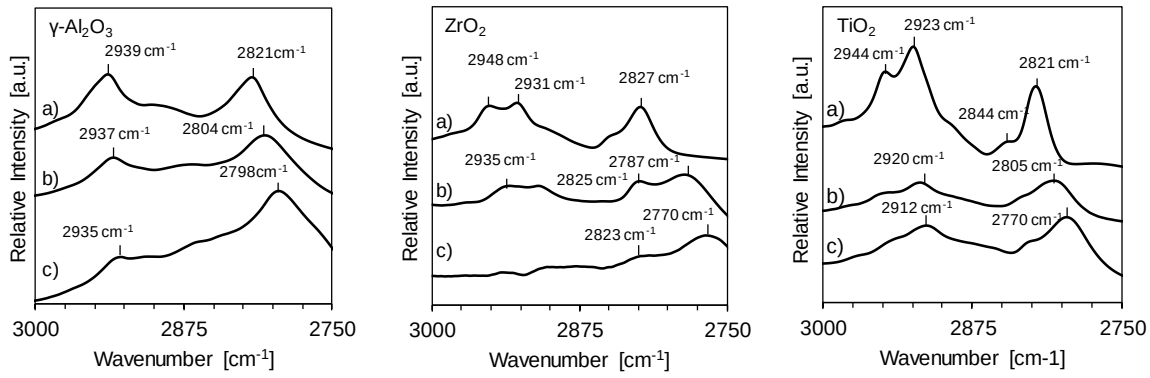

Figure 3.3. Spectra of methanol adsorbed on (Cs^+)Al_2O_3 (left), (Cs^+)ZrO_2 (Middle) and (Cs^+)TiO_2 (50 ºC and 0.1 mbar methanol partial pressure), without Cs^+ (a), 10 wt.% Cs^+(b) and 20 wt.% Cs^+ (c).

wavenumbers of alcoholate bands on the different supports and Cs^+ loadings is attributed to differences in electronegativity of the supports and the base strength of the Cs^+ catalysts.

The vibration region between 1000 and 1500 cm^{-1} is shown in Figure S3.4. The signals between 1360 and 1370 cm^{-1} in γ-Al_2O_3 are assigned to the bending vibration of the O-H bond during methanol dissociation, due to the formation of the bridging methoxides. [23] This signal is not observed on all strong Cs^+ modified samples and medium Cs^+ modified ZrO_2, indicating the absence of LAS. The signals between 1440 and 1460 cm^{-1} are assigned to the bending vibration of the C-H bond. A red shift is observed in the C-H bending vibration upon addition of Cs^+ on each metal oxide, similar to the red shift observed in the C-H stretching vibration. We hypothesize the differences in intensities observed for bridging methoxides during heating and alcoholate are strongly correlated to the selectivity to dimethyl ether and methanethiol, respectively.

3.4.2. Thiolation of methanol

3.4.2.1. Catalyst activity and reaction network

Initial rates for methanethiol (CH_3SH) formation are shown Figure 3.4. The highest rate in methanol thiolation was observed for TiO_2 (0.17-1.4·10^{-6} mol_{CH3SH} s^{-1} g_{cat}^{-1}), followed by γ-Al_2O_3 (0.13-0.9·10^{-6} mol_{CH3SH} s^{-1} g_{cat}^{-1}) and ZrO_2 (0.02-0.2·10^{-6} mol_{CH3SH} s^{-1} g_{cat}^{-1}). There is almost a factor five difference in the rates of methanethiol formation in between TiO_2 and ZrO_2 at 360 °C. The rates normalized to the concentration of LAS (Figure S3.7) shows comparable TOF for TiO_2 and γ-Al_2O_3, while that on ZrO_2 was 50% lower. The observed differences between the two former supports suggests the methanethiol formation is a function of the concentration of accessible active sites, since these hold a higher number of Lewis acid sites (454 and 749 µmol g^{-1} for γ-Al_2O_3 and TiO_2) than for ZrO_2 (220 µmol g^{-1}).

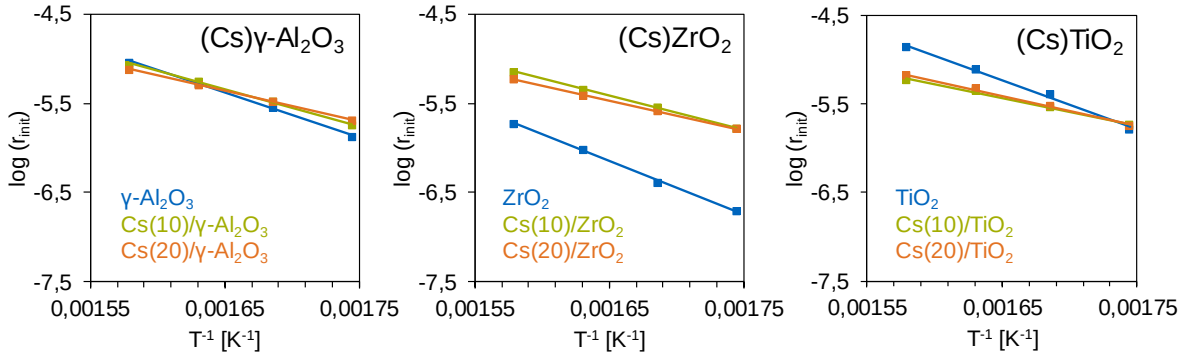

Figure 3.4. Initial rates for methanethiol formation for Cs^+/Al_2O_3 (left), Cs^+/ZrO_2 (middle) and Cs^+/TiO_2 (right) between 300 and 360°C at 9 bar for the pure metal oxides (blue), 10 wt Cs^+% (green) and 20 wt% Cs^+ (orange).

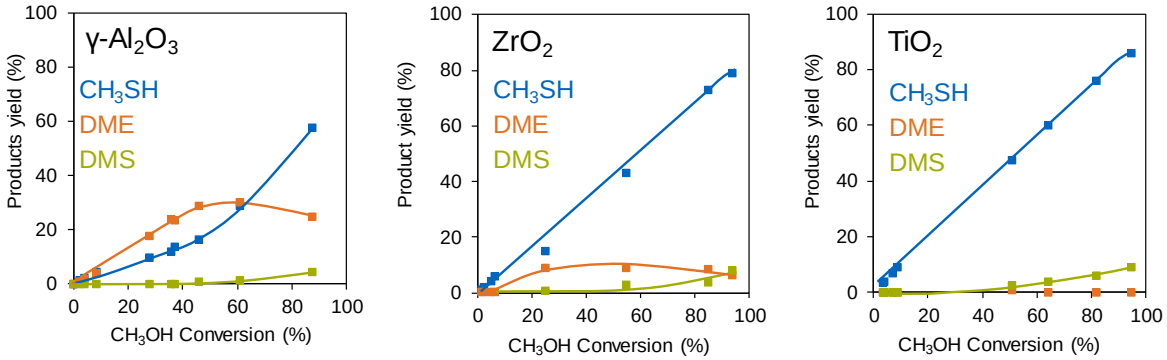

Figure 3.5. Y vs. X: Methanethiol (blue), DME (orange), DMS (green) on (Cs^+)Al_2O_3 (left), (Cs^+)ZrO_2 (middle) and (Cs^+/)TiO_2 (right) catalysts with T = 360 °C and 9 bar.

For Cs^+ containing catalysts all rates for methanethiol formation were approximately equal ($Cs^+(10)/\gamma\text{-}Al_2O_3$ ($1.8\text{-}8.7\cdot10^{-6}$ mol_{CH3SH} s^{-1} g_{cat}^{-1}), $Cs^+(10)/ZrO_2$ ($1.7\text{-}7.1\cdot10^{-6}$ mol_{CH3SH} s^{-1} g_{cat}^{-1}), $Cs^+(10)/TiO_2$ ($1.8\text{-}6.6\cdot10^{-6}$ mol_{CH3SH} s^{-1} g_{cat}^{-1})). Higher Cs^+ loading of 20 wt.% lead to a slightly lower activity. This indicates that the overall activity is solely determined by accessible Cs^+ species.

The yields of methanethiol, dimethyl ether (DME) and dimethyl sulfide (DMS) as a function of methanol conversion are compared in Figure 3.5 (metal oxides) and Figure 3.6 (Cs^+ modified metal oxides). On $\gamma\text{-}Al_2O_3$, methanethiol and dimethyl ether (DME) were primary products, with DME being the highest primary product until 60% of methanol conversion. At higher conversions, the yield of DME decreased to 20% at 90% conversion, with methanethiol being the main product. This indicates that DME formation is reversible. It should be noted in passing that a similar trend was also observed for W/Al_2O_3.[1] Similar results were observed with ZrO_2, however, methanethiol was the main primary product and dimethyl ether yield was below 10%.

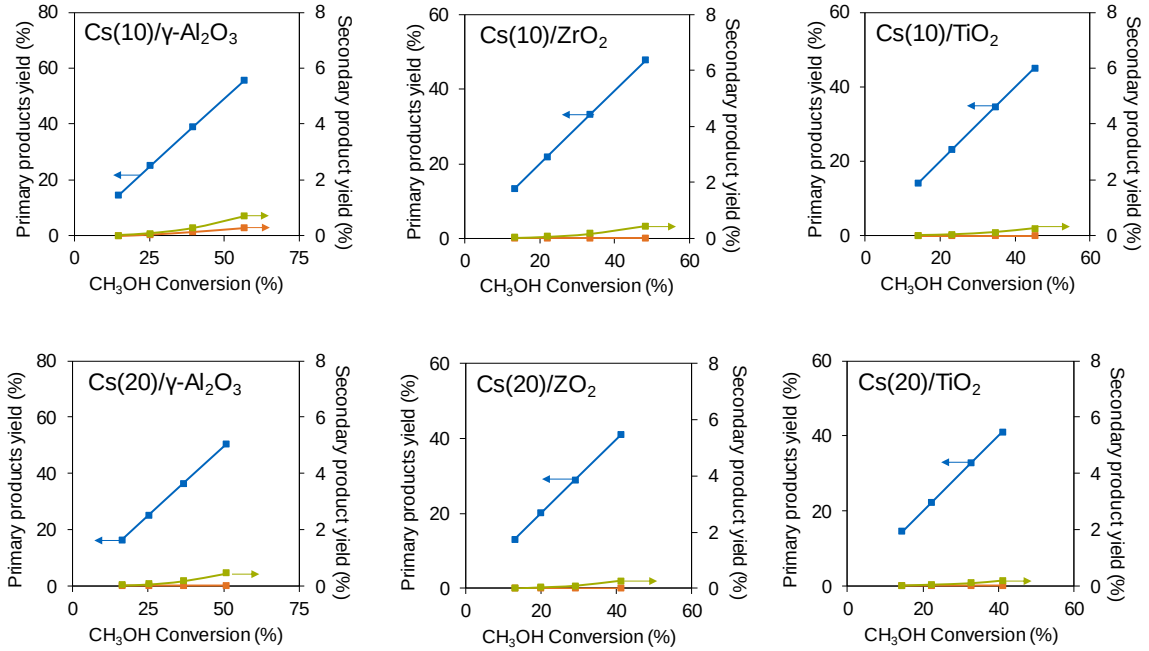

Figure 3.6. Y vs. X: Methanethiol (blue), DME (orange), DMS (green) on Cs^+/Al_2O_3 (left), Cs^+/ZrO_2 (middle) and Cs^+/TiO_2 (left) catalysts with T = 300-360 °C and 9 bar.

Remarkably, DME was not formed at conversions lower than 10%. On TiO_2, dimethyl ether was not observed. The reaction without H_2S on ZrO_2 and TiO_2 resulted in the formation of DME (Figure S3.6), the rates of DME being approximately 4 times higher than for ZrO_2 with H_2S ($4.4 \cdot 10^{-6}$ mol_{CH3SH} s^{-1} g_{cat}^{-1}compared to $1.1 \cdot 10^{-6}$ mol_{CH3SH} s^{-1} g_{cat}^{-1}). This points to a stronger preference for H_2S adsorption (relative to CH_3OH) on ZrO_2 and TiO_2. At 80-90% methanol conversion the yields to methanethiol increased in the order of: TiO_2 ~ZrO_2 > γ-Al_2O_3. On all materials, DMS was found at higher methanol conversion levels as a secondary product of methanethiol formation. Thus, the less acidic supports, such as ZrO_2 and TiO_2, favor the formation of methanethiol over dimethyl ether formation. The relative concentrations of methoxide and alcoholate on the catalysts surface, previously shown during methanol adsorption, influence the formation of dimethyl ether and methanethiol, respectively.

Scheme 3.1 shows the proposed general reaction network. As primary product methanethiol is formed via thiolation of methanol (Reaction 1); DME is formed by condensation of two CH_3OH (Reaction 2). As the reaction proceeds, DME undergoes a secondary reaction to methanethiol (Reaction 3), as seen from the maximum DME yield at 50% methanol conversion on γ-Al_2O_3 and ZrO_2. CH_3SH can further react to DMS (Reaction 4).

Comparing yields as a function of methanol conversion for catalysts with different Cs^+ loading (Figure 3.6), methanethiol was generally obtained as main product and only with $Cs^+(10)/Al_2O_3$ a small amount of dimethyl ether was formed. The main side product was dimethyl sulfide, with a maximum yield of 0.7% on $Cs^+(10)/Al_2O_3$ at 360 °C. The absence of DME in presence of Cs^+ is attributed to the absence of strong LAS as shown by spectroscopic characterization.[1]

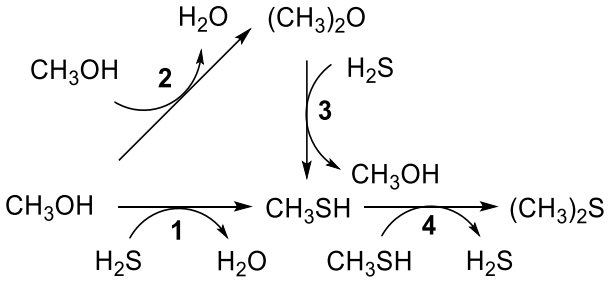

Scheme 3.1. Reaction network for the reaction of methanol with H_2S over metal oxides (the dominant reactions are (1) and (2)) and Cs^+-modified catalysts (the dominant reaction is (1)). The numbers in parenthesis correspond to the reaction numbers as described in the text. The figure is based on Scheme 1 of our previous work.[1]

3.4.2.2. Kinetic analysis

The reaction orders for CH_3OH and H_2S in the formation of methanethiol are shown in Table 3.2. The rates with variable pressure in methanol and H_2S of each catalyst are shown in Figure S3.5 and a summary for the reaction orders in Table 3.2.

Table 3.2. Reaction orders for methanethiol formation from H_2S and CH_3OH at 360°C and a total pressure of 9 bar.

Cs loading	Reaction order (CH_3OH)			Reaction order (H_2S)		
(wt.%)	Al_2O_3	TiO_2	ZrO_2	Al_2O_3	TiO_2	ZrO_2
0	0.4	0.3	0.3	0.4	0.5	0.4
10	0.5	0.6	0.5	0.4	0.2	0.2
20	0.3	0.6	0.6	0.6	0.2	0.2

The bimolecular reaction for a Langmuir-Hinshelwood mechanism between a dissociated methanol and dissociated hydrogen sulfide would require half order for both substrates (derivation in Section S3), having the following rate equation:

$$r_{CH_3SH} = \frac{k_5 K_2 K_3 [CH_3OH]^{0.5} [H_2S]^{0.5}}{b^2} \qquad (1)$$

with $b = (1 + K_2^{0.5}[CH_3OH]^{0.5} + K_3^{0.5}[H_2S]^{0.5} + [CH_3SH]^{0.5}/K_6^{0.5} + [H_2O]^{0.5}/K_7^{0.5})$. H_2S is known to adsorb dissociatively on the surface of the metal oxides, [1, 21] while CH_3OH also adsorbs dissociatively forming a methanolate on the Lewis acid-base pairs of the surface oxides, confirmed by the adsorption of methanol via IR (Species II). The observed reaction orders were in between 0.3-0.6 for methanol and 0.2-0.6 for H_2S. While a reaction order of 0.5-0.6 for CH_3OH is observed on Cs^+/TiO_2 and Cs^+/Al_2O_3, the reaction order of 0.2 for H_2S suggests that dissociated H_2S is a minority species. The partial coverage is also observed with CH_3OH on TiO_2 and ZrO_2 (without Cs^+), with a 0.3 reaction order for CH_3OH. Thus, it is suggested that both substrates dissociate on the same kind of strong basic sites and the addition of Cs^+ modifies the chemical affinity of the metal oxide.

The apparent activation energies of all catalysts are compiled in Table 3.3. The apparent activation energy for methanethiol formation varied between 115 and 107 kJ mol^{-1} on the parent oxides, while the addition of Cs^+ decreases the values to 78 - 66 kJ mol^{-1}. The lower activation energy of these catalysts, with respect to the metal oxides, is attributed to the increase in basicity and it was even lower for catalysts with 20 wt.% Cs. [19] It is hypothesized that Cs^+ reduces the concentration of hydroxyl groups on the surface.[29,30] Indeed, the IR spectra of adsorbed of pyridine and CO indicated the absence of OH bands and a complete replacement by Cs^+.

Table 3.3. Apparent activation energy for methanethiol formation at 9 bar, $CH_3OH:H_2S$ of 1:2 at 300-360°C.

Cs loading (wt.%)	Apparent activation energy (kJ mol^{-1}) of methanethiol formation		
	Al_2O_3	TiO_2	ZrO_2
0	112	105	115
10	78	66	73
20	65	59	64

Kinetic data for DME are shown in Table 3.4. The observed reaction order of 1.5 in CH_3OH for the formation of DME with γ-Al_2O_3 suggests an Eley-Rideal type bimolecular reaction (derivation Section S.3). On ZrO_2 and TiO_2 the reaction order for DME formation (without H_2S present) was found to be 0.7. This suggests a higher surface coverage of methanol than on γ-Al_2O_3. The higher coverage of the methanol molecule to form a surface methoxy group on TiO_2 and ZrO_2 will result in a higher apparent activation energy (91 and 93 kJ/mol, respectively) than with γ-Al_2O_3 (70 kJ/mol), reflecting energy differences in between the transition state intermediate and a point in between the mobile and adsorbed methanol.

The two transition metal oxides, TiO_2 and ZrO_2, provide mainly Lewis acid-base pairs for methanolate formation on the metal oxide surface upon methanol adsorption, while γ-Al_2O_3 contributes both strong and weak Lewis acid sites. Thus, the highest methanethiol rates (Figure 3.4) were observed with TiO_2. In addition, TiO_2 and ZrO_2 stabilize better Cs^+ cations, eliminating OH groups as adsorption sites and shutting down the methanol condensation pathway with Cs^+(10)/support. The addition of Cs^+ increases the surface base strength and inhibits the methanol condensation pathway. Thus, we propose the formation of methanethiol proceed via a bimolecular Langmuir-Hinshelwood mechanism (Scheme 3.2)

Table 3.4. Reaction order in H_2S and methanol and apparent activation energy for dimethyl ether formation.

	Reaction order (CH_3OH)	Reaction order (H_2S)	Apparent activation energy (kJ mol^{-1}) for dimethyl ether formation
Al_2O_3	1.5	0	70
TiO_2	0.7	n.d.	91
ZrO_2	0.7	n.d.	93

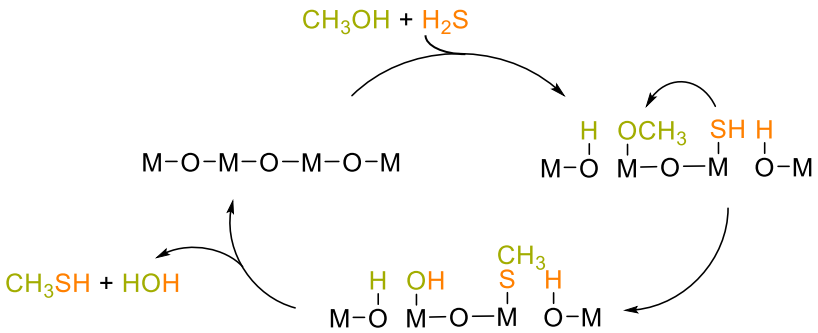

Scheme 3.2. Schematic reaction mechanism for the formation of methanethiol. M presents a metal cation like Cs^{+}, Ti^{4+}, Zr^{4+}, Al^{3+} and O, the corresponding O^{2-} anion.

In a first step, methanol and H_2S adsorb dissociatively on acid-base sites, forming a surface methanolate and SH, respectively. In a second step the SH^- attacks the methanolate in a SN_2 nucleophilic substitution to form the thiol and a hydroxyl group. After the recombination with H^+ methanethiol and water desorb from the surface.

Our results demonstrate that methanol thiolation is possible in the absence of the WS_2 used in the industrial catalyst. [8] The simultaneous addition of the SH nucleophile and the elimination of the hydroxyl species in a concerted step (SN_2 nucleophilic substitution) requires Lewis acid-base pairs with strong basic anions in the absence of strong Lewis acid sites.

3.5. Conclusion

On Cs^+ modified metal oxides, Cs^+ is bonded to the surface oxygen substituting the protons in OH groups, drastically increasing the strength of the base sites. This modification drastically impedes dimethyl ether formation. The increase in basicity leads to a decrease in the apparent activation energy, as the more basic sites favor thiolation. γ-Al_2O_3 contributes both strong and weak Lewis acid sites, while TiO_2 and ZrO_2 provide mainly Lewis acid-base pairs for methanolate formation on the metal oxide surface upon methanol adsorption and stabilize better the Cs^+ cations. Thiolation of methanol proceeds via a bimolecular Langmuir-Hinshelwood type mechanism, involving the dissociation of CH_3OH and H_2S to form a methanolate and a sulfhydryl group.

The results demonstrate that suitable catalysts for methanol thiolation do not require the presence of WS_2 to be active and stable. The overall insight allows now to develop new catalysts based on tailoring acid-base properties for highly selective methanol thiolation.

3.6. Acknowledgment

The authors would like to thank SAINT-GOBAIN NorPro for providing the ZrO_2 materials, used in this work. RBD would like to thank the Alexander von Humboldt foundation for financial support.

3.7. Literature

[1] Pashigreva, A. V.; Kondratieva, E.; Bermejo-Deval, R.; Gutiérrez, O. Y.; Lercher, J. A., Methanol thiolation over Al2O3 and WS2 catalysts modified with cesium. *Journal of Catalysis* **2017,** *345*, 308-318.

[2] Gutiérrez, O. Y.; Kaufmann, C.; Hrabar, A.; Zhu, Y.; Lercher, J. A., Synthesis of methyl mercaptan from carbonyl sulfide over sulfide K2MoO4/SiO2. *Journal of Catalysis* **2011,** *280* (2), 264-273.

[3] Gutiérrez, O. Y.; Kaufmann, C.; Lercher, J. A., Synthesis of Methanethiol from Carbonyl Sulfide and Carbon Disulfide on (Co)K-Promoted Sulfide Mo/SiO2 Catalysts. *ACS Catalysis* **2011,** *1* (11), 1595-1603.

[4] Gutiérrez, O. Y.; Zhong, L.; Zhu, Y.; Lercher, J. A., Synthesis of Methanethiol from CS2 on Ni-, Co-, and K-Doped MoS2/SiO2 Catalysts. *ChemCatChem* **2013,** *5* (11), 3249-3259.

[5] Wang, W.; Li, J.; He, Q.; Peng, S.; Yang, Y.; Li, M., Synthesis of Methanethiol from Methanol and Carbon Disulfide over CoKW/Al2O3 Catalysts: The Possible Reaction Network and Reaction Mechanism. *ChemistrySelect* **2018,** *3* (33), 9663-9671.

[6] Wang, W.; Li, Y.; Zhang, X.; Fang, W.; Yang, Y., Catalytic synthesis of methanethiol from methanol and carbon disulfide over KW/Al2O3 catalysts. *Catalysis Communications* **2015,** *69*, 104-108.

[7] Wang, W.; Zhang, X.; Xia, Z.; Fang, W.; Yang, Y., Catalytic Synthesis of Methanethiol from Carbon Disulfide and Hydrogen Over Sulfided KMo/Al2O3 Catalysts. *Catal Lett* **2015,** *145* (7), 1521-1528.

[8] Sauer, J.; Boeck, W.; Hippel, L. v.; Burkhardt, W.; Rautenberg, S.; Arntz, D.; Hofen, W. Catalyst, process for its preparation, and use for synthesis of methyl mercaptan 1998.

[9] Weber-Stockbauer, M.; Gutiérrez, O. Y.; Bermejo-Deval, R.; Lercher, J. A., The role of weak Lewis acid sites for methanol thiolation. *Catalysis Science & Technology* **2019,** *9* (2), 509-516.

[10] Bermejo-Deval, R.; Walter, R. M. H.; Gutierrez, O. Y.; Lercher, J. A., On the role of the alkali cations on methanol thiolation. *Catalysis Science & Technology* **2017,** *7* (19), 4437-4443.

[11] Maier, S. M.; Jentys, A.; Lercher, J. A., Steaming of Zeolite BEA and Its Effect on Acidity: A Comparative NMR and IR Spectroscopic Study. *The Journal of Physical Chemistry C* **2011,** *115* (16), 8005-8013.

[12] Morterra, C.; Magnacca, G., A case study: surface chemistry and surface structure of catalytic aluminas, as studied by vibrational spectroscopy of adsorbed species. *Catalysis Today* **1996,** *27* (3), 497-532.

[13] Zaki, M. I.; Hasan, M. A.; Pasupulety, L., Surface Reactions of Acetone on Al2O3, TiO2, ZrO2, and CeO2: IR Spectroscopic Assessment of Impacts of the Surface Acid−Base Properties. *Langmuir* **2001,** *17* (3), 768-774.

[14] Morterra, C.; Chiorino, A.; Ghiotti, G.; Fisicaro, E., Spectroscopic study of anatase properties. Part 5.—Surface modifications caused by K2O addition. *Journal of the Chemical Society, Faraday Transactions 1: Physical Chemistry in Condensed Phases* **1982,** *78* (9), 2649-2659.

[15] Miller, T. M.; Grassian, V. H., Environmental Catalysis: Adsorption and Decomposition of Nitrous Oxide on Zirconia. *Journal of the American Chemical Society* **1995,** *117* (44), 10969-10975.

[16] Awate, S. V.; Waghmode, S. B.; Agashe, M. S., Synthesis, characterization and catalytic evaluation of zirconia-pillared montmorillonite for linear alkylation of benzene. *Catalysis Communications* **2004,** *5* (8), 407-411.

[17] Manríquez, M. E.; López, T.; Gómez, R.; Navarrete, J., Preparation of TiO2–ZrO2 mixed oxides with controlled acid–basic properties. *Journal of Molecular Catalysis A: Chemical* **2004,** *220* (2), 229-237.

[18] Martin, C.; Martin, I.; Delmoral, C.; Rives, V., FT-IR Assessment Through Pyridine Adsorption of the Surface Acidity of Alkali-Doped MoO3/TiO2. *Journal of Catalysis* **1994,** *146* (2), 415-421.

[19] Busca, G.; Ramis, G., FT-IR study of the surface properties of K2O-TiO2. *Applied Surface Science* **1986,** *27* (1), 114-126.

[20] Bordiga, S.; Lamberti, C.; Geobaldo, F.; Zecchina, A.; Palomino, G. T.; Arean, C. O., Fourier-Transform Infrared Study of CO Adsorbed at 77 K on H-Mordenite and Alkali-Metal-Exchanged Mordenites. *Langmuir* **1995,** *11* (2), 527-533.

[21] Travert, A.; Manoilova, O. V.; Tsyganenko, A. A.; Maugé, F.; Lavalley, J. C., Effect of Hydrogen Sulfide and Methanethiol Adsorption on Acidic Properties of Metal Oxides: An Infrared Study. *The Journal of Physical Chemistry B* **2002,** *106* (6), 1350-1362.

[22] Montanari, T.; Castoldi, L.; Lietti, L.; Busca, G., Basic catalysis and catalysis assisted by basicity: FT-IR and TPD characterization of potassium-doped alumina. *Applied Catalysis A: General* **2011,** *400* (1), 61-69.

[23] Burcham, L. J.; Briand, L. E.; Wachs, I. E., Quantification of Active Sites for the Determination of Methanol Oxidation Turn-over Frequencies Using Methanol Chemisorption and in Situ Infrared Techniques. 1. Supported Metal Oxide Catalysts. *Langmuir* **2001,** *17* (20), 6164-6174.

[24] Derouault, J.; Le Calve, J.; Forel, M. T., Discussion des vibrations de valence v(CH3) and v(CD3) des groupes OCH3 and OCD3: Influence de la formation d'une liaison de coordination entre l'oxygéne and les halogénures d'aluminium ou le trifluorure de bore. *Spectrochimica Acta Part A: Molecular Spectroscopy* **1972,** *28* (2), 359-371.

[25] Rodriguez, J. A.; Chaturvedi, S.; Kuhn, M.; Hrbek, J., Reaction of H2S and S2 with Metal/Oxide Surfaces: Band-Gap Size and Chemical Reactivity. *The Journal of Physical Chemistry B* **1998,** *102* (28), 5511-5519.

[26] Busca, G.; Rossi, P. F.; Lorenzelli, V.; Benaissa, M.; Travert, J.; Lavalley, J. C., Microcalorimetric and Fourier transform infrared spectroscopic studies of methanol adsorption on alumina. *The Journal of Physical Chemistry* **1985,** *89* (25), 5433-5439.

[27] Lavalley, J. C., Infrared spectrometric studies of the surface basicity of metal oxides and zeolites using adsorbed probe molecules. *Catalysis Today* **1996,** *27* (3), 377-401.

[28] Busca, G.; Forzatti, P.; Tronconi, E.; Lavalley, J. C., A TPD, FT-IR and Catalytic Study of the Interaction of Methanol with Pure and KOH DOPED TiO2 Anatase. In *Studies in Surface Science and Catalysis*, Imelik, B.; Naccache, C.; Coudurier, G.; Taarit, Y. B.; Vedrine, J. C., Eds. Elsevier: 1985; Vol. 20, pp 15-24.

[29] Scokart, P. O.; Amin, A.; Defosse, C.; Rouxhet, P. G., Direct probing of the surface properties of alkali-treated aluminas by infrared and x-ray photoelectron spectroscopy. *The Journal of Physical Chemistry* **1981,** *85* (10), 1406-1412.

[30] Montagne, X.; Durand, C.; Mabilon, G., Influence of the Operating Conditions on the Morphology and Acidity of K2CO3/γ Al2O3. In *Studies in Surface Science and Catalysis*, Imelik, B.; Naccache, C.; Coudurier, G.; Taarit, Y. B.; Vedrine, J. C., Eds. Elsevier: 1985; Vol. 20, pp 33-43.

3.8 Supporting Information

S.1 Characterization

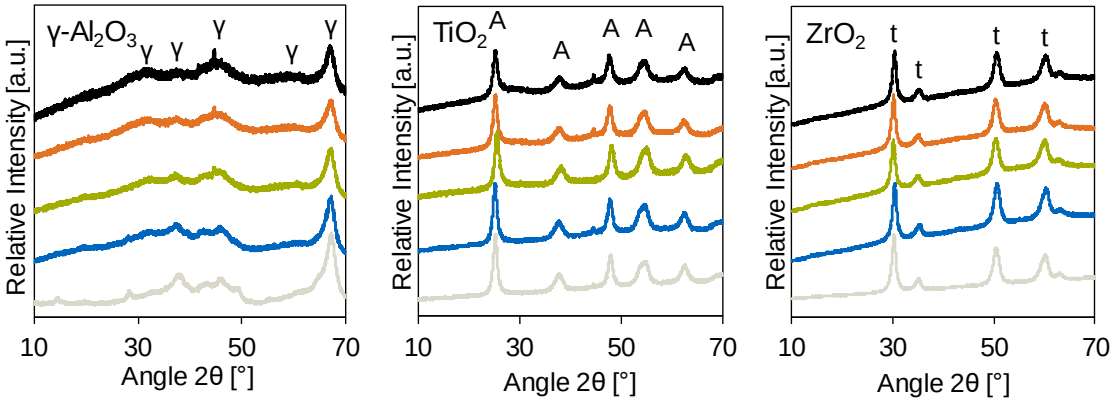

FigureS3.1: XRD pattern of Cs loaded metal oxides: pure metal oxide (grey), 5 wt.% (blue), 10wt% (green), 15 wt.% (orange), 20 wt.% (black).

Table S3.1 Assignments of pyridine adsorption bands on metal oxides.

	Wavenumber [cm^{-1}]	Vibration	Surface species
γ-Al_2O_3[1]	1620	$8a_{LAS,strong}$	Al^{IV}
	1612	$8a_{LAS,weak}$	Al^{IV}-Al^{VI}
	1593	$8a_H$	x-OH
	1573	8b	All Al + x-OH
	1450	$9b_{LAS}$	All Al
	1440	$9b_H$	x-OH
ZrO_2[2]	1604	$8a_{LAS,weak}$	Zr^{IV}
	1593	$8a_H$	x-OH
	1573	8b	Zr^{IV} and x-OH
	1445	9b	Zr^{IV}
TiO_2[2]	1604	$8a_{LAS,weak}$	Ti^{IV}
	1591	$8a_H$	x-OH
	1573	8b	Ti^{IV} and x-OH
	1445	9b	Ti^{IV}

Martin, C.; Martin, I.; Delmoral, C.; Rives, V., FT-IR Assessment Through Pyridine Adsorption of the Surface Acidity of Alkali-Doped MoO3/TiO2. *Journal of Catalysis* **1994,** *146* (2), 415-421.

Busca, G.; Ramis, G., FT-IR study of the surface properties of K2O-TiO2. *Applied Surface Science* **1986,** *27* (1), 114-126.

Table S3.2 Assignments of pyridine adsorption bands on Cs doped metal oxides.

	Wavenumber [cm^{-1}]	Vibration	Surface species
$Cs(10)/\gamma\text{-}Al_2O_3$	1612	$8a_{LAS,strong}$	$Al^{IV}\text{-}Al^{VI}$
	1583	$8a_{Cs}$	Cs^+
	1573	8b	$Al^{IV}\text{-}Al^{VI} + Cs^+$
	1450	$9b_{LAS}$	$Al^{IV}\text{-}Al^{VI}$
	1440	$9b_{Cs}$	Cs^+
$Cs(20)/\gamma\text{-}Al_2O_3$	1612	$8a_{LAS,strong}$	$Al^{IV}\text{-}Al^{VI}$
	1602	$1 + 6a_{Cs}$	Cs^+
	1583	$8a_{Cs}$	Cs^+
	1573	8b	$Al^{IV}\text{-}Al^{VI} + Cs^+$
	1450	$9b_{LAS}$	$Al^{IV}\text{-}Al^{VI}$
	1440	$9b_{Cs}$	Cs^+
$Cs(10)/ZrO_2$	1602	$1 + 6a_{Cs}$	Cs^+
	1583	$8a_{Cs}$	Cs^+
	1573	$8b_{Cs}$	Cs^+
	1440	$9b_{Cs}$	Cs^+
$Cs(20)/ZrO_2$	1602	$1 + 6a_{Cs}$	Cs^+
	1583	$8a_{Cs}$	Cs^+
	1573	$8b_{Cs}$	Cs^+
	1440	$9b_{Cs}$	Cs^+
$Cs(10)/TiO_2$	1604	$1 + 6a_{Cs}$	Cs^+
	1583	$8a_{Cs}$	Cs^+
	1573	$8b_{Cs}$	Cs^+
	1440	$9b_{Cs}$	Cs^+
$Cs(20)/TiO_2$	1602	$1 + 6a_{Cs}$	Cs^+
	1583	$8a_{Cs}$	Cs^+
	1573	$8b_{Cs}$	Cs^+

Martin, C.; Martin, I.; Delmoral, C.; Rives, V., FT-IR Assessment Through Pyridine Adsorption of the Surface Acidity of Alkali-Doped MoO3/TiO2. *Journal of Catalysis* **1994,** *146* (2), 415-421.

Busca, G.; Ramis, G., FT-IR study of the surface properties of K2O-TiO2. *Applied Surface Science* **1986,** *27* (1), 114-126.

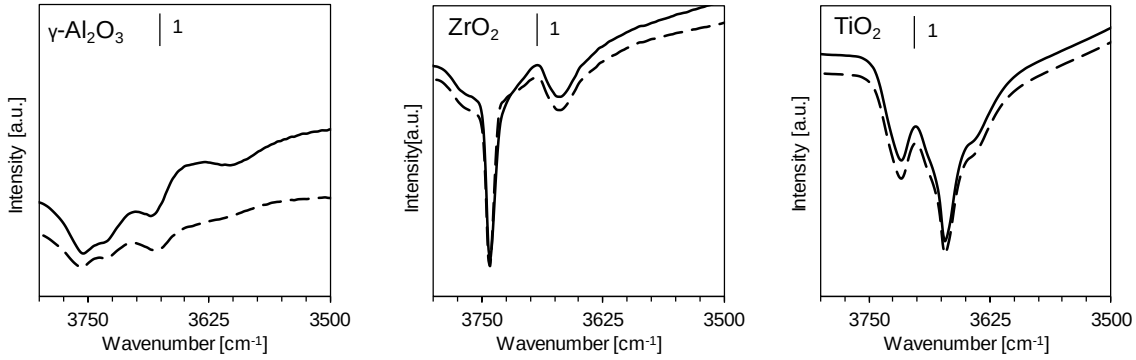

Figure S3.2: Difference spectra of the OH vibration region for γ-Al_2O_3, TiO_2 and ZrO_2 at 50 °C, at 0.1 mbar pyridine pressure (solid line) and after evacuation at 10^{-7} mbar (dashed line).

Table S3.3: Assignments of CO adsorbed on metal oxides and Cs doped equivalents.

	Metal oxides				10wt% Cs				20wt% Cs			
	CO_{LAS}	CO_{OH}	CO_{Cs+}	CO_{phys}	CO_{LAS}	CO_{OH}	CO_{Cs+}	CO_{phys}	CO_{LAS}	CO_{OH}	CO_{Cs+}	CO_{phys}
γ-Al_2O_3	2188	2150	-	-	2179	-	2146	2136	-	-	2146	2136
ZrO_2	2177	2154	-	-	-	-	2144	2136	-	-	-	-
TiO_2	2181	2150	-	-	-	-	2144	2138	-	-	2144	2133

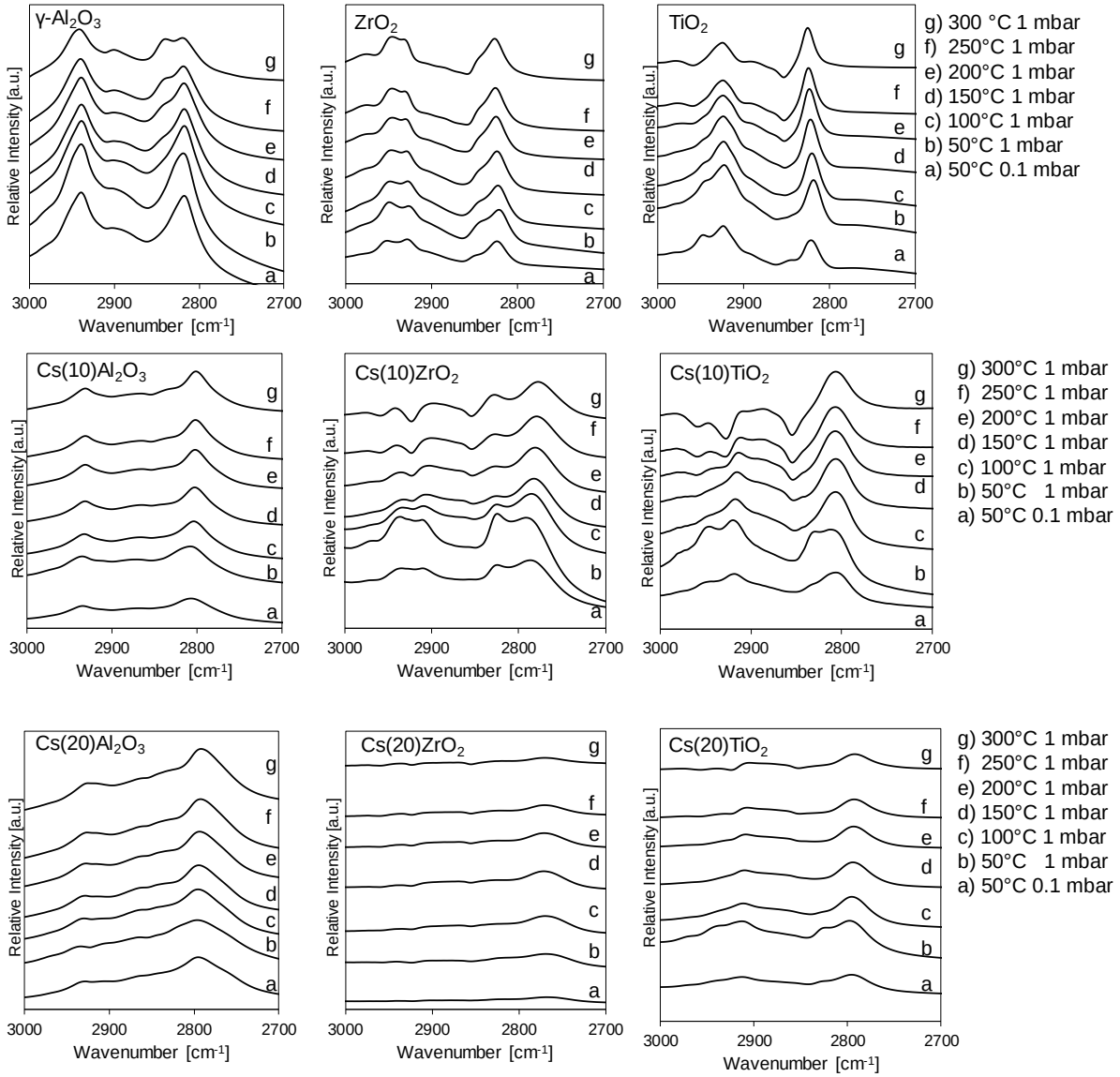

Figure S3.3 Methanol adsorption on all tested catalysts using different methanol partial pressure and Temperature in C-H stretching vibration region.

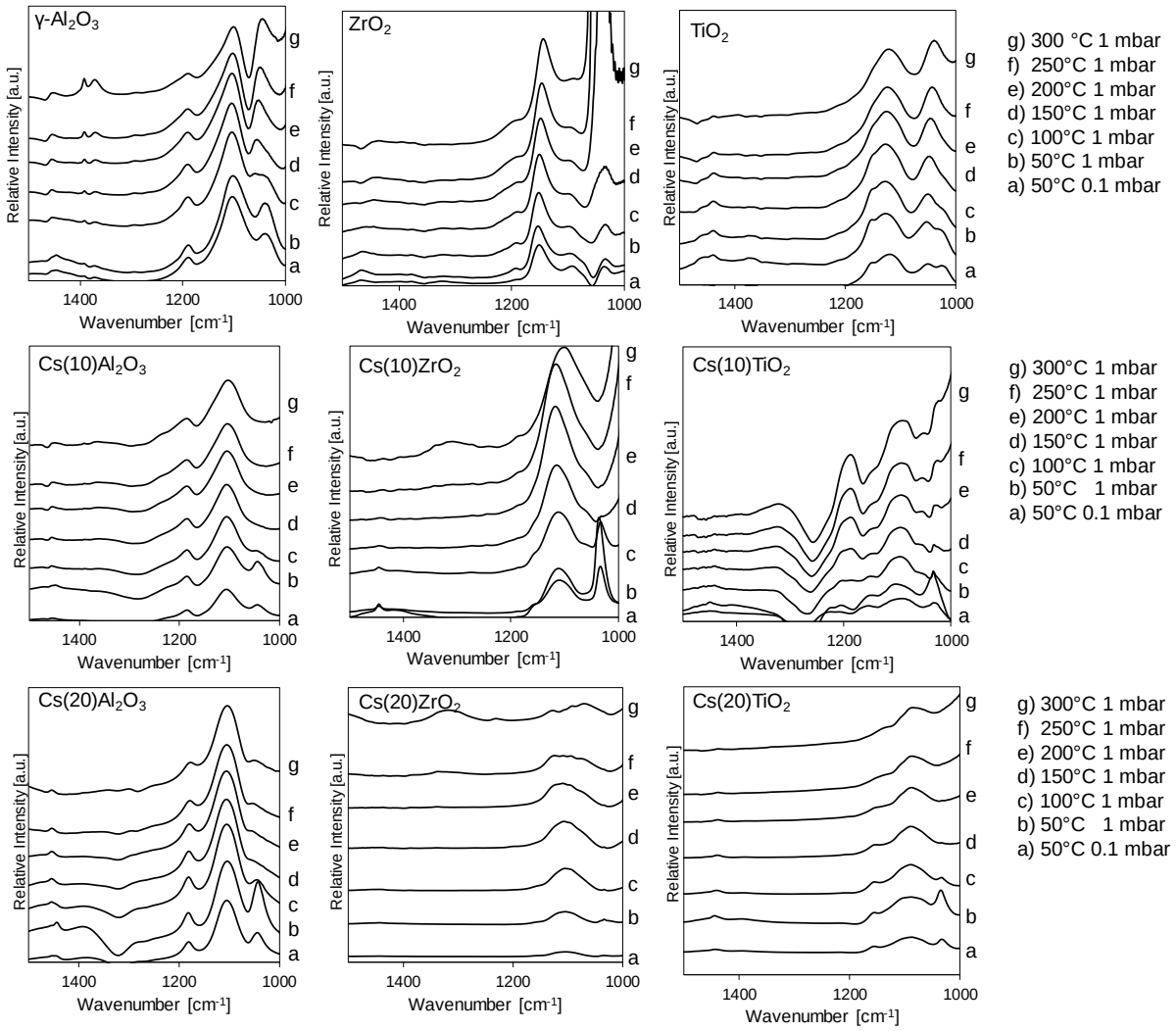

Figure S3.4. Methanol adsorption on all tested catalysts using different methanol partial pressure and Temperature in C-H bending vibration region.

S.2 Catalytic testing

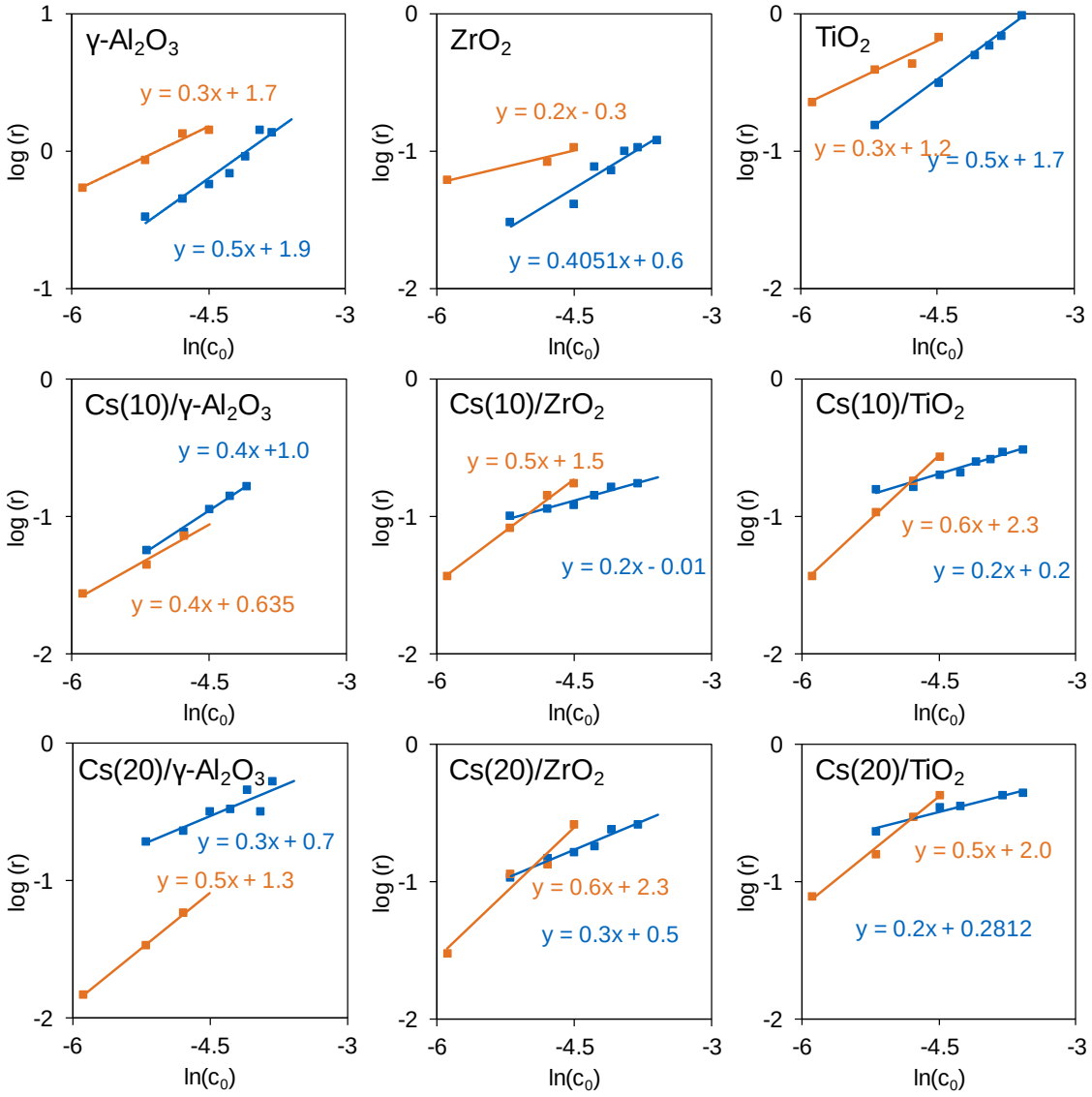

Figure S3.5 Dependency of methanethiol formation rate on concentration of H_2S (orange) and CH_3OH (blue) in mol/l at 360 °C and total pressure of 9 bar.

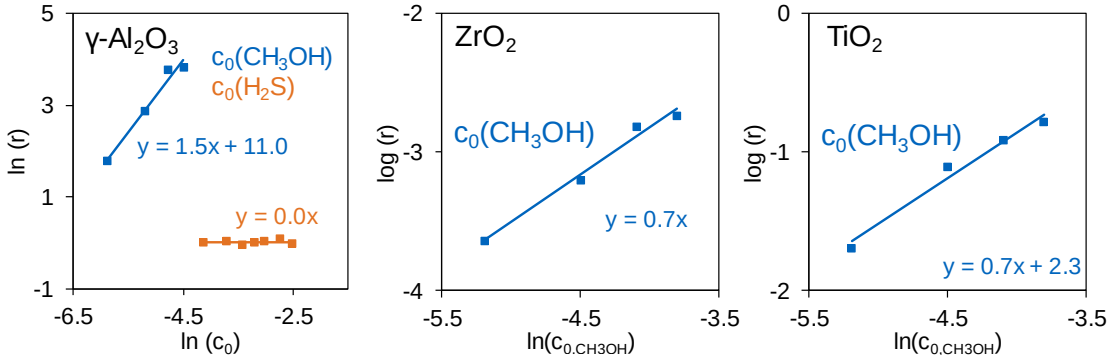

Figure S3.6 Dependency of DME formation rate on concentration of H_2S (orange; only γ-Al_2O_3) and CH_3OH (blue; γ-Al_2O_3, ZrO_2 and TiO_2) in mol/l at 360 °C and total pressure of 9 bar.

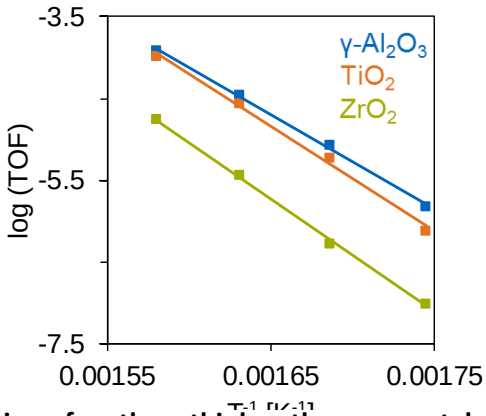

Figure S3.7 TOF for the formation of methanethiol on the pure metal oxides at 360°C, 9 bar.

4. Cesium modified Zeolites as thiolation catalysts

This chapter is based on a manuscript from

M. Weber-Stockbauer, O.Y. Gutiérrez Tinoco, R. Bermejo-Deval, J.A. Lercher[a]

which is planned to be submitted in a peer-review journal.

[a] M.W.-S. planned, designed and conducted the experiments, analyzed and interpreted the data and wrote the manuscript. R.B.-D., O.Y.G. and J.A.L. contributed to the discussion of the results and the correction of the manuscript anytime.

4.1. Abstract

Cs supported on zeolites were studied as catalysts for the selective thiolation of methanol. Next to Cs loading over impregnation, ion exchanged zeolites, providing single cation Cs sites were synthesized to study the catalytic behavior of such species, compared to the Cs phase formed by impregnation. Monitoring the acid-base properties via pyridine adsorption and evaluating the reaction kinetics we found that: Single Cs sites are not active in the bimolecular methanol thiolation; while the activity on those ion-exchanged systems is based on the presence of extra framework alumina and, as we suppose, in situ formed Cs clusters and BAS. Comparing an impregnated Cs zeolite to a benchmark catalyst show lower activity due to a lower ability to disperse Cs and selectivity (presence of extra framework alumina) on the Cs zeolite.

4.2 Introduction

Synthetic amino acids are largescale basic compounds for the pharmaceutic and nutrition industry. Next to glutamic acid, methionine is the amino acid with the second-largest volume produced per year (450 000 t a^{-1}). The main process for the industrial production of methionine is the so-called Degussa process, starting from methanethiol and acrolein. Methanethiol is produced over the catalytic thiolation of methanol with H_2S, using $CsWS_2/Al_2O_3$ as catalyst.[1] As recently shown, the formation of methanethiol is happens on solely basic sites.[2] For a better understanding of the mechanism, single Cs sites, as obtained in exchanged zeolites are studied and compared to impregnated Cs zeolite. Monitoring the acid-base properties via pyridine adsorption and evaluating the reaction kinetics will show potential of such catalysts for the methanol thiolation.

4.3 Experimental

4.3.1 Catalyst preparation

4.3.1.1 Synthesis of Cs loaded BEA catalysts

HBEA (Südchemie) with a Si/Al ratio of 12.5 was used as support for Cs. Two different methods were used to load Cs: Ion exchange and incipient wetness impregnation.

For a completely ion exchanged zeolite Cs(IE)/HBEA, 1.6 g of zeolite were added to 40 ml of an aqueous 0.25 M cesium acetate solution. After stirring for 8 hours the zeolite was separated from the solution by centrifugation; the procedure was repeated twice. Afterwards the ion exchanged zeolite was washed with double deionized water three times.

Cs(IWI)/HBEA was prepared by incipient wetness impregnation, using an aqueous solution of cesium acetate, added dropwise to the agitated solid. 245.9 mg of Cs acetate (Sigma Aldrich, ≥99.99%) were dissolved in 0.5 mL H_2O per 1 g of support targeting a Cs loading of 14 wt.%. The impregnated metal oxides were dried over night at 70 °C and successively calcined (0.5 °C min^{-1}, 400 °C, 2 h, in flowing synthetic air, 100 ml min^{-1}). All samples were activated by treatment in H_2S with flow rate of 20 ml/min at 360 °C for 2 hours.

4.3.1.2 Synthesis of Cs exchanged MFI zeolites

To further study the behavior of single Cs sites in the thiolation reaction and exclude effects of extra framework alumina, MFI type zeolites with a parent Si/Al ratio in the range of 12.5–100 were prepared by hydrothermal synthesis. For the synthesis of MFI zeolite with a Si/Al ratio of 12.5, 27.10 g (130 mmol) of tetraethyl orthosilicate, 5.29 g (26 mmol) of tetrapropyl ammonium hydroxide and 0.852 g (10.4 mmol) of sodium aluminate were added to 27.0 g of H_2O under stirring. For the other zeolites, the mass of sodium aluminate was different. That is, 0.426 g (5.2 mmol) for Si/Al = 25, 0.950 g (2.6 mmol) for Si/Al = 50 and 0.106 g (1.3 mmol) for Si/Al =

100.

After aging over night at room temperature the gel-containing liners, were placed in a rotating autoclave for 72 h (170 °C and 30 rpm). Afterwards the zeolites were washed three times with 100 mL deionized water, dried over night at 70 °C and calcined in a constant flow of synthetic air (10 °C min^{-1} up to 550 °C, for 8 h, synthetic air 100 mL min^{-1}). The obtained NaMFI zeolites were treated according to the method reported by Schallmoser et al.[3] The sodium containing zeolites were transformed into the ammonia form by stirring each 1 g of Na-zeolite for 2 h in 150 mL of an aqueous 1 M NH_4NO_3 solution at 80 °C. The procedure was repeated two times. The NH_4MFI samples were treated with 40 mL of an aqueous solution of $(NH_4)_2SiF_6$ (AHFS) per 1 g catalyst at 80°C for 5 h to remove the Lewis acid sites (LAS). A fourfold excess of AHFS to the Al content of the prepared zeolites was used: 5.812 g (41.9 mml) for MFI (Si/Al = 12.5), 2.906 g (21.0 mmol) for MFI (Si/Al = 25), 1.453 g (10.5 mmol) for MFI (Si/Al = 50) and 0.727 g (5.2 mmol) for MFI (Si/Al = 100). After the treatment the samples were washed 6 times in 80 °C hot water and calcined (550 °C, 10°C min^{-1}, 6 h, 100 mL min^{-1} synthetic air).

For exchange of ammonia against cesium, 1 g of the NH_4-MFI was stirred three times for 8 h in 50 mL of an aqueous 0.1 M $CsNO_3$ solution. Afterwards, the solid was washed with water and dried at 120 °C for 2 h. Finally, the Cs-zeolites were calcined (10 °min^{-1} up to 550 °C, for 8 h, synthetic air 100 mL min^{-1}).

4.3.2 Chemical and physicochemical characterization

The elemental composition of the prepared materials was determined by AAS. The measurements were performed on an *UNICAM 939 AA*-Spectrometer. XRD patterns were collected with a Philips X'Pert System (Cu Kα radiation, 0.1542 nm) operating at 45 kV/40 mA, using a nickel Kβ-filter and solid-state detector (X'Celerator). The measurements were carried out with a step size of 0.017° and scan time of 0.31 s per step. To determine the concentration of acid sites on the catalysts, pyridine adsorption was performed and monitored via IR, using a *Nicolet 5700* FT IR spectrometer. The samples were pressed into self-supporting wafers with a mass of around 20 mg. Before the adsorption of pyridine, the sample was activated for one hour at 450 °C at 10^{-5} mbar, with a heating ramp of 10 °C min^{-1}. Adsorption of 0.5 mbar pyridine was done at 50 °C. In order to remove physisorbed pyridine, desorption took place for 1 h at 10^{-5} mbar at 50 °C. All spectra were taken at 50 °C with a resolution of 4 cm^{-1}.

4.3.3 Catalytic testing

Before the reaction, 125.0 mg of catalyst (125-250 µm), diluted in 1 g of SiC, were sulfided in a flow of 20 mL min^{-1} H_2S at 360 °C and 9 bar. The reaction was performed with a flow of gaseous methanol of 10 mL min^{-1} mixed with H_2S (20 mL min^{-1}) and N_2 (20 mL min^{-1}). After stabilizing for 2 h, the reaction was performed at 360 °C for 7 h. Subsequently, the temperature was stepwise decreased to 340 °C, 320 °C, and 300 °C, holding every temperature for 5 h.

The product flow was periodically analyzed on-line with a *Shimadzu GC-2014* equipped with a HP-PLOT Q column (2.7 m, 2.0 mm inner diameter), using a TCD detector. Reaction rate constants were calculated using the integrated rate law for a reaction being 0.5 in H2S and methanol.

4.4 Results and Discussion

4.4.1 Physicochemical properties

The XRD patterns of all prepared Cs/zeolite catalysts are shown in Figure 4.1. For the commercial HBEA, no changes in the XRD pattern are visible, comparing the parent to the two different loaded samples, showing that the loading and the succeeding calcination procedure did not affect the HBEA framework. For the sake of clarity, only the reflections with the highest intensity were marked, corresponding to the reflections of the [302] (2θ = 22°) plane is shown. [4] For the five Cs exchanged zeolites only the reflections of the MFI framework were observed, showing that the MFI was successfully synthesized and that it was not affected by the chemical (AHFS treatment and Cs exchange) and thermal treatments. Again, only the reflections with the highest intensity were marked, corresponding to the reflections of the [011] (2θ = 7°) and the [051] (2θ = 23°) plane of the MFI framework.[5] To check the stability of the Cs/MFI catalysts in the thiolation reaction, the XRD patterns of Cs/MFI (Si/Al = 25) before and after the reaction are shown. Except the additional reflections of SiC (needed to pack the reactor), the XRD patterns remained constant showing that the zeolite structure is stable under the reaction conditions.

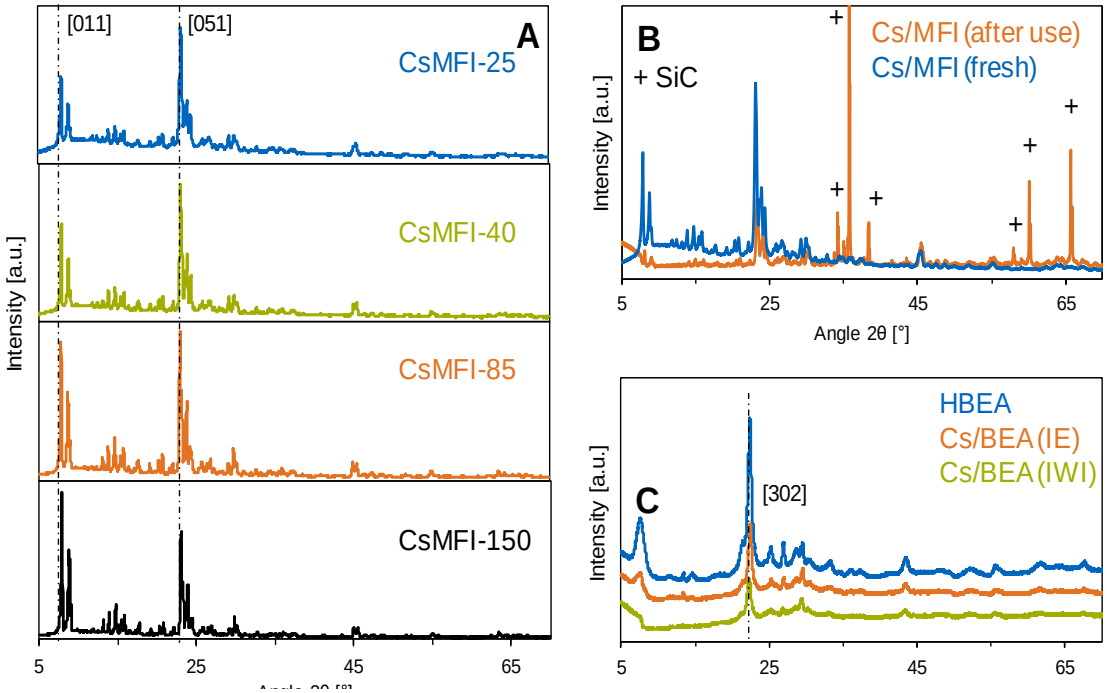

Figure 4.7 XRD patterns of Cs loaded zeolites. A) Cs exchanged MFI; the marked reflections correspond to the [011] and [051] planes. [2], B) Pure HBEA and loaded with Cs via ion exchange (Cs(IE)/HBEA and incipient wetness impregnation (Cs(IWI)/HBEA, the marked reflections correspond to the [302] plane [3], C) Cs/MFI-25 before (blue) and after reaction (orange), reflection patterns of the used catalyst show SiC used as catalyst diluent, marked as +.

.

The results of the elemental analysis of Cs loaded zeolites are shown in Table 4.1. The Cs content of Cs(IWI)/HBEA is close to the desired value of 14 wt.%. For Cs(IE)/HBEA Cs loading of 6.2 wt.% was obtained. This is only 40 % of the value, expected under the estimation that all aluminum of the zeolite forms BAS which are fully exchanged with Cs (14 wt.%). This could be explained that not all Al cations form BAS, due to the formation of Lewis acidic extra framework alumina or that not all BAS were exchanged. For the Cs/MFI zeolites, a Si/Al ratio of around 1 was obtained for all zeolites, indicating that all Cs^+ in the zeolite is associated to a Al^{3+} site (Brønsted acid site prior to ion exchange), without significant agglomeration of Cs within the pores (which would have resulted in Cs/Al molar ratios above 1). Not-exchanged Brønsted acid sites (BAS) or extra-framework alumina (EFA) remained in the zeolite are not likely, as both cases would decrease the Cs/Al ratio. Therefore, we conclude that both, the removal of EFA and the Cs exchange were complete. The Si/Al ratio calculated from the elemental analysis is in the range from 25–152. These ratios are higher than the expected Si/Al ratios (in the range of 12.5–100) due to the removal of alumina during the AHFS treatment. The Cs loading for the zeolites was in the range from 7.1 wt.% for Cs/MFI with Si/Al = 25 to 1.4 wt.% for Cs/MFI with Si/Al = 150.

Table 4.1 Elemental analysis of Cs loaded zeolites.

Catalyst	Cs loading [wt.%]	Cs content [mmol g^{-1}]	Al content [mmol g^{-1}]	Cs/Al ratio	Si/Al ratio
Cs(IE)/HBEA	6.2	0.46	1.2*	0.4	-
Cs(IWI)/HBEA	12.6	0.94	1.2*	0.8	-
Cs/MFI-25	7.1	0.53	0.60	0.9	25
Cs/MFI-40	5.1	0.38	0.40	1.0	39
Cs/MFI-85	2.3	0.17	0.19	0.9	84
Cs/MFI-150	1.4	0.11	0.11	1.0	152

*theoretical value, not measured

Pyridine adsorption on HBEA, ion exchanged HBEA and CS/MFI samples is shown in Figure 4.2. For the HBEA samples, the shown spectra were recorded at 150 °C, after evacuation. On the parent HBEA, the typical signals of pyridine adsorbed on LAS (1450 cm^{-1}), respectively BAS (1550 cm^{-1}) are detected.[6] In contrast, the signal of BAS is not detectable, while a minor signal of LAS is observed. Those changes confirm the exchange of the protons on BAS against Cs. The acid site concentration is 0.48 mmol g^{-1} BAS and 0.41 mmol g^{-1} LAS. Comparing those results to the elemental analysis of Cs, one gets a Cs to BAS ratio close to one, showing that all available BAS were Cs exchanged, while LAS, formed by extra framework alumina are at still present. Therefore we propose that the low Cs content is based on the formation of extra framework alumina, lowering the concentration of exchangeable BAS, forming Lewis acid sites instead.[3] As on all Cs/MFI samples, pyridine signals completely disappeared after evacuation (not shown), the shown spectra were taken at 0.1 mbar of pyridine and a decreased temperature of 50 °C. The absence of any adsorbed pyridine species under vacuum is in line with the of elemental analysis, as the atomic ratio of Cs/Al of 1 hints for full exchange of BAS and absence of extra framework alumina. At 0.1 mbar pyridine pressure, pyridine adsorption on Cs^{+} sites is visible from the signal at 1440 cm^{-1}.[7-9]

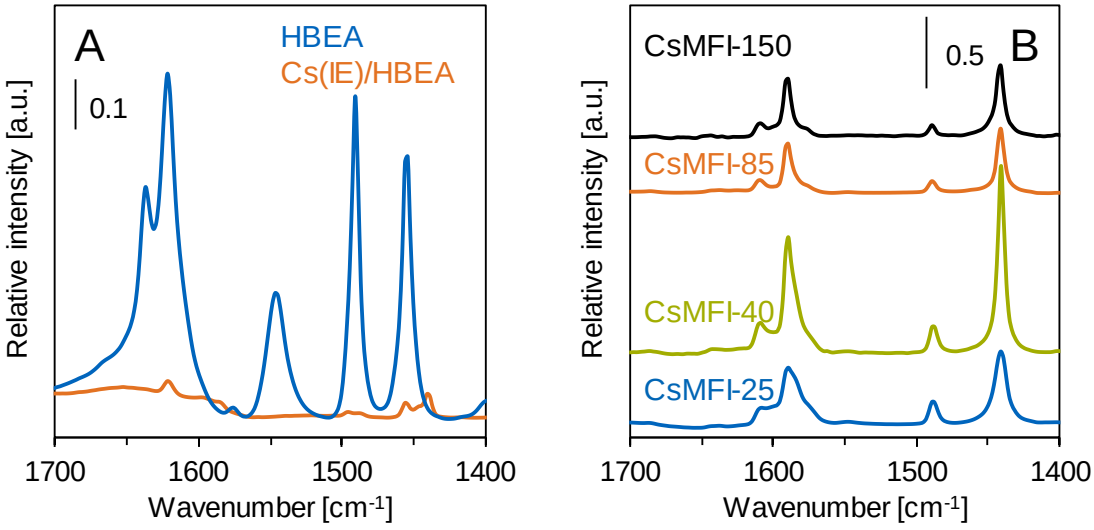

Figure 4.2 Background corrected difference IR spectra of pyridine adsorbed on A) HBEA at 150 °C after evacuation at 10^{-7} mbar, B) Cs/MFI at 50 °C and pyridine partial pressure of 0.1 mbar.

4.4.2 Results for the thiolation of methanol

The catalytic activity of all Cs zeolite samples is given as the initial rate of methanethiol formation in an Arrhenius-type plot (Figure 4.3); the yield and selectivity towards methanethiol and the apparent activation energy are summarized in Table 4.2.

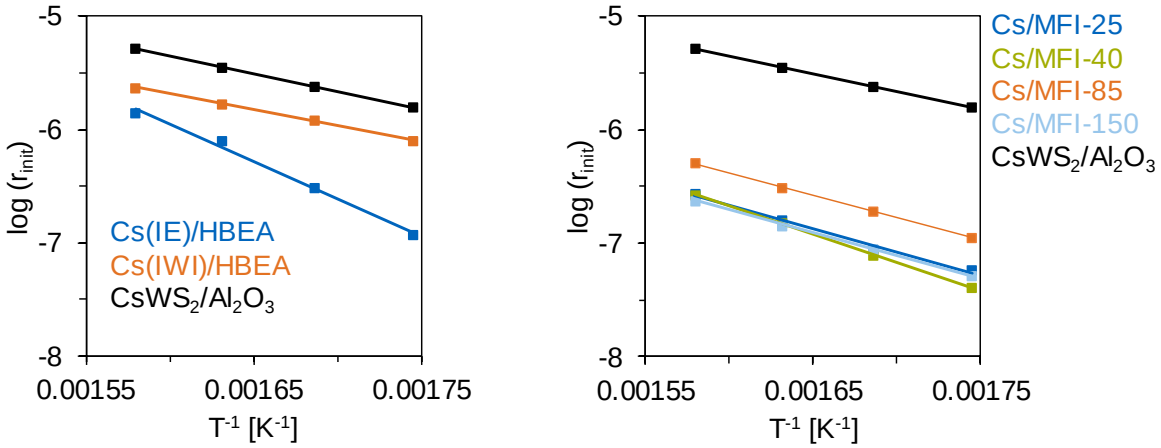

Figure 4.3 Logarithm of initial rate of methanethiol formation on A) Cs/HBEA and B) Cs/MFI catalysts at 300-360°C, 9 bar total pressure. Thiol formation rates on $CsWS_2/Al_2O_3$ for benchmarking were taken from a previous study. [1]

To compare the catalytic performance of the Cs zeolite catalysts, the data for $CsWS_2/Al_2O_3$, studied in a previous work are used.[2] For the two different Cs/HBEA samples, Cs(IWI)/HBEA higher activity and a lower apparent activation (54 to 126 kJ mol^{-1}), compared to Cs(IE)/HBEA, with selectivity to methanethiol (at 360 °C) also higher in Cs(IWI)/HBEA (85.5%) than on Cs(IE)/HBEA (76.6%). These results give a clear insight on the different active sites present on those two catalysts. Activation energy of 126 kJ mol^{-1} on Cs(IE)/HBEA is comparable to values, obtained on pure metal oxide catalysts, while the apparent activation energy of 54 kJ mol^{-1} is comparable to $CsWS_2/Al_2O_3$ (67 kJ mol^{-1}).[2] At 360 °C the rates for methanethiol formation are factor 2 (Cs(IWI)/HBEA), respectively factor 4 ($Cs(IE)/Al_2O_3$) lower compared to $CsWS_2/Al_2O_3$. From these results we suppose that on Cs(IWI)/HBEA methanethiol is formed over Cs based sites, while on Cs(IE)/HBEA LAS, formed by extra framework alumina are responsible for the methanethiol formation. Cs located on former BAS seems to be not active for the reaction; taking into account that a bimolecular reaction mechanism, involving two active sites, this seems reasonable. From the higher activity of $CsWS_2/Al_2O_3$ compared to $Cs(IWI)/Al_2O_3$ compared to, both with comparable Cs loading, compared to Cs on HBEA.

All Cs/MFI catalysts were at least one order of magnitude less active, compared to $CsWS_2/Al_2O_3$, while no correlation between the Cs content and the catalyst activity or selectivity was observed. As shown in Figure 4.1 the zeolite framework is stable under reaction conditions, therefore a collapse of the framework is excluded as a reason for the low catalytic activity. As for Cs(IE)/HBEA we assume, that the low activity of these catalysts is based on the atomic dispersion of Cs^+ in the MFI framework. A single Cs^+ cation is not able to activate two

molecules, methanol and H_2S, suppressing the methanol thiolation. The appearance of DME as the only major product (Table S4.1), next to methanethiol, shows that the acid properties of the catalyst changes during the reaction, as pyridine adsorption only showed the presence of low Lewis acidic Cs sites. These changes can also explain the fact why the catalyst is active at all for methanol conversion, respectively methanethiol formation. While a single Cs site is not active, agglomeration to larger Cs clusters can create new active sites, releasing also the BAS, being attached to Cs before, which can act as active site. The apparent activation energies are comparable to the one obtained for $CsWS_2/Al_2O_3$, implying that indeed Cs clusters are responsible for methanethiol formation, while DME could be formed on the in situ formed BAS.[10]

Table 4.2: Catalytic thiolation of methanol on Cs loaded zeolites, with the conversion of methanol (X_{MeOH}), Yield of methanethiol (Y_{MeSH}), selectivity S to methanethiol (S_{MeSH}), methanethiol formation rate $r_{360°C}$ and apparent activation energy E_{app}.

Catalyst	Cs content [mmol g^{-1}]	$r_{360°C}$ [mmol $g^{-1}s^{-1}$]	$E_{a,app}$ [kJ mol^{-1}]	$X_{MeOH360°C}$ [%]	$Y_{MeSH360°C}$ [%]	$S_{MeSH360°C}$ [%]
Cs(IWI)/HBEA	0.46	$2.3\ 10^{-6}$	54	21.3	18.2	85.5
Cs(IE)/HBEA	0.94	$1.4\ 10^{-6}$	126	14.7	11.3	76.6
Cs/MFI-25	0.53	$2.7\ 10^{-7}$	79	7.8	2.3	29.3
Cs/MFI-40	0.38	$2.7\ 10^{-7}$	94	2.5	2.2	89.3
Cs/MFI-85	0.17	$5.2\ 10^{-7}$	75	5.5	4.3	77.6
Cs/MFI-150	0.11	$2.4\ 10^{-7}$	76	6.1	2.0	32.9
$CsWS_2/Al_2O_3$[57]	1.08	$5.2\ 10^{-6}$	76	40.3	37.5	93.0

4.5 Conclusion

Catalysts with single Cs sites, as in Cs-exchanged zeolites, showed low activity for the thiolation reaction. As shown, in ion exchanged HBEA, extra framework alumina acts as active site for methanethiol formation, while the single Cs sites seem to be inactive for the reaction. This is further proofed by using Cs/MFI, where extra framework alumina was removed by AHFS treatment. All of those catalysts exhibit only minor activity for methanol conversion at all. As no relation between Cs site concentration and activity was observed, the low activity for methanethiol and DME formation is assumed to be not related to single Cs sites, but to Cs clusters and BAS formed during activation.

Cs supported on HBEA over incipient wetness impregnation resulted in a catalyst showing lower activity and selectivity, compared to a benchmark $CsWS_2/Al_2O_3$. We assume that on WS_2/Al_2O_3 higher Cs dispersion is achieved, leading to higher activity, compared to Cs on HBEA. The lower selectivity on the latter can be explained by the present of extra framework alumina, on which DME can be formed.

4.6 Literature

[1] M. Breuer, K. Ditrich, T. Habicher, B. Hauer, M. Keßeler, R. Stürmer, T. Zelinski, Industrial Methods for the Production of Optically Active Intermediates, Angewandte Chemie International Edition, 43 (2004) 788-824.

[2] M. Weber-Stockbauer, O.Y. Gutiérrez Tinoco, R. Bermejo-Deval, J.A. Lercher, The role of weak Lewis acid sites for methanol thiolation, Catalysis Science & Technology, (2019).

[3] S. Schallmoser, T. Ikuno, M.F. Wagenhofer, R. Kolvenbach, G.L. Haller, M. Sanchez-Sanchez, J.A. Lercher, Impact of the local environment of Brønsted acid sites in ZSM-5 on the catalytic activity in n-pentane cracking, Journal of Catalysis, 316 (2014) 93-102.

[4] A. Simon-Masseron, J.P. Marques, J.M. Lopes, F.R. Ribeiro, I. Gener, M. Guisnet, Influence of the Si/Al ratio and crystal size on the acidity and activity of HBEA zeolites, Applied Catalysis A: General, 316 (2007) 75-82.

[5] H. van Koningsveld, H. van Bekkum, J.C. Jansen, On the location and disorder of the tetrapropylammonium (TPA) ion in zeolite ZSM-5 with improved framework accuracy, Acta Crystallographica Section B, 43 (1987) 127-132.

[6] S.M. Maier, A. Jentys, J.A. Lercher, Steaming of Zeolite BEA and Its Effect on Acidity: A Comparative NMR and IR Spectroscopic Study, The Journal of Physical Chemistry C, 115 (2011) 8005-8013.

[7] C. Morterra, A. Chiorino, G. Ghiotti, E. Fisicaro, Spectroscopic study of anatase properties. Part 5.—Surface modifications caused by K2O addition, Journal of the Chemical Society, Faraday Transactions 1: Physical Chemistry in Condensed Phases, 78 (1982) 2649-2659.

[8] C. Martin, I. Martin, C. Delmoral, V. Rives, FT-IR Assessment Through Pyridine Adsorption of the Surface Acidity of Alkali-Doped MoO3/TiO2, Journal of Catalysis, 146 (1994) 415-421.

[9] G. Busca, G. Ramis, FT-IR study of the surface properties of K2O-TiO2, Applied Surface Science, 27 (1986) 114-126.

[10] S.R. Blaszkowski, R.A. van Santen, The Mechanism of Dimethyl Ether Formation from Methanol Catalyzed by Zeolitic Protons, Journal of the American Chemical Society, 118 (1996) 5152-5153.

4.7 Supporting information

Table S4.1 Conversion, yield and selectivity of all tested Cs zeolite samples, between 300 and 360 °C.

	Temperature [°C]	X(CH_3OH) [%]	Y(CH_3SH) [%]	Y(DME) [%]	Y(DMS) [%]	S(CH_3SH) [%]	S(DME) [%]	S(DMS) [%]
Cs(IWI)/HBEA	360	21.3	18.2	0.5	2.4	85.5	2.5	11.2
	340	15.3	13.6	0.4	1.3	89.2	2.4	8.5
	320	10.5	9.8	0.2	0.6	92.9	1.8	5.7
	300	6.8	6.5	0.1	0.2	95.3	1.3	3.4
Cs(IE)/HBEA	360	14.7	11.3	2.0	1.3	76.6	13.4	9.1
	340	8.6	6.5	1.5	0.6	75.9	17.0	7.1
	320	3.3	2.5	0.7	0.1	77.2	22.4	2.9
	300	1.3	1.0	0.3	0.0	76.9	22.4	0.4
Cs/MFI-25	360	7.8	2.3	5.3	0.2	29.3	68.4	2.4
	340	4.9	1.4	3.5	0.1	28.0	70.8	1.2
	320	2.6	0.8	1.8	0.0	29.4	70.6	0.0
	300	1.4	0.5	0.9	0.0	34.8	65.2	0.0
Cs/MFI-40	360	2.5	2.2	0.3	0.0	89.3	10.2	0.5
	340	1.4	1.3	0.1	0.0	92.9	7.1	0.0
	320	0.7	0.7	0.0	0.0	100.0	0.0	0.0
	300	0.3	0.3	0.0	0.0	100.0	0.0	0.0
Cs/MFI-85	360	5.5	4.3	1.0	0.2	77.6	19.0	3.3
	340	3.2	2.6	0.5	0.1	81.3	16.2	2.0
	320	1.9	1.6	0.3	0.0	85.9	14.1	0.0
	300	1.1	1.0	0.2	0.0	83.4	16.6	0.0
Cs/MFI-150	360	6.1	2.0	3.7	0.3	32.9	60.5	5.1
	340	3.9	1.2	2.6	0.1	31.1	66.3	2.6
	320	2.6	0.8	1.8	0.0	29.2	70.3	0.5
	300	1.6	0.4	1.2	0.0	27.2	72.8	0.0

5. Mg-Al mixed oxides as basic catalysts for the synthesis of methanethiol

This chapter is based on a manuscript from

M. Weber-Stockbauer, Martin Baumgärtl O.Y. Gutiérrez Tinoco, R. Bermejo-Deval, J.A. Lercher[a]

which is has been accepted and is going to be published in Catalysis Letters.

[a] M.W.-S. planned, designed and conducted the experiments, analyzed and interpreted the data and wrote the manuscript, expect for IR studies of adsorbed CO_2, which were done by M.B. and analyzed by R. B.-D.). R.B.-D., O.Y.G. and J.A.L. contributed to the discussion of the results and the correction of the manuscript anytime.

5.1. Abstract

Mixed aluminum–magnesium oxides were studied systematically for the thiolation of methanol with H_2S. We found that these systems surpass the catalytic activity of the current used Cs-catalysts by one order of magnitude. The Mg/Al ratio of the metal oxides had a tremendous effect on the catalytic activity and selectivity of the catalysts. IR studies, combined with temperature programmed desorption of CO_2 showed that decreasing the aluminum content decreases the surface area of the Mg/Al oxides, as well as its acidic properties, increasing the concentration of strong basic sites. The highest rate and selectivity was obtained for equal concentrations of Mg and Al, giving an optimum ratio between basic and weak Lewis acid sites.

5.2. Introduction

Methanethiol is a key intermediate step for the industrial synthesis of methionine.[1] While hydrogenation of carbonyl sulfide represents an effective route for its synthesis [2-5], high selectivity to methanethiol combined with higher rates make methanol thiolation the dominating reaction pathway using catalyst with Cs^+ dispersed on WS_2/Al_2O_3.[1, 6-8]

The dispersed presence of Cs^+ on WS_2/Al_2O_3 leads to high surface basicity. It limits the concentration of strong Lewis acid sites that catalyze the formation of dimethyl ether and increases, in turn, the concentration of moderately strong Lewis acid-base pairs active in methanol thiolation.[1, 6] The addition of Cs^+ on other metal oxide supports, such as titania and zirconia, results in similar activity and selectivity for methanol thiolation (Third chapter of this thesis). These materials show, however, somewhat lower methanethiol formation rates than the current benchmark catalyst. As moderately strong Lewis acid-base pairs have been observed to be the key to high rates and selectivities, we explore here magnesium aluminum mixed oxides that have been known for their high concentration of balanced acid-base pair sites. [9-12]

Thus, the present manuscript explores the catalytic properties of such oxides derived from hydrotalcite for methanol thiolation. Acid sites are probed by IR spectra of adsorbed pyridine, while basic sites are probed by CO_2 adsorption-desorption studies. Equimolar Al and Mg concentrations seem to be optimal for a high methanethiol rate formation, surpassing those observed previously with alkali dispersed on tungsten sulfide and/or metal oxides.

5.3. Experimental

5.3.1. Catalyst preparation

Magnesium-Aluminum mixed oxides with an Aluminum content in between 2.5 mol% and 50 mol% were prepared by co-precipitation in aqueous solution, following the synthesis procedure described by Shen *et al*.[9]. Stoichiometric quantities of $Mg(NO_3)_2$•6 H_2O (*Merck, ACS Reag. Ph. Eur*) and $Al(NO_3)_3$•9 H_2O (*Merck*, ≥ 98.5%) were dissolved in deionized water to form a solution with a total cation concentration of 1 M. A second aqueous solution is prepared by diluting a 25% ammonium hydroxide solution (*Sigma Aldrich,* ≥ 98.5%) with deionized water and adding $(NH_4)_2CO_3$ (*Sigma Aldrich*, ≥ 98.5%), using the relations $n(NH_4OH) = 2.2\ n(Mg^{2+}) + 3.2\ n(Al^{3+})$ and $n(NH_4CO_3) = 0.5\ n(Al^{3+})$. The two solutions were added dropwise simultaneously into a stirring beaker containing 125 mL deionized water over a time of 30 minutes (40°C, keeping pH value constant at 8-9). During the process, a white precipitate was formed. After adding the solutions, the resulting suspension was stirred for another 30 minutes at 40°C. After aging overnight, the precipitate was filtered, washed with deionized water, dried at 70°C and calcined (0.5 °C min^{-1}, 400 °C, 2 h, in a flow of synthetic air, 100 mL min^{-1}).

5.3.2. Physicochemical characterization

The elemental composition of the prepared materials was determined by AAS. The measurements were performed on an *UNICAM 939 AA*-Spectrometer. To determine the textural properties, N_2 physisorption was performed on a *Porous Materials Inc. BET-121* sorptometer. After activation at 250 °C for 2 h under vacuum, N_2 was adsorbed at a temperature of 77.4 K. The surface area was calculated using the BET-method. The crystalline structure of the catalysts was determined by powder X-ray diffraction. XRD patterns were collected with a Philips X'Pert System (Cu Kα 1 radiation, 0.1542 nm) operating at 45 kV/40 mA, using a nickel Kβ-filter and solid-state detector (X'Celerator). The measurements were carried out with a step size of 0.017° (2θ) and scan time of 0.31 s per step.

Basic site characterization was done over adsorption followed by temperature programmed desorption of CO_2, using a flow apparatus equipped with a mass spectrometer (QME 200, Pfeiffer Vacuum). A sample of 100 mg of catalyst was loaded in a quartz reactor and activated in situ under a flow of 10 mL min^{-1} 10% H_2S in N_2 at 360 °C for 0.5 h. CO_2 adsorption took place at 50 °C, after flushing for 1 h with He, flushing 1 vol% CO_2 diluted in He over the sample for 0.5 h. For temperature controlled desorption of CO_2, temperature was increased up to 400 °C with a ramp of 1 °C min^{-1}, monitored via MS.

Pyridine adsorption was performed and monitored via IR, using a *Nicolet 5700* FT IR spectrometer. The samples were pressed into self-supporting wafers with a mass of around 20 mg. Before the adsorption of pyridine, the sample was heated to 360 °C under He flow

(heating ramp of 10 °C min^{-1}) and treated for 0.5 h with a flow of 10 mL min^{-1} of 10 vol% H2S in N_2. To remove physisorbed H_2S, the sample was flushed with He flow of 10 mL min^{-1} for another 15 min, before it was evacuated to 10^{-5} mbar and cooled down to 50 °C. Adsorption of 0.5 mbar pyridine was done at 50 °C. In order to remove physisorbed pyridine, desorption took place for 1 h at 10^{-5} mbar at 50 °C. All spectra were taken at 50 °C with a resolution of 4 cm^{-1}.

IR spectra of the surface carbonate of the mixed oxides were studied using a Bruker IFS 66v/S. The powdered sample was carefully dispersed in isopropanol, dropped on a CaF_2 infrared window, and dried, creating a thin uniform layer. These samples were heated to 400°C for 1h below 10^{-6} mbar (10 °C min^{-1}). The spectra were recorded at 50°C below 10^{-6} mbar.

5.3.3. Catalytic testing and kinetic experiments

Prior reaction, 10.0 mg of catalyst (125-250 µm), diluted in 1 g of SiC, were sulfided in a flow of 20 mL min^{-1} H_2S at 360 °C and 9 bar. To determine activation energies, the reaction was performed with a flow of gaseous methanol of 10 mL min^{-1} mixed with H_2S (20 mL min^{-1}) and N_2 (20 mL min^{-1}), varying the temperature between 300 and 360 °C. Additionally to the Mg-Al-mixed oxide materials, the reaction as performed with γ-Al_2O_3 as benchmark system, its physicochemical properties have been evaluated in a previous work.[63] To compare the selectivity of the different mixed oxides, product yields versus methanol conversion plots were obtained over the whole conversion range at 360 °C, changing the residence time in the range of 0.004 s to 0.4 s. Online analysis of the product flow was done using a *Shimadzu GC-2014* equipped with a HP-PLOT Q column (2.7 m, 2.0 mm inner diameter), using a TCD detector.

5.4. Results and discussion

5.4.1. Physicochemical characterization

The main results of the physicochemical characterizations are shown in Table 5.1. The elemental analysis shows that the Al content of the calcined mixed oxides increases from 17 to 86 mol% (MgAl-17 to MgAl-86), in line with the Al concentration in the solution during co-precipitation. The X-ray diffractograms showed varying crystallinity with the Mg/Al ratio (Figure 5.1). In the low-aluminum mixed oxides (MgAl-17 and MgAl-25) two phases were found, i.e., hydrotalcite (JCPDS 22-700) $MgAl_2O_4$ and a mixed oxide phase Mg(Al)Ox in cubic MgO lattice structure (periclase) (JCPDS 87-0653).[14] Above 25 mol % Al, reflections of hydrotalcite were not observed by X-ray diffraction. In addition, the increase in Al concentration results in broadening of periclase bands, hinting for a higher degree of structural distortion. In MgAl-86 the periclase phase is not observed by means of XRD, reflecting only the diffraction band for γ-Al_2O_3

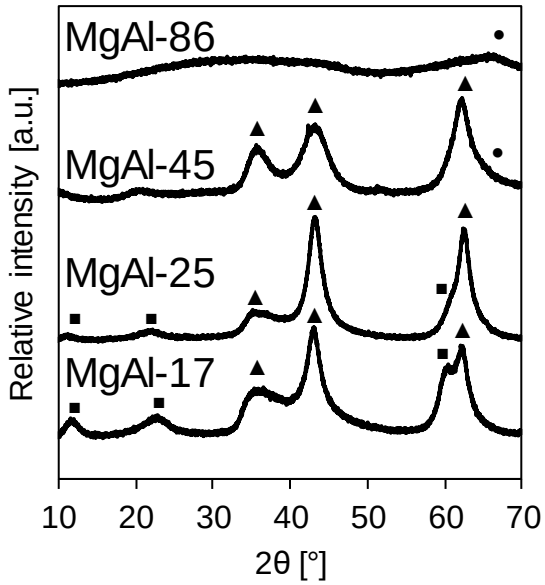

Figure 5.1 XRD patterns of Mg/Al mixed oxides; hydrotalcite (■), periclase (▲), γ-Al_2O_3 (●).

Table 5.1: Results of physicochemical characterization of the MgAl-x materials.

Material	Al/(Al+Mg) [mol%]	Al/Mg [-]	SSA_{BET} [$m^2\ g^{-1}$]	Pore volume [$cm^3\ g^{-1}$]	Uptake $CO_{2,\ High\ T}$ [$\mu mol\ g^{-1}$]	Uptake $CO_{2,\ Low\ T}$ [$\mu mol\ g^{-1}$]	Uptake pyridine [$\mu mol\ g^{-1}$]	Crystalline phases
Al-17	16.9	1:5	<5	n.d.	260	2	-	Hydrotalcite, Periclase
Al-25	24.6	1:3	<5	n.d.	261	19	-	Hydrotalcite, Periclase
Al-45	44.9	2:3	48	0.10	-	38	185	Periclase
Al-86	86.0	6:1	132	0.20	-	11	166	Al_2O_3

The increase in Al concentration led to an increase in surface area and pore volume, increasing the former from less than 5 to 132 m^2/g. SEM micrographs showed a change in the morphology of the Mg/Al mixed oxides with the Al concentration (Figure S1), transitioning from a rough surface with particles between 3-5 µm in diameter to the formation of merged granules that induce cavities of 50 nm or smaller, as in the case of MgAl-86. The formation of these cavities are hypothesized to increase the surface area of the Mg/Al mixed oxide.

The Mg/Al oxides were pre-sulfided and probed with CO_2 at 50°C. Its desorption was measured to determine its basic properties. CO_2 desorption with a maximum at 90 °C, attributed to desorption of physisorbed CO_2, was observed on all samples. On MgAl-17 and MgAl-25 additional desorption maxima were observed at 350 °C and 360 °C (Figure S2) with a concentration of 260 and 261 µmol g^{-1}, respectively This signal is attributed to the loss of carbonates, leading to the formation of MgO on the surface of the mixed oxides.[15]

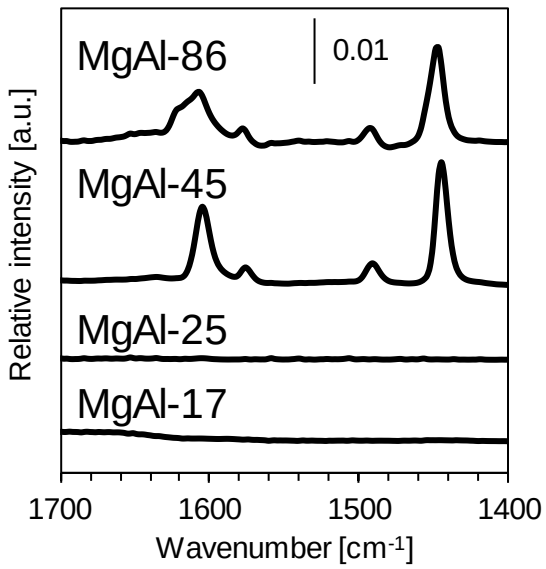

Figure 5.2 Background corrected difference IR spectra of pyridine adsorption at 10-8 mbar after adsorption of 0.1 mbar pyridine at 50 °C for MgAl-17, MgAl-25, MgAl-45 and MgAl-86.

The missing high desorption peak of CO_2 on MgAl-45 and MgAl-86 implies that after sulfidation with H_2S there is no formation of carbonates due to its strong acidic properties.

The IR spectra of the MgAl prior sulfidation showed bands in between 1200-1700 cm^{-1} that are characteristic of the carbonates (Figure S3). The bands at 1530 and 1298 cm^{-1} correspond to the O-C-O antisymmetric and symmetric stretching vibrations of bidentate carbonate, respectively, the bands at 1434 and 1384 cm^{-1} to the O-C-O antisymmetric and symmetric stretching vibrations of the monodentate carbonate.[16] A shift to higher wavenumbers of the antisymmetric stretching vibration and lower wavenumbers of the symmetric stretching vibration of the bidentate carbonate indicates a higher polarity of the carbonate induced by higher base strength, as in the case of MgAl-17.[17] We had shown previously the conversion of carbonates into sulfur oxyanions in alkali/Al_2O_3 catalysts upon sulfidation with H_2S above 300°C.[7] We suggest similar changes of these Mg/Al oxides, able to adsorb CO_2 after sulfidation on those materials with stronger basic sites, such as the transformations observed with MgAl-17 and MgAl-25.

Previously, we showed that acid site strength and concentration strongly impacts the selectivity.[6] Therefore, pyridine adsorption was studied by IR spectroscopy Figure 5.2). Pyridine did not adsorb on MgAl-17 and MgAl-25 at 50°C, highlighting their low acid strength. Bands between 1580 and 1620 cm^{-1} are assigned to pyridine coordinatively bound to Lewis acid sites. [18] Both strong (1621 cm^{-1}) and weak (1606 cm^{-1}) Lewis acid sites were observed on MgAl-86, while only weak (1604 cm^{-1}) Lewis acid sites were observed with MgAl-45. The band between 1440-1455 cm^{-1} is used as a qualitative and quantitative measure for LAS. The blue shift observed with increasing Al content in the Mg/Al oxides suggests an increase of the Lewis acid strength (1444 and 1447 cm^{-1} for 45 % and 86% Al, respectively). We hypothesize the differences in the acid-base properties observed for Mg/Al oxides are strongly correlated to the selectivity of methanethiol.

5.4.2. Catalytic test reaction

The rates of methanethiol formation with Mg/Al oxide catalysts are shown in Figure 5.3. At 360 °C the highest rate of methanethiol was observed with MgAl-45 ($1.0 \cdot 10^{-4}$ mol g^{-1} s^{-1}) and the lowest with MgAl-86 ($0.2 \cdot 10^{-4}$ mol g^{-1} s^{-1}). The almost identical rates on MgAl-17 and MgAl-25 ($1.0 \cdot 10^{-4}$ mol g^{-1} s^{-1}) were in between. Surprisingly, these rates are an order of magnitude higher than those observed with alkali dispersed on tungsten sulfide and/or metal oxides (Chapter 3 of this thesis). [6]

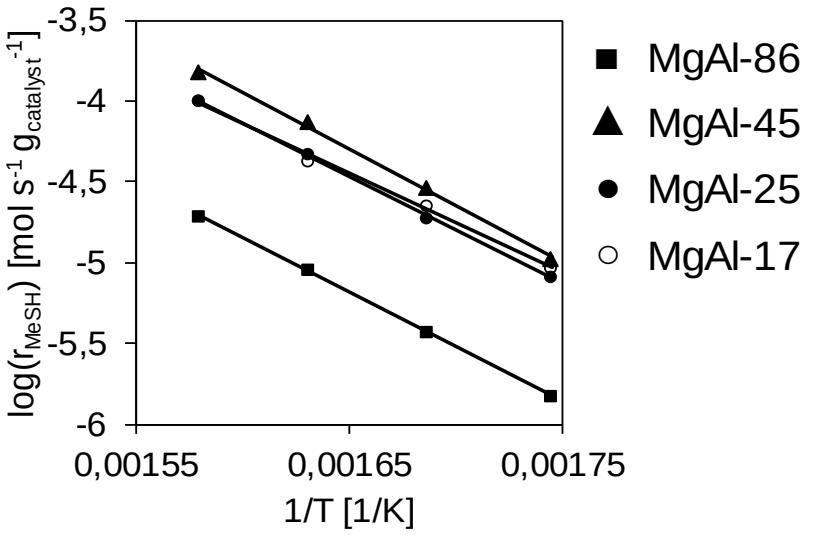

Figure 5.3 Logarithm of initial rate of methanethiol formation on Mg/Al mixed oxides for MgAl-17 (○ circles), MgAl-25 (●), MgAl-45 (▲) and MgAl-86 (■).

The yields of methanethiol, dimethyl sulfide (DMS) and dimethyl ether (DME) with increasing methanol conversion are shown in Figure 5.4. For MgAl-17, MgAl-25 and MgAl-45 the main product is methanethiol, with DMS as the only byproduct, forming at conversions above 40 % and reaching a maximum yield of 10% at full methanol conversion. Thus, methanethiol is a primary product and DMS is a secondary product. On MgAl-86, DME is a primary product, increasing its yield in between 0-20% methanol conversion and remaining constant (10% Yield of DME) until 65% methanol conversion. The change in the slope of methanethiol before and after 20% methanol conversions indicates methanethiol is formed both as primary and secondary product, via reaction with DME, in analogy to results with γ-Al_2O_3.[1, 6]

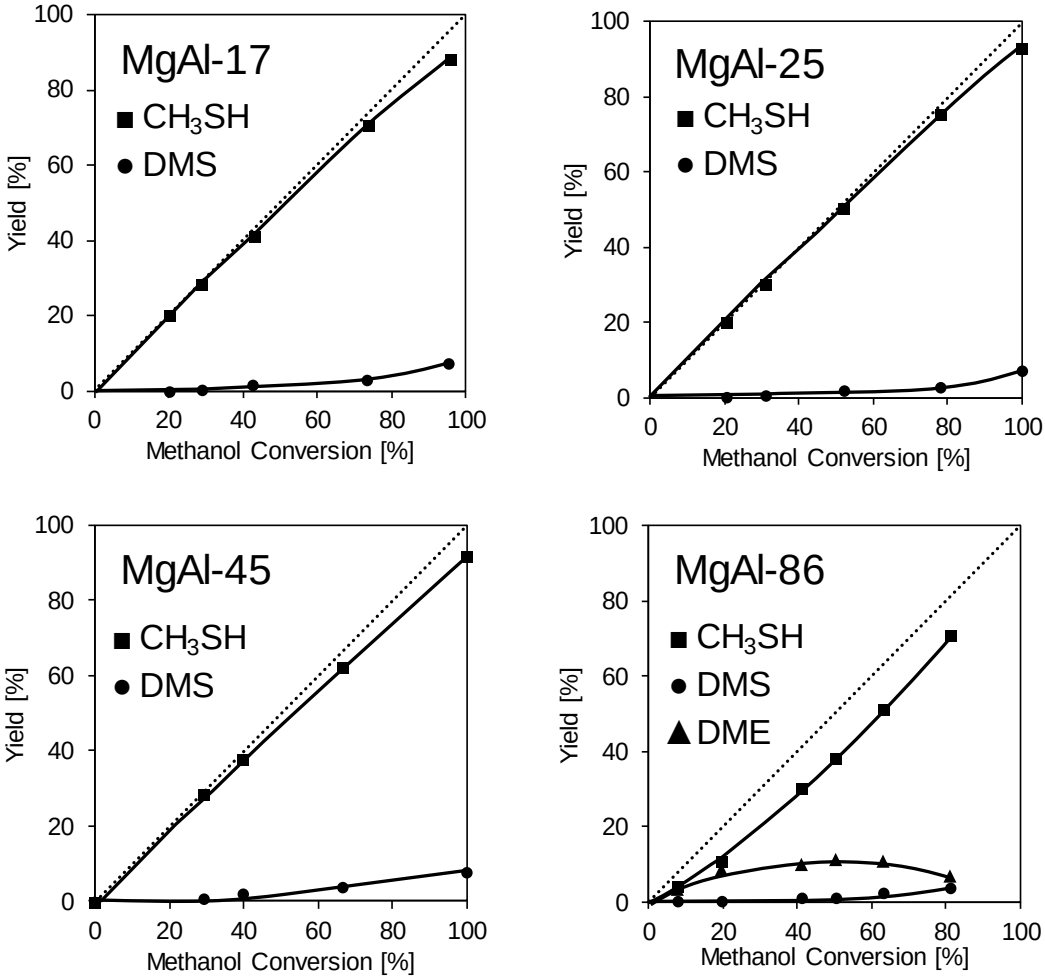

Figure 5.4 Yield vs. conversion: Methanethiol (■), DME (▲), DMS (●) with T = 360 °C and 9 bar.

The apparent activation energy increased monotonously with the Al concentration from 111 for MgAl-17 to 128 mol^{-1} for MgAl-86 (Table 5.2). The decrease in the apparent activation energy with higher Mg content correlates well with the lowest acid strength, as shown by pyridine and carbon dioxide adsorption. MgAl-86 contained both, strong and weak Lewis acid sites and did not adsorb carbon dioxide, while MgAl-17 did not adsorb pyridine but its strong basic sites are bound to carbon dioxide. Similar results were observed in our previous work with potassium, rubidium and cesium dispersed on γ-Al_2O_3, observing the lowest enthalpic barrier on the most basic mixed oxide (Cesium on γ-Al_2O_3). [7]

Table 5.2 Initial formation rates at 360 °C and apparent activation energy for methanethiol formation on Mg-Al mixed oxides.

Material	$r_{CH3SH,360°C}$ [mmol g^{-1} s^{-1}]	$E_{app,CH3SH}$ [kJ mol^{-1}]
MgAl-17	$1.0*10^{-4}$	111
MgAl-25	$1.0*10^{-4}$	121
MgAl-45	$1.5*10^{-4}$	127
MgAl-86	$0.2*10^{-4}$	128

It is hypothesized that only Al^{3+} sites act as part of the active sites, because MgO catalyzes methanol thiolation only with low rates. [19] However, a threshold of optimum aluminum content seems to be observed to prevent the formation of strong Lewis acid sites which induces methanol dehydration and induce the formation of Lewis acid-base pairs that catalyze methanol thiolation. Thus, the oxygen anions neighbored next to the Al^{3+} sites are affected by the presence of Mg^{2+}, making them more basic and favoring the formation of the methanethiol (Scheme 5.1).

Following the rational from our previous work with alkalis (K, Rb and Cs)[7] dispersed on metal oxides (Al_2O_3, TiO_2 and ZrO_2)(Third chapter of this thesis) and WS_2[1], methanol and H_2S adsorb dissociatively on Lewis acid-base pairs, forming a surface methanolate and SH^-, respectively(Third chapter of this thesis) In a second concerted step the SH^- attacks the methanolate through a SN_2 nucleophilic substitution to form the thiol and a hydroxyl group. After the recombination of the hydroxide and the thiol with the protons, the methanethiol and the water will desorb from the surface, respectively.

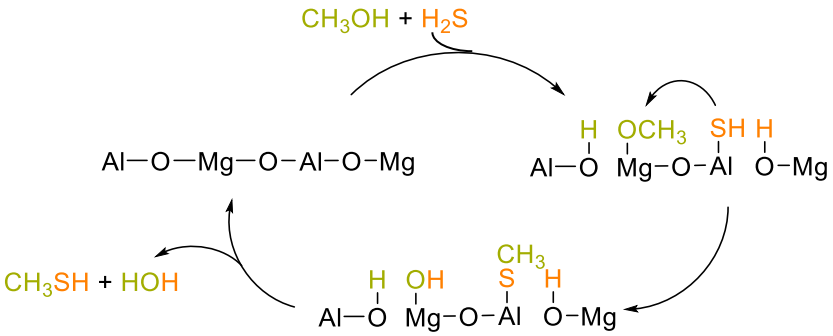

Scheme 5.1 Reaction mechanism for the formation of methanethiol, with Al^{3+} and Mg^{2+} cations and corresponding O^{2-} anion as active sites. This scheme is based on the mechanism proposed in our previous publication (Third chapter of this thesis).

5.5. Conclusion

Mg/Al mixed oxides are active in the thiolation of methanol, with higher rates per gram than with catalysts containing alkali dispersed on tungsten sulfide and/or mixed oxides. The mixed oxides with 25 Al mol % or lower introduce strong basic sites that do not adsorb the basic pyridine molecule, while those Mg/Al mixed oxides with higher than 25 Al mol % produce weak and strong Lewis acid sites that do not adsorb the acidic carbon dioxide molecule. The key factor for the inhibition of dimethyl ether is the absence of strong Lewis acid sites, which are required for this reaction, while strong basic sites form methanethiol. To achieve these requirements, Mg-Al mixed oxides with an aluminum content lower than 50 mol % seem to be highly suitable, achieving an intrinsic optimum of surface area and site density for methanol thiolation.

5.6. Literature

[1] A.V. Pashigreva, E. Kondratieva, R. Bermejo-Deval, O.Y. Gutiérrez, J.A. Lercher, Methanol thiolation over Al2O3 and WS2 catalysts modified with cesium, Journal of Catalysis, 345 (2017) 308-318.

[2] O.Y. Gutiérrez, C. Kaufmann, A. Hrabar, Y. Zhu, J.A. Lercher, Synthesis of methyl mercaptan from carbonyl sulfide over sulfide K2MoO4/SiO2, Journal of Catalysis, 280 (2011) 264-273.

[3] O.Y. Gutiérrez, C. Kaufmann, J.A. Lercher, Synthesis of Methanethiol from Carbonyl Sulfide and Carbon Disulfide on (Co)K-Promoted Sulfide Mo/SiO2 Catalysts, ACS Catalysis, 1 (2011) 1595-1603.

[4] C. Kaufmann, O.Y. Gutiérrez, Y. Zhu, J.A. Lercher, Effect of H2 in the synthesis of COS using liquid sulfur and CO or CO2 as reactants, Research on Chemical Intermediates, 36 (2010) 211-225.

[5] W. Taifan, J. Baltrusaitis, Minireview: direct catalytic conversion of sour natural gas (CH4 + H2S + CO2) components to high value chemicals and fuels, Catalysis Science & Technology, 7 (2017) 2919-2929.

[6] M. Weber-Stockbauer, O.Y. Gutiérrez, R. Bermejo-Deval, J.A. Lercher, The role of weak Lewis acid sites for methanol thiolation, Catalysis Science & Technology, 9 (2019) 509-516.

[7] R. Bermejo-Deval, R.M.H. Walter, O.Y. Gutierrez, J.A. Lercher, On the role of the alkali cations on methanol thiolation, Catalysis Science & Technology, 7 (2017) 4437-4443.

[8] J. Sauer, W. Boeck, L.v. Hippel, W. Burkhardt, S. Rautenberg, D. Arntz, W. Hofen, Catalyst, process for its preparation, and use for synthesis of methyl mercaptan in: E.D. GmbH (Ed.), 1998.

[9] J.A. Lercher, Acid - Base Properties of Al2O3/MgO Oxides I. I.r. Study of Adsorption of Acetone, in: Zeitschrift für Physikalische Chemie, 1982, pp. 209.

[10] J.A. Lercher, Acid-base properties of Al2O3/MgO oxides, II. Infrared study of adsorption of pyridine, 20 (1982) 409-413.

[11] J.A. Lercher, C. Colombier, H. Noller, Acid - Base Properties of Al2O3/MgO Oxides III. I.r. Study of Adsorption of Pyrrole in: Zeitschrift für Physikalische Chemie, 1982, pp. 111.

[12] J.A. Lercher, C. Colombier, H. Noller, Acid–base properties of alumina–magnesia mixed oxides. Part 4.—Infrared study of adsorption of carbon dioxide, Journal of the Chemical Society, Faraday Transactions 1: Physical Chemistry in Condensed Phases, 80 (1984) 949-959.

[13] J. Shen, J.M. Kobe, Y. Chen, J.A. Dumesic, Synthesis and Surface Acid/Base Properties of Magnesium-Aluminum Mixed Oxides Obtained from Hydrotalcites, Langmuir, 10 (1994) 3902-3908.

[14] S. Abelló, F. Medina, D. Tichit, J. Pérez-Ramírez, J.C. Groen, J.E. Sueiras, P. Salagre, Y. Cesteros, Aldol Condensations Over Reconstructed Mg–Al Hydrotalcites: Structure–Activity Relationships Related to the Rehydration Method, Chemistry – A European Journal, 11 (2005) 728-739.

[15] L.M. Parker, N.B. Milestone, R.H. Newman, The Use of Hydrotalcite as an Anion Absorbent, Industrial & Engineering Chemistry Research, 34 (1995) 1196-1202.

[16] G. Busca, V. Lorenzelli, Infrared spectroscopic identification of species arising from reactive adsorption of carbon oxides on metal oxide surfaces, Materials Chemistry, 7 (1982) 89-126.

[17] T. Montanari, L. Castoldi, L. Lietti, G. Busca, Basic catalysis and catalysis assisted by basicity: FT-IR and TPD characterization of potassium-doped alumina, Applied Catalysis A: General, 400 (2011) 61-69.

[18] C. Morterra, G. Magnacca, A case study: surface chemistry and surface structure of catalytic aluminas, as studied by vibrational spectroscopy of adsorbed species, Catalysis Today, 27 (1996) 497-532.

[19] M. Ziolek, J. Kujawa, O. Saur, J.C. Lavalley, Metal oxides as catalysts for the reaction between methanol and hydrogen sulfide, The Journal of Physical Chemistry, 97 (1993) 9761-9766.

.

5.7 Supplementary Information

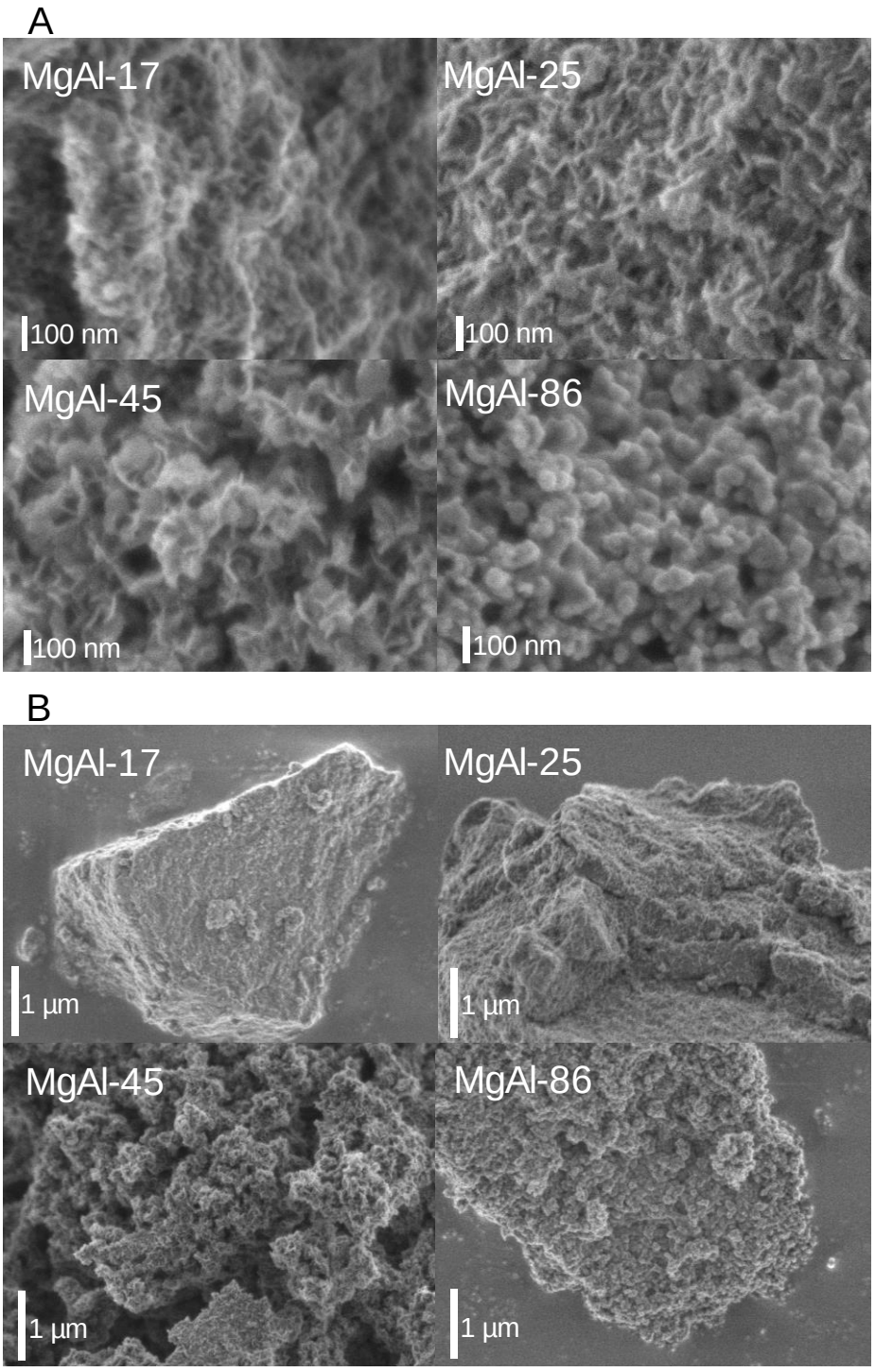

Figure S5.1 SEM micrographs of the Mg/Al mixed oxides at different scales.

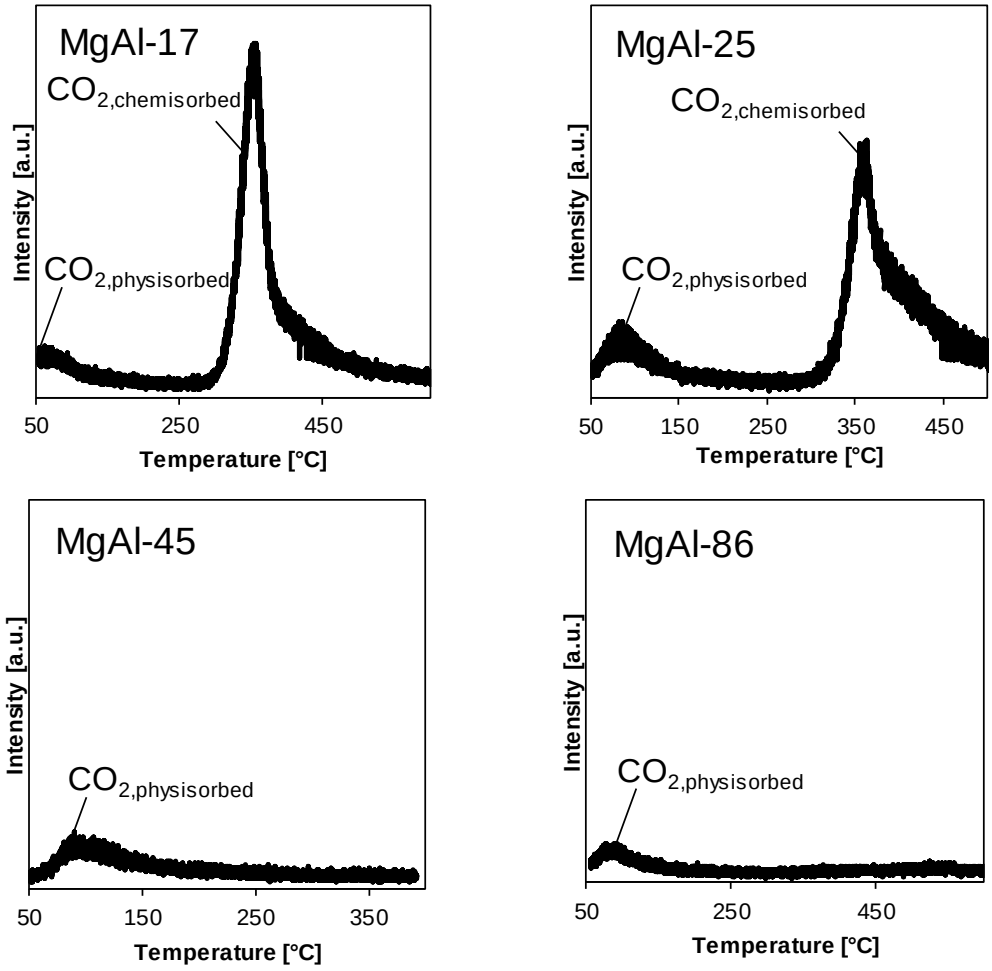

Figure S5.2 CO_2 desorption profiles from 50 to 500 °C (1°C/min) on sulfided mixed oxides.

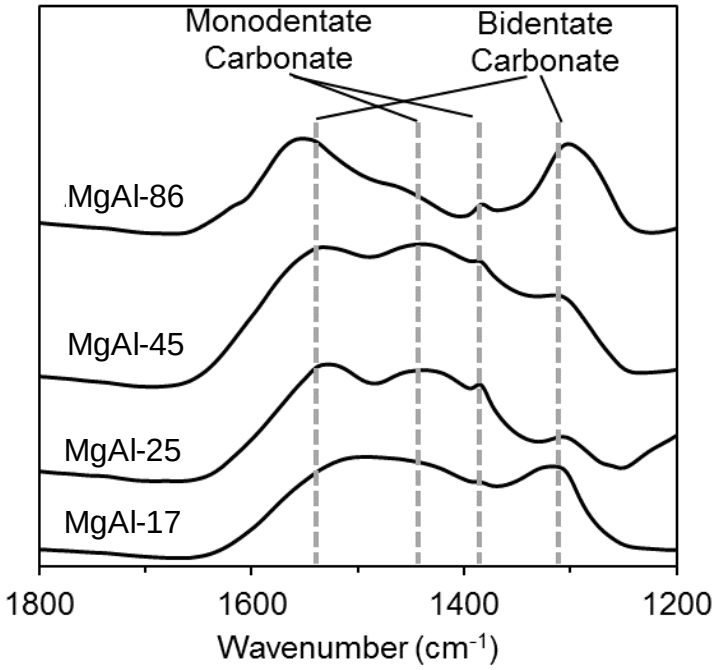

Figure S5.3 IR spectra of the Mg/Al mixed oxides at 50°C and below 10^{-6} mbar vacuum.

6. Summary

Methanethiol forms under reaction of H_2S and methanol adsorbed on Lewis acid-base pairs with strong basic sites, respectively weak Lewis acid sites. Addition of Cs^+ enhances the base strength on all supports, being metal oxides and metal sulfides. Dimethyl ether, as the major side product is formed on strong Lewis acid sites, only formed in the absence of Cs^+ as those strong Lewis acid sites are physically blocked or weakened by electronic effects of the alkali cation. The dehydration of methanol into dimethyl ether follows an Eley-Rideal mechanism involving a surface methoxy group and a weakly sorbed methanol on strong Lewis acid sites. Methanethiol formation follows a Langmuir-Hinshelwood mechanism: Methanolate reacting with a sulfhydryl, both being formed on the surface by dissociation of methanol, respectively H_2S. The dissociative adsorption of both reactants was clearly indicated by pyridine and methanol adsorption, as well as of a reaction order close to 0.5 in methanol thiolation with γ-Al_2O_3 and Cs/Al_2O_3. Tough the reaction mechanism is the same, the intrinsic properties of the strong basic sites determine the energetic barriers in the methanol thiolation: While on Cs/Al_2O_3 and CsW/Al_2O_3 a similar relatively low apparent activation energy (69 and 67 kJ/mol) was measured and similar pyridine bands in the IR were obtained, on γ-Al_2O_3 the higher apparent activation energy for methanol thiolation was dramatically higher (113 kJ/mol).

On Cs^+ modified metal oxides, Cs^+ is bound to the surface oxygen substituting the protons of OH groups, drastically increasing the strength of the base sites. The increase in basicity leads to a decrease in the apparent activation energy, as the more basic sites favor the thiolation reaction. Further investigating the influence of the surface properties of different metal oxides showed that on Al_2O_3 strong and weak Lewis acid sites act as reaction sites (forming methanethiol and dimethyl ether), while TiO_2 and ZrO_2 mainly provide Lewis acid-base pairs for methanethiol formation.

The results of Cs ion exchanged zeolite catalysts showed that discrete single sites are not active for the thiolation of methanol, supporting our proposed reaction mechanism, involving two acid-base sites, one for very reactant, H_2S and methanol.

Mixed Magnesium-Aluminum metal oxides were found to be the most active thiolation catalysts, related to mass, having been studied so far. On these systems the Mg/Al ratio was found to be the key parameter, with Mg/Al ratio of 1 being the optimum. With a ratio lower 1, catalysts with low surface area (<5 m^2g^{-1}) were found, which limits the reactivity of the catalyst due to a low concentration of accessible active sites, while at a higher ratio, strong Lewis acid sites were formed, leading to a decreased methanethiol selectivity, due to dimethyl ether formation.

7. Zusammenfassung

Methanthiol wird aus der Reaktion von H_2S und Methanol gebildet, welche an starken Base-, beziehungsweise schwachen Lewis-Säurezentren adsorbiert sind. Durch Cs^+ erhöht sich die Basenstärke auf allen Trägermaterialen (Metalloxide und -sulfide). Die Bildung von Dimethylether als Hauptnebenprodukt (auf starken Lewis-Säurezentren) findet nur in der Abwesenheit von Cs^+ statt. Wir schlossen aus unseren Ergebnissen, dass die starke Lewis-Säurezentren durch Cs^+ physikalisch blockiert oder durch elektronische Effekte des Alkalikations geschwächt werden. Die Dehydratisierung von Methanol zu Dimethylether folgt einen Eley-Rideal-Mechanismus, durch die Reaktion einer Oberflächenmethoxygruppe und eines Methanolmoleküles, schwach adsorbiert auf starken Lewis-Säurezentren.

Die Bildung von Methanthiol folgt einen Langmuir-Hinshelwood-Mechanismus:

Die Annahme der dissoziativen Adsorption beider Reaktanden auf der Oberfläche wird sowohl durch die Adsorption von Pyridin und Methanol, sowie einer Reaktionsordnung von 0.5 mit γ-Al_2O_3 und Cs/Al_2O_3 gestützt. Obwohl der Mechanismus auf beiden Katalysatoren gleich ist, sind die intrinsischen Eigenschaften der starken Basezentren ausschlaggebend, für die energetische Barriere der Thiolbildung, wie aus einer ähnlichen apparenten Aktivierungsenergie für Cs/Al_2O_3 und CsW/Al_2O_3 (69 und 67 kJ/mol), dem Fund der gleichen Pyridin-banden im IR-Spektrum der Cs^+-Katalysatoren, sowie der deutlich höheren apparenten Aktivierungsenergie für die Thiolbildung auf γ-Al_2O_3, 113 kJ/mol, ersichtlich wird.

Weitere Studien über die aktiven Zentren der Methanol-Thiolierung stützten unsere Schlussfolgerungen: In Cs^+ modifizierten Metalloxiden ist das Cs^+ an Oberflächensauerstoff gebunden, wobei es die Protonen und OH-Gruppen ersetzt, wodurch sich die Basizität signifikant erhöht. Durch diese sinkt die apparente Aktivierungsenergie, da stärkere Basezentren die Bildung von Methanthiol begünstigen. Weitere Untersuchungen zum Einfluss der Oberflächeneigenschaften verschiedener Metalloxiden zeigten, dass auf Al_2O_3 starke und schwache Lewis-Säurezentren als Reaktionszentren für die Bildung von Methanthiol und Dimethylether dienen, während auf vor allem Lewis-Säure-base-Paare für die Bildung von Methanthiol vorhanden sind.

Studien an mit Cäsium getauschten Zeolithen zeigten, dass einzelne voneinander getrennte Zentren keine Aktivität für die Reaktion von H_2S und Methanol zeigen, was den von uns vorgeschlagenen Mechanismus unterstützt, der zwei Säure-Base-Zentren beinhalte, jeweils eine pro Reaktant, H_2S und Methanol.

Aus diesen Ergebnissen folgerten wir, dass die Säure-Basen-Eigenschaften von Magnesium-Aluminium-Mischoxide für die Synthese von Methanthiol sein könnten. Tatsächlich fanden wir, dass diese, bezogen auf die Masse, die aktivste bisher gefundenen Katalysatoren für diese

Reaktion sind. Wir fanden, dass in diesen Systemen das Mg/Al-Verhältnis den entscheidenden Faktor darstellt, wobei das Optimum bei einem Mg/Al-Verhältnis von 1 lag. Mit einem Mg/Al-Verhältnis kleiner 1 wurden nur Katalysatoren mit einer unzureichend großen Oberfläche (kleiner 5 $m^2 g^{-1}$) gefunden, was die katalytische Aktivität aufgrund der geringen Konzentration an aktiven Zentren limitiert. Ein Verhältnis größer 1 begünstigte die Bildung von starken Lews-Säure-Zentren, was zu einer verringerten Methanthiol-Selektivität aufgrund der Bildung von Dimethylether führt.